

Aus dem
Institut für Prophylaxe und Epidemiologie der Kreislaufkrankheiten (IPEK)
Großhadern Institut der Ludwig-Maximilians-Universität München



Role of macrophage CB1 in atherosclerosis

Dissertation
zum Erwerb des Doctor of Philosophy (Ph.D.) an der
Medizinischen Fakultät der
Ludwig-Maximilians-Universität München

vorgelegt von:
Yong Wang

Aus:
Xingtai of HeBei
province, China

Jahr:
2024

Mit Genehmigung der Medizinischen Fakultät der Ludwig-
Maximilians-Universität München

Erstes Gutachten von: Prof. Dr. Sabine Marten-Steffens

Zweites Gutachten von: Prof. Dr. Alexander Faußner

Drittes Gutachten von: Priv. Doz. Dr. Michael Czihal

Viertes Gutachten von: Prof. Dr. Gerd Juchem

Dekan: Prof. Dr. med. Thomas Gudermann

Datum der Verteidigung:

13.03.2024

Eidesstattliche Versicherung

Wang, Yong

Name, Vorname

Ich erkläre hiermit an Eides statt,
dass ich die vorliegende Dissertation mit dem Thema

Role of macrophage CB1 in atherosclerosis

selbständig verfasst, mich außer der angegebenen keiner weiteren Hilfsmittel bedient und alle Erkenntnisse, die aus dem Schrifttum ganz oder annähernd übernommen sind, als solche kenntlich gemacht und nach ihrer Herkunft unter Bezeichnung der Fundstelle einzeln nachgewiesen habe.

Ich erkläre des Weiteren, dass die hier vorgelegte Dissertation nicht in gleicher oder in ähnlicher Form bei einer anderen Stelle zur Erlangung eines akademischen Grades eingereicht wurde.

München, 28.11.2023

Ort, Datum Unterschrift Doktorand

Yong Wang

The results of this work were published in:

Yong Wang, Guo Li, Bingni Chen, George Shakir, Mario Volz, Emiel P.C. van der Vorst, Sanne L. Maas, Carolin Muley, Alexander Bartelt, Zhaolong Li, Nadja Sachs, Lars Maegdefessel, Maliheh Nazari Jahantigh, Michael Hristov, Michael Lacy, Beat Lutz, Christian Weber, Stephan Herzig, Raquel Guillamat Prats, Sabine Steffens

bioRxiv preprint doi: <https://doi.org/10.1101/2023.04.06.535832>

The results of this work were presented at the following conferences:

ORAL PRESENTATIONS

09/2022 **IRTG 1123 Annual Retreat**, Tutzing, Germany

POSTER PRESENTATIONS

10/2019 **IRTG1123 Annual Retreat**, Grainau, Germany

09/2021 **44th Annual ELC Scientific Meeting**, Tutzing, Germany

10/2021 **IRTG1123 Annual Retreat**, Venice, Italy

04/2022 **88th Annual DGK Meeting**, Mannheim, Germany

05/2022 **90th EAS Congress**, Milan, Italy

10/2022 **CRC1123 Atherosclerosis International Symposium**, Munich, Germany

04/2023 **89th Annual DGK Meeting**, Mannheim, Germany

04/2023 **CRC1123 Atherosclerosis Annual Retreat**, Grainau, Germany

06/2023 **IRTG1123 Annual Retreat**, Venice, Italy

08/2023 **ESC Congress 2023**, Amsterdam, Netherlands

TABLE OF CONTENT

TABLE OF CONTENT	I
LIST OF FIGURES	V
LIST OF TABLES	VII
ABBREVIATIONS	VIII
1. SUMMARY	1
2. ZUSAMMENFASSUNG.....	2
3. INTRODUCTION	3
3.1 Cardiovascular diseases	3
3.2 Atherosclerosis.....	4
3.2.1 Pathogenesis of atherosclerosis	5
3.2.1.1 Cellular components of atherosclerosis	6
3.2.1.1.1 Endothelial cells	6
3.2.1.1.2 Smooth muscle cells	7
3.2.1.1.3 Leukocytes.....	8
3.2.1.1.3.1 Myeloid cell.....	9
3.2.1.1.3.2 Lymphocytes.....	12
3.2.1.2 Special features of atherosclerotic plaques.....	13
3.2.1.2.1 Lipid-rich core.....	13
3.2.1.2.2 Cell death.....	14
3.2.1.2.3 Plaque erosion	14
3.2.1.2.4 Plaque rupture.....	15
3.2.2 Mouse models of atherosclerosis.....	15
3.2.2.1 <i>Apoe</i> ^{-/-} mouse model.....	16
3.2.2.2 <i>Ldlr</i> ^{-/-} mouse model	17
3.3 Endocannabinoid system	17
3.3.1 Cannabinoid CB1 receptor.....	18
3.3.2 Pharmacological tools to activate or block CB1.....	20
3.3.2.1 Globally active CB1 antagonists	20
3.3.2.2 Peripherally active CB1 inhibitors	20
3.3.2.3 CB1 activator ACEA.....	20
3.4 Aim of the study.....	22

4. MATERIALS AND METHODS	23
4.1 Materials	23
4.1.1 Chemical and reagents	23
4.1.2 Buffers and solutions	25
4.1.3 Kits	26
4.1.4 Primers	26
4.1.5 Antibodies	27
4.1.6 Enzymes	29
4.1.7 Consumables	29
4.1.8 Equipment	30
4.1.9 Software	31
4.2 Methods	31
4.2.1 Mouse model	31
4.2.2 Mouse dissection	32
4.2.3 Plasma cholesterol and triglycerides measurement	33
4.2.4 Plaque analysis in descending aorta	33
4.2.5 Histology and immunofluorescence	33
4.2.5.1 ORO staining of aortic root	34
4.2.5.2 Hematoxylin-eosin staining of arch	34
4.2.5.3 Masson's trichrome stain	35
4.2.5.4 Immunofluorescence staining	35
4.2.5.5 Macrophage co-staining with Nile Red	35
4.2.5.6 TUNEL staining	36
4.2.6 <i>In situ</i> hybridization	36
4.2.7 Laser capture microdissection (LCM)	37
4.2.8 Monocyte adoptive transfer	38
4.2.9 Flow cytometry	38
4.2.9.1 Determination of myeloid and lymphoid cell subsets counts in blood and bone marrow	39
4.2.9.2 Flow cytometric cell sorting	39
4.2.10 BMDMs were utilized in <i>in vitro</i> assays	39
4.2.10.1 BMDM ROS production assay	40
4.2.10.2 BMDM mitochondrial activity assay	40
4.2.10.3 BMDM oxLDL uptaking assay	41
4.2.10.4 BMDM proliferation rate assay	41
4.2.10.5 BMDM apoptosis assay	41
4.2.10.6 Murine IL1 β ELISA	42

4.2.10.7	BMDM p53 nuclear immunofluorescence staining	42
4.2.11	mRNA expression analysis.....	43
4.2.11.1	RNA isolation.....	43
4.2.11.2	Reverse transcription.....	43
4.2.11.3	Quantitative real time polymerase chain reaction (qRT-PCR).....	44
4.2.11.4	Droplet digital PCR.....	45
4.2.11.5	RNA-sequencing	46
4.2.12	Phospho kinase array.....	47
4.2.13	Extracellular Flux Analysis.....	48
4.2.14	Statistical analysis	48
5.	RESULTS.....	50
5.1	Reduced formation of early and advanced atherosclerotic plaques through inactivation of myeloid CB1	50
5.1.1	CB1 expression and mouse model establishment.....	50
5.1.2	The impact of CB1 receptor deficiency in myeloid cells on atherosclerosis progression.....	51
5.1.3	The impact of CB1 deficiency in myeloid cells on plaque progression.....	53
5.1.4	The effect of CB1 receptor deficiency in myeloid cells on metabolic parameters	56
5.2	Arterial monocyte recruitment is diminished due to a decrease in chemokine receptor expression in absence of myeloid CB1	57
5.2.1	The influence of CB1 deficiency in myeloid cells on the number of circulating leukocyte subsets	57
5.2.2	Impact of CB1 deficiency in myeloid cells on the expression of growth factor and chemokine receptors	60
5.2.3	Arterial monocyte recruitment is impacted by the absence of CB1 in myeloid cells	61
5.2.4	The regulation of chemokine receptor expression by CB1 signaling in BMDM61	
5.3	Myeloid CB1 deficiency hampers macrophage growth by modulating p53 signalling	62
5.3.1	Impact of myeloid CB1 deficiency in macrophages proliferation.....	62
5.3.2	The activation of CB1 receptors influences kinase activity and promotes the translocation of p53 into the nucleus.....	64
5.4	Myeloid CB1 deficiency reduces pro-inflammatory macrophage phenotype	65
5.4.1	The involvement of CB1 in macrophage polarization and the uptake of oxLDL	65
5.4.2	Impact of myeloid CB1 deficiency on macrophage apoptosis.....	68
5.4.3	Macrophage inflammatory reprogramming is regulated by CB1 signaling	69

5.5	CB1 profoundly regulates the transcriptional, translational, and metabolic profiles of BMDMs	69
5.5.1	CB1 stimulation significantly influences the transcriptomic profile of BMDMs.	69
5.5.2	Validation of the key regulated genes in BMDMs and plaques of <i>Cnr1</i> -deficient mice.....	71
5.5.3	CB1 signaling in macrophages influences mitochondrial function	72
5.6	Plaque progression in atherosclerosis is inhibited by peripheral CB1 antagonism.	74
5.6.1	Metabolic parameters after treatment with peripheral antagonist	74
5.6.2	Effect of peripheral CB1 antagonism impact on plaque progression	74
6.	DISCUSSION	77
6.1	Pleiotropic effects of myeloid cell CB1 signaling in atherosclerosis	77
6.2	Regulation of cellular cholesterol metabolism and proliferation by CB1	77
6.3	Regulation of inflammation, apoptosis and plaque stability by CB1	78
6.4	The absence of myeloid <i>Cnr1</i> is linked to changes in p53 and cyclin dependent kinase activity.....	78
6.5	CB1 regulates the expression of chemokines and chemokine receptors	79
6.6	Role of macrophage CB1 in mitochondrial regulation and metabolism	79
6.7	Long-term treatment with a peripheral CB1 antagonist suppresses plaque macrophage build-up, proliferation, and inflammatory polarization	80
6.8	Inverse correlation between <i>CNR1</i> and crucial cellular pathways in the pathophysiology of human atherosclerosis.....	80
6.9	Limitations of this study	81
6.10	Conclusion and future perspectives.....	82
7.	REFERENCES	83
8.	ACKNOWLEDGEMENTS	99
9.	CONFIRMATION OF CONGRUENCY	100

LIST OF FIGURES

Figure 1: Stages of fatty streaks and atheroma formation.....	4
Figure 2: The risk factors for cardiovascular disease.....	7
Figure 3: The mechanisms that control monocyte recruitment and accumulation in plaques. 8	
Figure 4: Possible macrophage origins in atherosclerotic plaques in metabolic disease.....	11
Figure 5: The human body's CB1 and CB2 receptors have distinct physiological roles and localized distributions.	18
Figure 6: CB1 signaling: Peripheral metabolic effects.....	19
Figure 7: Representative long-chain endocannabinoids and their synthetic analogs.	21
Figure 8: The expression of murine Cnr1 in various myeloid cell subsets and BMDMs.....	50
Figure 9: The expression of murine Cnr1 in atherosclerotic plaques and BMDMs.....	51
Figure 10: The influence of deficient CB1 receptors in myeloid cells on the development of atherosclerosis.....	52
Figure 11: The influence of deficient CB1 receptors in myeloid cells on the advancement of arterial plaque.	53
Figure 12: Examining the influence of myeloid CB1 deficiency on advanced atherosclerosis.	54
Figure 13: Impact of myeloid Cnr1 deficiency on advanced plaque composition.	55
Figure 14: Examining the influence of myeloid CB1 deficiency on advanced of arterial arch plaque.	56
Figure 15: Effects of the absence of CB1 receptors in myeloid cells on metabolic parameters.	57
Figure 16: Myeloid CB1 deficiency impact on blood myeloid subset counts.	58
Figure 17: Myeloid CB1 deficiency impact on femur myeloid subset counts.....	59
Figure 18: Myeloid CB1 deficiency impact on lymphocyte counts.	59
Figure 19: Myeloid CB1 deficiency impact on CSF1R expression.....	60
Figure 20: Myeloid CB1 deficiency's impact on chemokine receptor expression.	60
Figure 21: The impact of Cnr1 deficiency in myeloid cells on the mobilization of arterial monocytes.	61
Figure 22: Impact of myeloid CB1 deficiency on chemokine receptors in BMDMs.	62
Figure 23: Impact of myeloid CB1 deficiency on macrophages proliferation.....	63
Figure 24: The effects of stimulating CB1 on kinase activity.	64
Figure 25: The effects of stimulating CB1 on the translocation of p53 to the nucleus.	65
Figure 26: The role of CB1 in macrophage polarization.	66

Figure 27: The role of CB1 in macrophage oxLDL uptake.	67
Figure 28: Effects of myeloid CB1 deficiency on plaque macrophage apoptosis.	68
Figure 29: CB1-dependent regulation of macrophage inflammatory reprogramming.	69
Figure 30: The effects of stimulating CB1 on the transcriptomic profile of BMDM.	70
Figure 31: Transcriptomic profile of BMDMs after CB1 agonist stimulation.	71
Figure 32: The effect of CB1 signaling in macrophages gene expression and mitochondrial function.	72
Figure 33: The influence of CB1 signaling in macrophages mitochondrial function.	73
Figure 34: Peripheral CB1 antagonism's impact on metabolic parameters.	74
Figure 35: Peripheral CB1 antagonism's impact on plaque progression.	75
Figure 36: Peripheral CB1 antagonism impact on the advancement of arterial plaque.	76

LIST OF TABLES

Table 1: Animal models of atherosclerosis: advantages and limitations.	5
Table 2: Chemicals and reagents.....	23
Table 3: Buffers and solutions.....	25
Table 4: Kits	26
Table 5: Primers for qPCR analysis	26
Table 6: Murine antibodies for flow cytometry	27
Table 7: Antibodies used for immunohistochemistry	28
Table 8: Isotype controls for immunohistochemistry.....	28
Table 9: Secondary antibodies for immunohistochemistry	29
Table 10: Enzymes	29
Table 11: Material.....	29
Table 12: Equipment.....	30
Table 13: Software	31
Table 14: RT reaction mix.....	44
Table 15: RT program	44
Table 16: Primer-probe mix	44
Table 17: qPCR reaction mix	45
Table 18: qPCR FAST program.....	45

ABBREVIATIONS

ACK	Ammonium chloride potassium
AF	AlexaFluor
ANOVA	Analysis of variance
APC	Allophycocyanin
ApoE	Apolipoprotein E
ATP	Adenosine triphosphate
BMDMs	Bone marrow derived macrophages
BSA	Bovine serum albumin
BV	Brilliant violet
CB1	Cannabinoid receptor type 1
CB2	Cannabinoid receptor type 2
CCR	C-C motif chemokine receptor
cDNA	Complementary DNA
CFSE	Carboxyfluorescein succinimidyl ester
Chil3	Chitinase-like 3
CSF1R	Colony stimulating factor 1 receptor
CVD	Cardiovascular disease
Cy	Cyanine
ddH ₂ O	double-distilled water
ddPCR	Droplet Digital PCR
DEGs	Differentially expressed genes
DMSO	Dimethyl sulfoxide
DNA	Deoxyribonucleic acid
DNase	Deoxyribonuclease
EDTA	Ethylenediaminetetraacetic acid
ELISA	Enzyme-linked immunosorbent assay
ECS	Endocannabinoid system
FACS	Fluorescence-activated cell sorting
FCCP	Carbonyl cyanide 4-(trifluoromethoxy)phenylhydrazone
FDR	False discovery rate
Fwd	Forward
GPCR	G-protein-coupled receptor
GO	Gene Ontology

GSEA	Gene Set Enrichment Analysis
HBSS	Hank's balanced salt solution
HEPES	4-(2-hydroxyethyl)-1-piperazineethanesulfonic acid
H&E	Hematoxylin and eosin
Hprt	Hypoxanthine-guanine phosphoribosyltransferase
IEL	Internal elastic lamina
IFN γ	Interferon gamma
IgG	Immunoglobulin G
IL	Interleukin
i.p.	Intraperitoneal
IRF	interferon regulatory factor
JIR	Jackson Immuno Research
LCM	Laser capture microdissection
LDL	Low-density lipoprotein
LDLR	Low-density lipoprotein receptors
LPS	Lipopolysaccharide
M-CSF	Macrophage colony-stimulating factor
MFI	Mean fluorescence intensity
MIF	Macrophage migration inhibitory factor
mRNA	Messenger RNA
NCOR1	Nuclear receptor corepressor 1
NDUFA6	Ubiquinone oxidoreductase subunit A6
NOS2	Nitric oxide synthase 2
OCR	Oxygen consumption rate
oxLDL	Oxidized low density lipoprotein
ORO	Oil Red O
PBS	Phosphate buffered saline
PCR	Polymerase chain reaction
PE	Phycoerythrin
PFT α	Pifithrin- α
PerCP	Peridinin chlorophyll
PFA	Paraformaldehyde
qPCR	Quantitative PCR
Rev	Reverse
RNA	Ribonucleic acid

RNase	Ribonuclease
ROS	Reactive oxygen species
RPMI	Roswell Park Memorial Institute
RT	Reverse transcription
RT	Room temperature
STK	Serine-Threonine kinase
TG	Triglyceride
TMB	Tetramethylbenzidine
TNF α	Tumor necrosis factor alpha
WD	Western diet
WHO	World Health Organization

1. SUMMARY

Although the potential connection between the cannabinoid CB1 receptor and atherosclerosis has been suggested, the specific influence it exerts on the various cell types involved in the disease remains unclear. Here, we investigated its role in myeloid cells, which are key cellular effectors in atherosclerosis. Male mice with myeloid-specific knockout of the CB1-encoding gene (*Cnr1*) on an atherogenic apolipoprotein E (*ApoE*) deficiency background exhibited notably smaller lesions and necrotic cores compared to the control group. However, in females, only moderate effects were observed, and primarily at an advanced stage of the disease. The atheroprotective effects in male mice were attributed to reduced recruitment of arterial monocytes, decreased proliferation of plaque macrophages, and a less inflammatory polarization state. Interestingly, the sex-specific variances in CB1 signaling within murine macrophages were reproducible *in vitro* and mitigated by estradiol treatment. Detailed analysis of kinase activity profiling revealed the involvement of p53 signaling and cyclin-dependent kinases in mediating the effects of CB1. Unbiased transcriptomic profiling further confirmed the role of CB1 in regulating macrophage oxidative metabolism, which was subsequently validated by metabolic flux assays. Notably, CB1 deficiency or antagonism led to an improvement in oxidative energy metabolism. Additionally, the peripherally acting CB1 antagonist JD5037 halted early plaque formation in male mice. To summarize, impaired CB1 signaling in macrophages reduces their recruitment to arteries, local proliferation, and inflammatory reprogramming, leading to protection against atherosclerosis, especially during the early disease stages. The phenotype was only observed in male mice, which may hint to a sex-specific difference of macrophage CB1 signaling.

2. ZUSAMMENFASSUNG

Obwohl ein möglicher Zusammenhang zwischen dem Cannabinoid-CB1-Rezeptor und Arteriosklerose vermutet wurde, bleibt der spezifische Einfluss, den er auf die verschiedenen an der Krankheit beteiligten Zelltypen ausübt, unklar. Hier untersuchten wir seine Rolle in myeloischen Zellen, die eine Schlüsselrolle in der Atherosklerose spielen. Männliche Mäuse mit myeloidspezifischem Knockout des CB1-kodierenden Gens (*Cnr1*) und Apolipoprotein E (*ApoE*) Knockout zeigten im Vergleich zur Kontrollgruppe deutlich kleinere atherosklerotische Läsionen und nekrotische Kerne. Bei weiblichen Mäusen wurden jedoch nur mäßige Auswirkungen beobachtet, und zwar vor allem in einem fortgeschrittenen Krankheitsstadium. Die atheroprotektiven Wirkungen bei männlichen Mäusen wurden auf eine verringerte Rekrutierung arterieller Monozyten, eine verringerte Proliferation von Plaque-Makrophagen und einen weniger entzündlichen Phänotyp zurückgeführt. Interessanterweise waren die geschlechtsspezifischen Unterschiede in der CB1-Signalübertragung in murinen Makrophagen *in vitro* reproduzierbar und wurden durch die Behandlung mit Östradiol gehemmt. Eine detaillierte Analyse der Kinaseaktivitätsprofile ergab die Beteiligung von p53-Signalwegen und Cyclin-abhängigen Kinasen an der Vermittlung der Wirkung von CB1. Die RNA Sequenzierung von *Cnr1*-defizienten Makrophagen zeigte außerdem eine CB1-abhängige bei der Regulierung des oxidativen Metabolismus von Makrophagen, was anschließend durch Stoffwechselflussassays *in vitro* validiert wurde. Eine genetische CB1-Defizienz oder pharmakologische Antagonisierung führte zu einer Verbesserung des oxidativen Energiestoffwechsels. Darüber hinaus hemmte die chronische Verabreichung von JD5037, einem nur peripher wirkenden CB1-Antagonisten, die frühe Plaquebildung bei männlichen Mäusen. Zusammenfassend lässt sich sagen, dass eine Blockierung des CB1 Rezeptors in Makrophagen deren Rekrutierung in die Arterien, die lokale Proliferation und die entzündliche Neuprogrammierung verringert, was zu weniger Atherosklerose führt. Männliche Mäuse zeigen einen stärkeren Einfluss der Makrophagen-CB1-Signalisierung, insbesondere in den frühen Krankheitsstadien, was auf einen geschlechtsspezifische Rolle schließen lässt.

3. INTRODUCTION

3.1 Cardiovascular diseases

Cardiovascular disease (CVD) is a significant global contributor to mortality, encompassing a range of heart and blood vessel disorders, as per the definition provided by the World Health Organization (WHO). Approximately 17 million deaths occur annually due to CVD, emphasizing its profound impact on public health worldwide [9]. CVD includes heart-related conditions like coronary heart disease, stroke, and heart failure, among others. The underlying causes of CVD are complex and multifactorial. The commonly recognized risk factors for CVD encompass elevated blood pressure, increased cholesterol levels, smoking habits (Figure 1), lack of physical activity, obesity, diabetes, and a family history of the condition. Age and sex are also important factors, with CVD incidence increasing with age and being higher in men than women. The field of CVD research has made notable advancements in comprehending the underlying mechanisms, leading to an improved understanding of the pathophysiology and the emergence of novel diagnostic and therapeutic strategies. Studies have identified genetic and environmental factors that contribute to CVD, as well as the role of inflammation, oxidative stress, and endothelial dysfunction [10]. The present treatment approaches for CVD encompass lifestyle modifications, such as dietary adjustments and regular exercise, along with the utilization of lipid-lowering medications, including statins, antihypertensive drugs, and antiplatelet agents. Additional research is essential to enhance both preventive measures and treatment approaches for CVD. This is particularly crucial for high-risk populations, specifically focusing on low- and middle-income countries. Despite notable progress in this field, the burden of CVD remains substantial in these regions, emphasizing the need for further advancements.

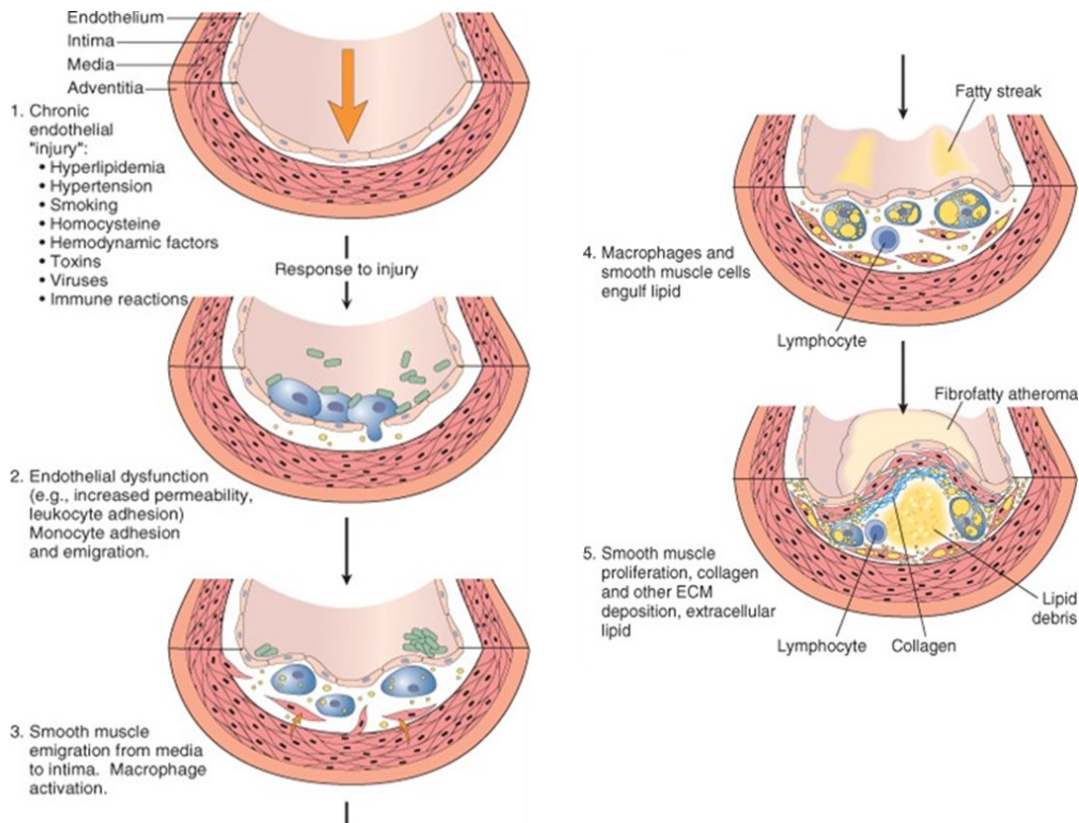


Figure 1: Stages of fatty streaks and atheroma formation.

1) At the onset of atherosclerosis, LDL cholesterol becomes trapped at the lesion site, initiating the disease progression. This process results in an increased accumulation of LDL within the intima and prolongs its residence in the lesion. As a consequence, these factors promote the spontaneous oxidation of LDL and subsequent oxidation of cells that have captured these particles [5]. 2) The activation of endothelial cells by cytokines and oxidized lipids triggers the onset of atherosclerosis, as it attracts monocytes and T lymphocytes to the inner layer of blood vessels, known as the vascular intima [6]. 3) In the initial stages of atherosclerosis, immune cells like monocytes and T cells become activated and move from the bloodstream through the healthy endothelium, crossing the walls of the blood vessels. 4) In the intima, mononuclear phagocytes undergo transformation into macrophages. Subsequently, these macrophages uptake and retain ox-LDL through scavenger receptors, which ultimately results in the formation of foam cells [7]. 5) Atheroma formation involves macrophages and T lymphocytes at plaque borders. Macrophages secrete metalloproteinases that degrade the extracellular matrix, and T cells produce TNF- α , inhibiting collagen synthesis in smooth muscle cells (SMCs). Adapted from Mahmoud Rafieian-Kopaei *et al* [8].

3.2 Atherosclerosis

Atherosclerosis is characterized as a persistent inflammatory condition that primarily impacts large and medium-sized arteries. This condition leads to the development of plaques, which impede blood flow and elevate the risk of an acute cardiovascular event [11]. Risk factors, including smoking, hypertension, elevated cholesterol levels, and diabetes, exert an influence on the progression of the condition. It involves the gradual buildup of cholesterol and other lipids within the arterial wall, initiating the formation of fatty streaks. Over time, these fatty streaks progress and transform into atherosclerotic plaques, comprising diverse cell types and proteins [8]. Despite advancements in prevention and treatment, atherosclerosis continues to

be a significant global contributor to illness and mortality [12]. In order to enhance our comprehension of the disease and foster the development of novel therapeutic approaches, various animal models, including mice, rabbits, and pigs (Table 1), have been developed to mimic the human disease to varying degrees [13, 14]. These insights have been helpful in elucidating the significance of inflammation, lipid metabolism, and immune modulation in the pathogenesis of atherosclerosis [15]. Recent research in mouse models has focused on identifying new therapeutic targets, including immune cells and the gut microbiome [16-18]. Advancements in technologies like single-cell sequencing and imaging have enabled a more comprehensive understanding of the disease [19-21]. However, translating preclinical findings to the clinical setting remains a significant challenge. Further research in mouse models of atherosclerosis is essential to continue advancing our understanding of the disease and developing new treatments for this prevalent condition [22, 23].

Table 1: Animal models of atherosclerosis: advantages and limitations.

Mouse	(1) Rapid development of atherosclerotic plaques (2) Short reproductive cycle (3) Relative ease of genome manipulation	(1) Only partial resemblance to humans (2) More atherosclerotic than atherothrombosis model (3) Very high levels of blood lipids
Rat	Easy, available, and cheap	Do not develop atheroma
Rabbit	(1) Medium size (2) Fibroatheroma lesions (3) Useful for restenosis models	(1) Need for high blood cholesterol levels (2) No plaque rupture model
Porcine	(1) Lesions more similar to human disease (2) Valid for restenosis studies	(1) High cost (2) Difficult handling

Modified from Carlos Zaragoza *et al* [13].

3.2.1 Pathogenesis of atherosclerosis

Atherosclerosis development includes multiple factors, including endothelial dysfunction, inflammation, oxidative stress, and immune system activation (Figure 1) [8]. The initial stage in the progression of atherosclerosis involves damage or dysfunction of the endothelial lining of the artery (Figure 1). Subsequently, this leads to low-density lipoprotein (LDL) cholesterol buildup in arterial walls and activates inflammatory cells. High cholesterol, smoking, and diabetes increase the risk of facilitating this process [24]. As the plaques grow, they protrude

into the lumen of the artery, narrowing it and reducing blood flow. Plaque rupture can lead to blood clot formation, blocking arteries and causing heart attacks or strokes (Figure 1). Atherosclerosis can cause artery narrowing and hardening, leading to complications like angina, peripheral artery disease, and chronic kidney disease [25]. Lifestyle changes such as exercise, diet, and smoking cessation can help to slow the progression of atherosclerosis. Statins, blood pressure medication, and antiplatelet drugs can slow or stop disease progression [26]. In severe cases, the restoration of blood flow to the affected area may require invasive procedures like angioplasty or bypass surgery. However, early detection and proactive management of risk factors are vital for preventing or delaying complications linked to atherosclerosis [27]. Understanding the pathogenesis and progression of atherosclerosis can aid in the development of effective prevention and treatment strategies for this complex disease [28].

3.2.1.1 Cellular components of atherosclerosis

3.2.1.1.1 Endothelial cells

Occupying the innermost layer of blood vessels, endothelial cells assume a pivotal role in governing vascular function and regulation [2]. Atherosclerosis emerges when endothelial cells are triggered by various risk factors, such as high blood pressure, increased cholesterol levels, and tobacco use (Figure 2). As a consequence of this activation, Endothelial cell activation increases adhesion molecules and cytokine expression, promoting the recruitment of white blood cells and lipoproteins to the arterial wall. Endothelial cells also regulate the production of nitric oxide, a molecule that helps maintain vascular tone and prevent the formation of blood clots [29]. Endothelial cells serve a dual purpose in the progression of atherosclerosis, contributing to its development while also supporting the stability of plaques. On one hand, activated endothelial cells facilitate the adhesion and migration of monocytes into the subendothelial space. Monocytes then differentiate into macrophages, which take up oxidized LDL particles and transform into foam cells, a hallmark of early atherosclerotic lesions. On the other hand, endothelial cells also play a critical role in maintaining the stability of atherosclerotic plaques. As the disease progresses, some plaques become vulnerable and prone to rupture. Endothelial cells within stable plaques help promote stability through fibrous cap formation. Endothelial cells stimulate the synthesis and secretion of extracellular matrix components, particularly collagen and elastin fibers. These fibers contribute to the formation of a fibrous cap over the plaque, providing structural support and stability [30].

Risk factors for CVD

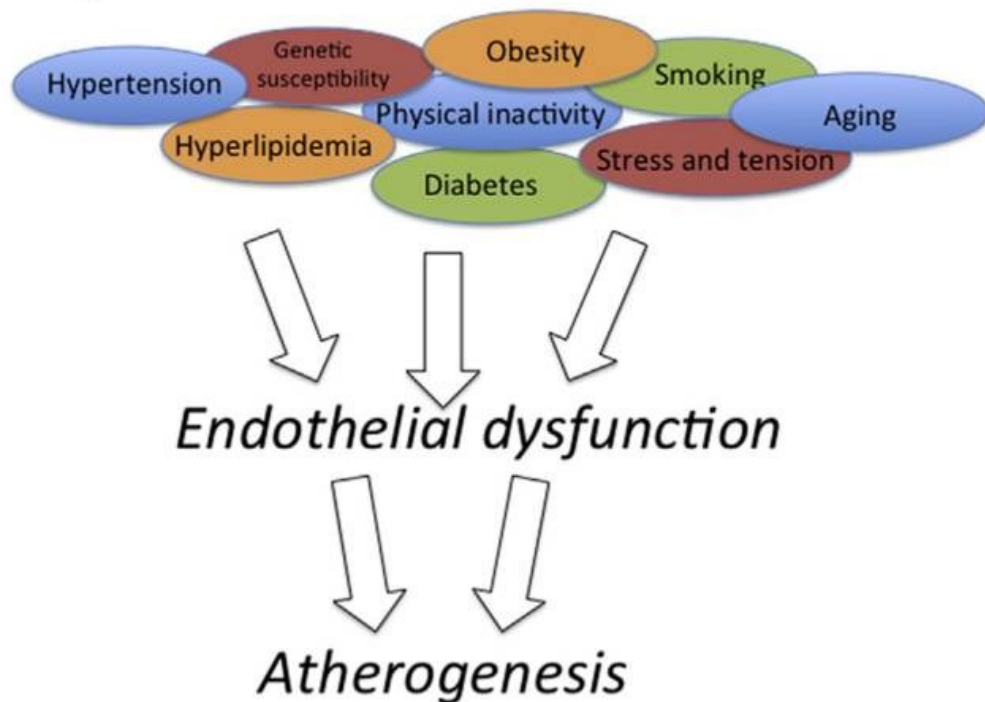


Figure 2: The risk factors for cardiovascular disease.

Common risk factors for CVD, including those mentioned, are linked to "endothelial dysfunction." This condition is characterized by a decline in the biological activity of nitric oxide and is considered an initiating factor in the development of atherosclerosis. Adapted from Cahill PA *et al* [2].

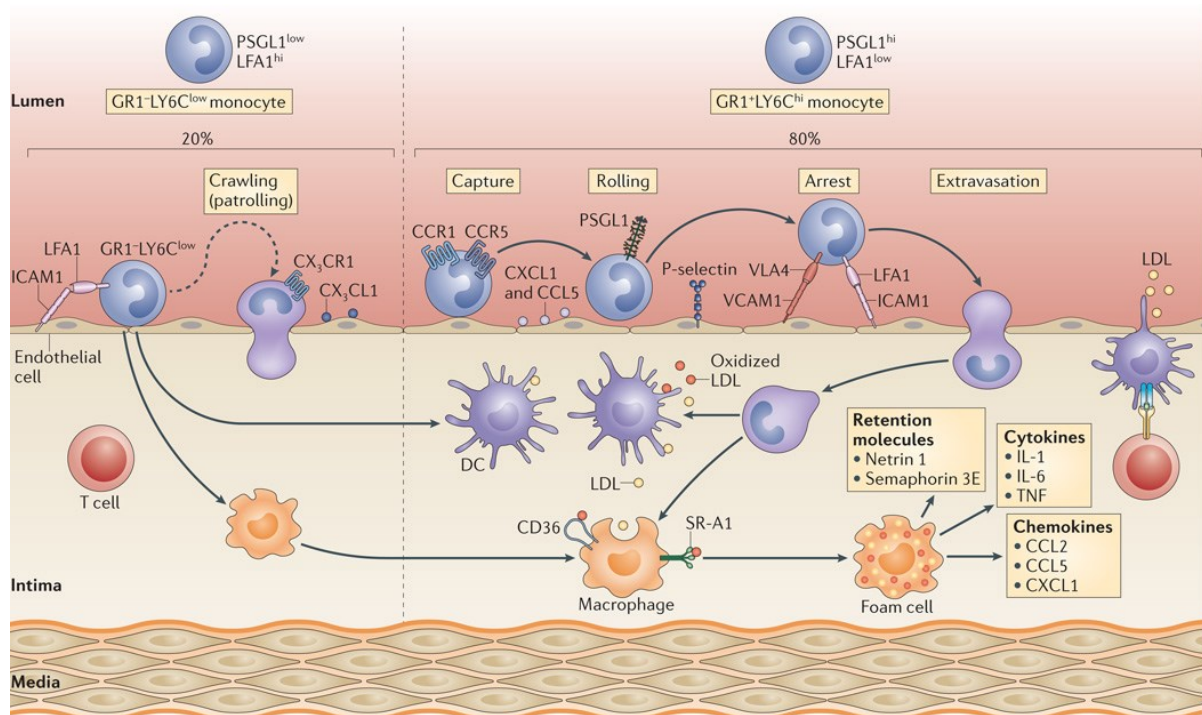
3.2.1.1.2 Smooth muscle cells

SMCs represent the predominant cellular component within the tunica media layer of arterial walls. They are crucial for preserving the structural integrity and contractile function of blood vessels. In atherosclerosis, SMCs transition from a contractile to a synthetic state, characterized by enhanced proliferation, migration, and synthesis of extracellular matrix components. As the disease progresses, the immune-inflammatory response is accompanied by a fibroproliferative reaction orchestrated by SMCs in the innermost layer of the blood vessels. The SMCs have a vital function in repairing and repairing damages to arteries, thereby actively participating in the process of recovery. Nevertheless, they also play a significant role in the development of plaque rupture, a pivotal occurrence that can result in acute cardiovascular incidents such as myocardial infarction and stroke. The fibrous cap's stability is crucial for preventing plaque rupture. It provides structural support to the plaque and resists mechanical forces generated by blood flow. Over time, atherosclerotic plaques can undergo changes that make them more prone to rupture. These changes include the thinning and weakening of the fibrous cap, increased inflammation, and the accumulation of inflammatory cells and enzymes within the plaque. When the fibrous cap becomes sufficiently

weakened and cannot withstand the mechanical stresses, it can rupture, allowing the fatty core to be exposed to the blood. However, the presence of SMCs and the collagen-based matrix they generate make plaques more stable, reducing the likelihood of severe issues like plaque rupture and blood clot formation [31-33].

3.2.1.1.3 Leukocytes

Leukocytes can stick to blood vessel walls and move into artery walls due to risk factors like high cholesterol [34]. This process contributes to the development of atherosclerosis. The continuous presence of this cellular reaction seems to propel the advancement of the condition. After penetrating the intima layer, monocytes undergo a metamorphosis into macrophages, assuming a pivotal role in absorbing atherogenic lipoproteins [35]. This absorption process is facilitated through specialized receptors located on the surface of macrophages, specifically scavenger receptors such as SR-A and CD36 [36]. Foam cells emerge when lipid-laden macrophages (Figure 3) accumulate, serving as a crucial hallmark in both early and advanced atherosclerotic lesions [37].



Nature Reviews | Immunology

Figure 3: The mechanisms that control monocyte recruitment and accumulation in plaques.

Multiple mechanisms influence the recruitment and accumulation of monocytes in atherosclerotic plaques. In the context of mouse atherosclerosis, the majority of recruited monocytes (approximately 80%) are GR1⁺LY6C^{hi} monocytes, which are increased in response to hyperlipidemia. The remaining monocytes are the GR1⁻LY6C^{low} patrolling monocytes. Once recruited, monocytes undergo differentiation into macrophages or dendritic cells within the intima. These cells interact with atherogenic lipoproteins present in the environment. Macrophages, in particular, internalize both native and modified

LDL through processes such as macropinocytosis or scavenger receptor-mediated pathways, which involve receptors like scavenger receptor A (SRA) and CD36. Internalization results in foam cell formation, a key aspect of atherosclerotic plaques. Inflammation is significantly influenced by the active secretion of pro-inflammatory cytokines like IL-1, IL-6, and TNF by foam cells. Adapted from Kathryn J Moore *et al* [37].

Macrophages maintain their ability to ingest atherogenic lipoproteins without down-regulating scavenger receptors due to the persistent supply of these lipids. As a result, when macrophages undergo apoptosis and necrosis, this triggers the development of a destabilizing necrotic core within the plaque. This core is distinguished by its significant accumulation of lipid content. Macrophages possess the ability to transport cellular cholesterol to high-density lipoprotein (HDL) particles outside the cell via membrane transporters when LDL levels are low and HDL levels are high, under ideal circumstances. This phenomenon is commonly referred to as "reverse cholesterol transport" [38-40]. In addition to their scavenging function, macrophages also possess proteolytic enzymes such as matrix metalloproteinases (MMPs) and tissue factor. These enzymes play important roles in various biological processes. Moreover, macrophages exhibit distinct characteristics that contribute to the instability of plaques [41].

3.2.1.1.3.1 Myeloid cell

In the context of mouse models, myeloid cells, comprising monocytes, neutrophils, macrophages, and dendritic cells, have crucial involvement in the development and progression of atherosclerosis [42-44]. The recruitment of myeloid cells to inflamed tissue is a highly regulated process involving several chemotactic signals, adhesion molecules, and cytokines [45, 46]. Understanding the mechanisms of myeloid cell recruitment to inflamed tissue is essential for developing therapies for inflammatory diseases.

3.2.1.1.3.1.1 Monocytes

Atherosclerosis involves lipid and immune cell buildup, mainly monocytes and macrophages, in arterial walls [47, 48]. Multiple cytokines and receptors have been reported to be involved in monocyte recruitment to atherosclerotic plaques such as CCL2/CCR2, CCL5/CCR5, and CX3CL1/CX3CR1 [49, 50]. The process is facilitated by the interaction between adhesion molecules on endothelial cell surfaces and integrins on monocyte surfaces. The interaction results in the rolling of monocytes along the endothelium, followed by firm adhesion and transmigration into the subendothelial space [50, 51]. There are two main subsets of monocytes in mice, which are often distinguished based on the expression of cell surface markers. These subsets are known as "classical" or "inflammatory" monocytes (Ly6C^{high} in mice) and "non-classical" or "patrolling" monocytes (Ly6C^{low} in mice) [52]. Classical monocytes

are typically the predominant subset recruited to atherosclerotic lesions in mice [53]. Once monocytes infiltrate the arterial wall and differentiate into macrophages, they can take up modified lipoproteins, particularly LDL, and transform into foam cells [53, 54]. Foam cells contribute to the formation of fatty streaks, which are the earliest visible lesions in atherosclerosis. Foam cells accumulate cholesterol and lipids, leading to the development of necrotic cores within the plaques [55, 56]. Moreover, monocytes and macrophages secrete pro-inflammatory cytokines, such as interleukin-1 (IL-1), interleukin-6 (IL-6), and tumor necrosis factor-alpha (TNF- α), which further contribute to the inflammatory milieu within the arterial wall. This chronic inflammation promotes the recruitment of more monocytes, perpetuating the cycle of plaque development and progression [57, 58].

3.2.1.1.3.1.2 Macrophages

Macrophages are actively involved in the formation of atherosclerotic lesions, and their proliferation is integral to the disease progression (Figure 4) [59]. In the initial phases of atherosclerosis, macrophage accumulation within the lesion and the formation of a fibrous cap can be attributed to their proliferation [25]. As the disease advances, macrophages remain crucial in forming advanced plaques by releasing cytokines and chemokines that attract more immune cells to the injury site during persistent inflammation. The recruitment of immune cells can worsen inflammation, ultimately leading to the formation of a fibrous cap covering the lipid core of the plaque [53]. Macrophage growth aids lesion expansion and fibrous cap formation, promoting stability and minimizing rupture risk [60]. Nevertheless, an overabundance of macrophages can lead to the emergence of a necrotic core, weakening of the fibrous cap, and an increased susceptibility to plaque rupture and thrombosis. Research has revealed that local macrophage proliferation is responsible for sustaining the accumulation of macrophages in both inflammatory and normal tissues. In advanced atherosclerotic plaques, macrophage proliferation becomes prominent and accounts for over 80% of the local macrophage accumulation within a one-month timeframe [61, 62]. This highlights the significant role of macrophage proliferation in atherosclerosis progression and advanced plaque formation.

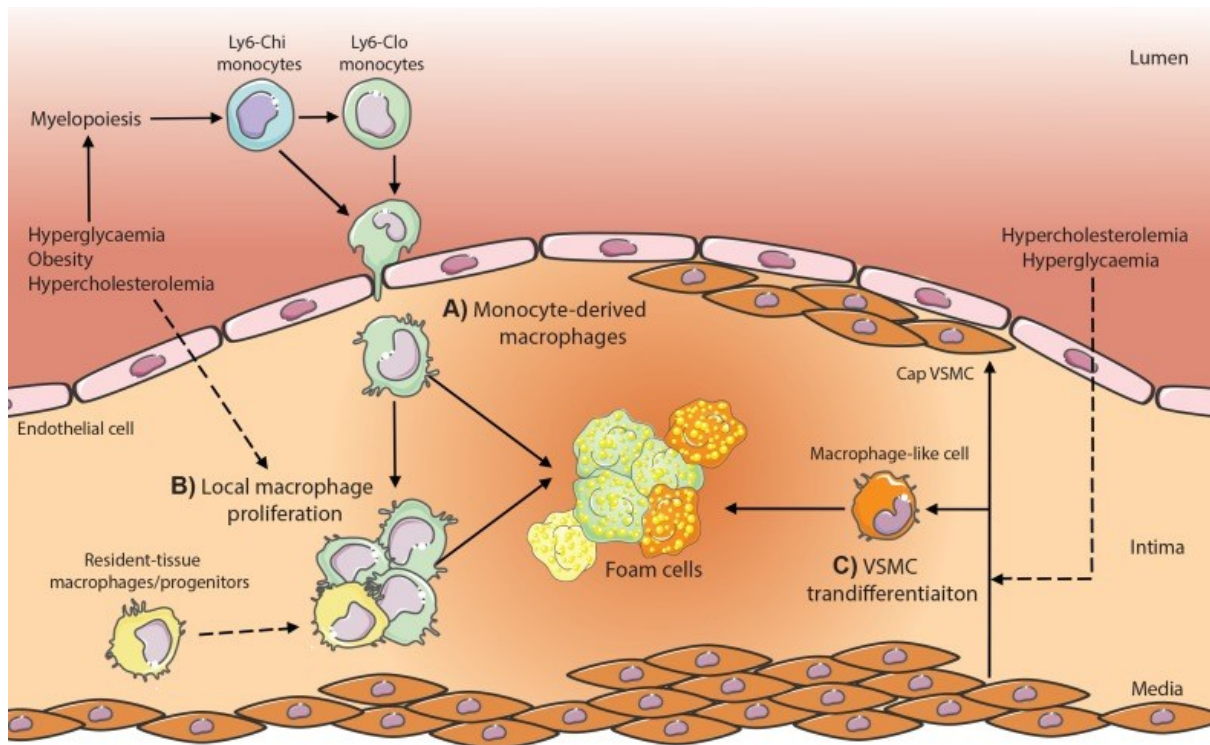


Figure 4: Possible macrophage origins in atherosclerotic plaques in metabolic disease. (A) Conditions such as hyperglycemia, hypercholesterolemia, or obesity-associated fat inflammation stimulate increased myelopoiesis, the process by which bone marrow cells form and differentiate, leading to the production of monocyte-derived macrophages. These macrophages infiltrate the atherosclerotic plaque and undergo transformation into foam cells due to lipid-loading. (B) Moreover, the plaque's foam cell formation can potentially be influenced by local macrophage proliferation and (C) the transdifferentiation of vascular smooth muscle cells. However, the specific impact of metabolic dysregulation (such as hypercholesterolemia or hyperglycemia) on these processes is still under investigation *in vivo*. Adapted from Michelle C Flynn *et al* [63].

3.2.1.1.3.1.3 Neutrophils

Neutrophils are vital components of the immune system, serving as white blood cells that are crucial for the body's defense against infections [64, 65]. While not as prominent as macrophages in atherosclerosis development, neutrophils do contribute to various stages of the disease process [44]. During the initial stages of atherosclerosis, chemokines and other signals released by activated endothelial cells attract neutrophils to the injured site in the arterial wall. Once present, neutrophils can interact with other immune cells, including macrophages, and participate in the formation of the early atherosclerotic lesion [66, 67]. Neutrophils can potentially contribute to the progression of atherosclerosis by releasing enzymes that can cause damage to the endothelial cells and other structures within the arterial wall. The occurrence of such damage can enhance the inflammatory response and facilitate the attraction of extra immune cells to the location of the injury [68]. Activated neutrophils have the ability to generate extracellular traps, consisting of DNA, histones, and antimicrobial proteins, known as web-like structures. These extracellular traps are released by neutrophils and can serve various functions in the immune response. Neutrophils extracellular traps have

been implicated in various inflammatory conditions, including atherosclerosis, and may contribute to the progression of the disease by promoting thrombosis and plaque rupture [69, 70].

3.2.1.1.3.1.4 Involvement of cells derived from the bone marrow

Several studies have demonstrated the significant contribution of cells derived from the bone marrow, specifically bone marrow-derived cells (BMDCs) to the pathogenesis of this condition [71, 72]. BMDCs, including hematopoietic stem cells, monocytes and macrophages are known to infiltrate atherosclerotic lesions. These cells are recruited to the site of vascular injury or inflammation through chemokine signaling and adhesive interactions with endothelial cells [53, 73]. Once present in the arterial wall, BMDCs actively participate in various processes that drive atherosclerosis progression [74]. Monocytes and macrophages which derived from the bone marrow infiltrate the subendothelial space and take up oxidized low density lipoprotein (oxLDL) particles, leading to the formation of foam cells. Foam cells contribute to plaque development and trigger an inflammatory response by releasing pro-inflammatory cytokines and chemokines, perpetuating the recruitment of more immune cells [42, 75].

3.2.1.1.3.2 Lymphocytes

The immune system remains continuously active within atherosclerotic lesions, contributing to their progression. While the initiation of atherosclerosis does not solely depend on lymphocytes, the immune system plays a vital role in controlling its development. The lesion contains a variety of antigens that have been identified as potential triggers for immune system activation. These antigens include heat-shock proteins, modified LDL, beta-2-glycoprotein I, and microbial antigens. Among these, oxLDL stands out with substantial evidence supporting its significant involvement, as it is prominently present within atherosclerotic plaques and recognized by T cells [76, 77].

3.2.1.1.3.2.1 T cells

CD4⁺ T cells, often known as helper T cells, play a vital role in coordinating the immune response against pathogens or foreign substances. Additionally, they have been associated with the progression of atherosclerosis. In atherosclerosis, CD4⁺ T cells contribute significantly to the pathological processes occurring in the blood vessels. CD4⁺ T cells are mobilized and recruited to the arterial wall, actively participating in the inflammatory processes that propel the development of plaque formation. CD8⁺ T cells, often referred to as cytotoxic T cells, take on the crucial role of eradicating cells infected by viruses or cells that have

experienced malignant changes. They possess the ability to target and destroy such compromised cells. In atherosclerosis, CD8+ T cells may contribute to plaque instability by killing smooth muscle cells in the arterial wall.

3.2.1.1.3.2.2 B cells

B cells are another type of lymphocyte that produces antibodies, which are proteins that bind to specific antigens, such as bacteria or viruses, and help to neutralize or eliminate them from the body. In atherosclerosis, B cells are also recruited to the arterial wall and produce antibodies against oxLDL, a type of cholesterol that accumulates in the arterial wall and contributes to plaque formation. Ongoing research is dedicated to exploring the involvement of B cells in atherosclerosis and aims to improve our understanding. Several studies have put forth the notion of B cells potentially playing a protective role in the onset and advancement of the disease. However, more research is necessary to fully grasp the extent of B cells' involvement in atherosclerosis.

3.2.1.2 Special features of atherosclerotic plaques

Atherosclerotic plaques are abnormal structures that form within the inner walls of arteries and are associated with CVD [78]. These plaques are composed of a variety of cellular and extracellular components, and their specific features can vary depending on their location in the arterial system and other factors. Some of the special features of atherosclerotic plaques include the presence of lipid deposits, cell death, plaque erosion, and thrombosis [8, 78].

3.2.1.2.1 Lipid-rich core

The accumulation of cholesterol and triglycerides within the inner layers of atherosclerotic plaques, which are fatty deposits in the arteries, leads to the development of a lipid-rich core [8]. This core, characterized by a high concentration of lipids, is formed as a result of the gradual deposition and retention of cholesterol and triglycerides over time. As these substances accumulate, they undergo various biochemical processes, such as oxidation and modification, which contribute to the formation of a complex mixture within the plaque [79]. In addition to the lipid-rich core, the atherosclerotic plaque structure consists of a fibrous cap [80]. This cap, situated on the surface of the plaque, serves as a protective layer separating the lipid core from the bloodstream. The fibrous cap is primarily composed of smooth muscle cells, which are specialized cells responsible for the contraction and relaxation of blood vessels, and various proteins present in the extracellular matrix [81]. In the early stages of atherosclerosis, macrophages eliminate atherogenic lipoproteins from the intima and produce

foam cells, which can help protect against plaque formation. If foam cells die, the remaining lipids contribute to an unstable necrotic core in the plaque, making it more vulnerable [37]. The accumulation of atherogenic lipoproteins in the intima can occur independently of foam cell participation, resulting in the development of a core rich in lipids within an atheromatous lesion [82]. The lipid-rich core, characterized by its avascular nature, low cellularity, and absence of supportive collagen, significantly undermines its stability. Additionally, the size of the lipid-rich core significantly impacts the overall stability of the plaque [83].

3.2.1.2.2 Cell death

This programmed cell death plays a crucial role in the progression of atherosclerosis disease. Additionally, although less common, there is also a certain occurrence of necrotic cell death in atherosclerosis, albeit to a lesser extent [84]. Necrosis is a form of cell death resulting from injury or inadequate blood supply, and it contributes to overall cellular damage and tissue inflammation observed in this condition. The interplay between apoptotic and necrotic cell death in atherosclerosis highlights the intricate and diverse nature of the disease process [85, 86]. The disintegration of foam cells and the reduction in smooth muscle cells can cause adverse effects, resulting in various harmful outcomes, ultimately leading to the formation of a plaque with a high concentration of lipids at its core [56, 87]. These cascading events can set off a chain reaction of complications within the arterial walls, paving the way for various health risks and complications. As foam cells disintegrate, their contents, primarily consist of cholesterol and fatty substances, are released into the surrounding tissues [8]. This release can further exacerbate the formation and progression of atherosclerotic plaques, which are the fatty deposits that build up within the arteries [88]. The accumulation of these lipids within the plaque results in the formation of a lipid-rich core characterized by a high concentration of cholesterol and other lipoproteins. Furthermore, the process of apoptosis, known as programmed cell death, plays a vital role in the increased activity of tissue factor and the heightened thrombogenicity observed within the lipid-rich core. Although cell death can outweigh cell proliferation, plaque growth can still happen by attracting new cells instead of local cell division [89, 90].

3.2.1.2.3 Plaque erosion

Plaque erosion is a phenomenon observed during the progression of atherosclerosis, wherein the fibrous cap encasing an atherosclerotic plaque erodes. This event renders the plaque unstable, increasing the risk of complications such as heart attacks or strokes. Plaque erosion is caused by a complex interplay of factors, including inflammation, endothelial dysfunction, and changes in the extracellular matrix composition [91, 92]. Inflammatory cells, like

macrophages and T lymphocytes, accumulate in the plaque, causing the release of cytokines and chemokines. These substances can activate endothelial cells and trigger apoptosis [53, 93]. The clinical significance of plaque erosion is noteworthy as it is associated with younger age and less severe atherosclerotic burden, indicating that it may represent a distinct phenotype of atherosclerosis [78, 94]. Diagnosing plaque erosion is challenging since it requires a histological examination of the coronary artery [95, 96]. However, non-invasive imaging techniques like optical coherence tomography and intravascular ultrasound can aid in detecting features suggestive of plaque erosion [96]. In conclusion, understanding the molecular and cellular processes behind plaque erosion is crucial for developing effective diagnostic and therapeutic approaches to reduce the morbidity and mortality related to this form of atherosclerotic lesion.

3.2.1.2.4 Plaque rupture

Plaque rupture is a critical event in the pathogenesis of atherosclerosis; this process involves the disruption of a vulnerable atherosclerotic plaque, leading to the exposure of highly thrombogenic material and subsequent formation of a blood clot. Plaque rupture is considered a major trigger for acute cardiovascular events, such as myocardial infarction and ischemic stroke. Multiple factors contribute to the vulnerability of atherosclerotic plaques, including inflammation, oxidative stress, and the presence of a necrotic core. Inflammatory cells, particularly macrophages and T lymphocytes, play a crucial role in plaque destabilization through the release of pro-inflammatory cytokines and enzymes that weaken the fibrous cap. Moreover, matrix metalloproteinases produced by activated macrophages contribute to the degradation of the extracellular matrix within the plaque, further compromising its structural integrity. Once a vulnerable plaque ruptures, it exposes the underlying thrombogenic material, including tissue factor, collagen, and lipid-rich debris. This triggers platelet activation and aggregation, leading to the formation of a thrombus that obstructs blood flow. The resulting ischemia and inflammation can cause irreversible damage to downstream tissues, leading to clinical manifestations of acute cardiovascular events.

3.2.2 Mouse models of atherosclerosis

Mouse models have played a crucial role in unraveling the underlying mechanisms and identifying potential therapeutic targets for atherosclerosis [23]. The different mouse models used in the study of atherosclerosis each have their strengths and limitations to advance our understanding of this ubiquitous cardiovascular disease [97]. Genetically modified mouse models have been extensively used to study specific genes and signaling pathways implicated in atherosclerosis development and progression [98]. *ApoE*^{-/-} and *Ldlr*^{-/-} mice are frequently

used models because they develop atherosclerotic lesions when they are fed a diet rich in high-fat and cholesterol [99]. These models mimic the hyperlipidemic conditions observed in humans and exhibit key features of human atherosclerosis, including lipid accumulation, inflammation, and plaque formation [100]. However, in mice with a genetic predisposition, the consumption of a diet rich in fats and cholesterol has been found to expedite the development of lesions and worsen the severity of the disease [101]. These diet-induced models enable the study of dietary factors, lipid metabolism, and their impact on atherosclerosis progression. Beyond genetic induced models, approaches have emerged to refine our understanding of atherosclerosis pathophysiology. For instance, bone marrow transplantation allows for the investigation of the contribution of hematopoietic cells to atherosclerotic plaque development [102]. By transplanting bone marrow from normal C57BL/6J mice or *Ldlr*^{-/-} mice into *Ldlr*^{-/-} recipients, the role of immune cells in disease initiation and progression can be discerned [103]. Mouse models, in particular, have been instrumental in studying the disease in a controlled environment and testing potential interventions. These mouse models are genetically engineered to carry specific genetic modifications, for example, cell-specific expression, some transgenic mouse lines are engineered to restrict the expression of a gene to specific cell types or tissues [104]. This cell-specific expression allows the investigation of gene function within a particular cellular context. By targeting a gene's expression to specific cell populations, we can gain insights into the gene's role in specific cell types, developmental processes, or disease mechanisms [105].

3.2.2.1 *ApoE*^{-/-} mouse model

ApoE^{-/-} mice have become a widely used animal model for studying atherosclerosis, a condition characterized by the build-up of plaque in the arteries [106]. This model is valuable for investigating the underlying mechanisms of atherosclerosis and developing potential therapeutic interventions [107, 108]. ApoE, a protein predominantly produced by the liver and macrophages, assumes a crucial function in the regulation of lipid metabolism and transport. It acts as a ligand for specific receptors involved in the uptake and clearance of cholesterol-rich lipoproteins, such as LDL particles [109, 110]. In the absence of functional ApoE, *ApoE*^{-/-} mice exhibit dysregulation in lipid homeostasis, leading to elevated levels of total cholesterol and VLDL cholesterol in their circulation [111]. The mice exhibit a diminished capacity to eliminate cholesterol from the bloodstream, leading to the accumulation of cholesterol within the walls of the arteries. Over time, this process leads to the formation of atherosclerotic plaques, which contain cholesterol, lipids, immune cells, and extracellular matrix components [112, 113]. *ApoE*^{-/-} mice serve as an experimental model to explore the impact of genetic and environmental elements on the advancement and course of atherosclerosis [114]. These mice provide a valuable tool for examining the role of specific genes, signalling pathways, and

cellular interactions in atherosclerotic lesion formation. It is possible to manipulate the genetic background of these mice or introduce additional genetic modifications to explore the influence of specific genes or pathways on atherosclerosis. In addition, the utilization of *ApoE*^{-/-} mice presents an opportunity to evaluate the effectiveness of prospective therapeutic approaches targeting atherosclerosis [107]. It is possible to test the effects of pharmacological agents, dietary interventions, or gene therapies on the progression or regression of atherosclerotic lesions in these mice. The utilization of this preclinical model enables the assessment of innovative therapeutic targets and the formulation of treatment approaches focused on diminishing plaque accumulation and averting cardiovascular complications linked to atherosclerosis [107, 115, 116].

3.2.2.2 *Ldlr*^{-/-} mouse model

The *Ldlr*^{-/-} mouse model is extensively employed in atherosclerosis research, which focuses on investigating a chronic inflammatory condition characterized by the accumulation of plaques rich in cholesterol within the arterial walls [115]. This mouse model is particularly valuable because it recapitulates many key features of human atherosclerosis and provides insights into disease development, progression, and potential therapeutic interventions. The *Ldlr*^{-/-} mouse model is created by genetically modifying mice to lack functional low-density lipoprotein receptors [117]. Low-density lipoprotein receptors are responsible for the uptake of LDL cholesterol from the bloodstream [118]. Familial hypercholesterolemia is a condition in humans characterized by elevated levels of LDL cholesterol and an increased risk of atherosclerosis. This condition arises from mutations occurring in the *Ldlr* gene [119]. *Ldlr*^{-/-} mice exhibit the formation of atherosclerotic lesions similar to those observed in humans with atherosclerosis when they are provided with a diet high in fat and cholesterol [120]. These lesions typically occur in the aortic root, aortic arch, and other major arteries. The combination of a diet-induced increase in cholesterol levels and the absence of LDL receptor-mediated clearance mechanisms results in the accumulation of cholesterol within the arterial wall, thereby initiating an inflammatory reaction [100, 108]. As an alternative model, similar to the *ApoE* KO model. The *Ldlr*^{-/-} mouse model is instrumental in evaluating potential therapeutic strategies for atherosclerosis [121]. It is possible to test the effectiveness of cholesterol-lowering drugs, anti-inflammatory agents, and novel interventions aimed at promoting plaque stability or regression [122].

3.3 Endocannabinoid system

The endocannabinoid system (ECS) influences cardiovascular disorders and other physiological and pathological conditions [123, 124]. The ECS is composed of endogenous

lipid mediators, referred to as endocannabinoids, and two primary cannabinoid receptors: CB1 and CB2 (Figure 5) [125, 126]. The endocannabinoids most extensively studied to date are N-arachidonylethanolamine (also known as anandamide) and 2-arachidonoyl glycerol, but ongoing research is expanding our understanding of this system [127, 128]. Fatty acid amide hydrolase and monoacylglycerol lipase are the primary enzymes responsible for the metabolism of endocannabinoids [129-131]. Apart from CB1 and CB2 receptors, the endocannabinoid system may involve other receptors such as GPR55, GPR3, GPR6, GPR12, and GPR18, which are all G-protein-coupled receptors [132, 133].

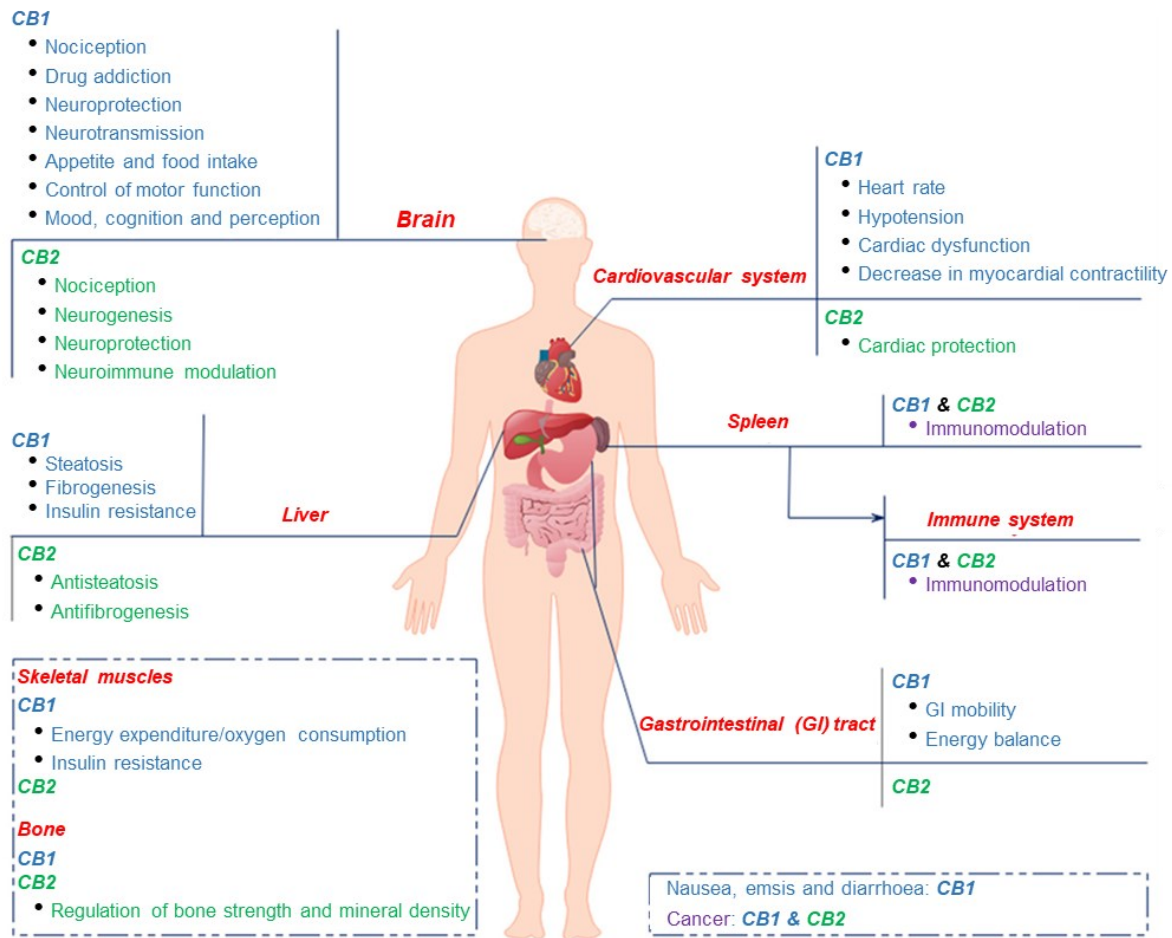


Figure 5: The human body's CB1 and CB2 receptors have distinct physiological roles and localized distributions.

CB1 receptors are primarily expressed in the brain, where they regulate a wide range of neurological activities. They also have a presence in peripheral tissues, although to a lesser extent, where they contribute to the modulation of local tissue functions. On the other hand, CB2 receptors are predominantly expressed in the immune system, particularly in organs like the spleen, where they play a significant role in immune modulation. Adapted from Dongchen An *et al* [134].

3.3.1 Cannabinoid CB1 receptor

The involvement of the endocannabinoid system, particularly CB1, in the development of atherosclerosis has been well-documented (Figure 6) [135]. The CB1 receptor is found in the central peripheral nervous system, nervous system, cardiac muscle, adipose tissue, liver, and

blood vessels [136]. Research findings indicate that the activation of CB1 in animal models of atherosclerosis contributes to the development of plaques and plaque instability. For instance, activating the CB1 receptor promotes adhesion molecules expression and upregulates monocyte adhesion [137]. Activation of CB1 impedes endothelial function while promoting proliferation and migration of vascular smooth muscle cells. These effects collectively contribute to the initiation and advancement of atherosclerosis [138]. On the other hand, inhibiting CB1 has demonstrated a beneficial effect by reducing the formation of atherosclerotic lesions. For example, treatment with CB1 antagonists rimonabant in the *Ldlr^{-/-}* reduced cholesterol levels and decreased plaque formation in animal models of atherosclerosis [139].

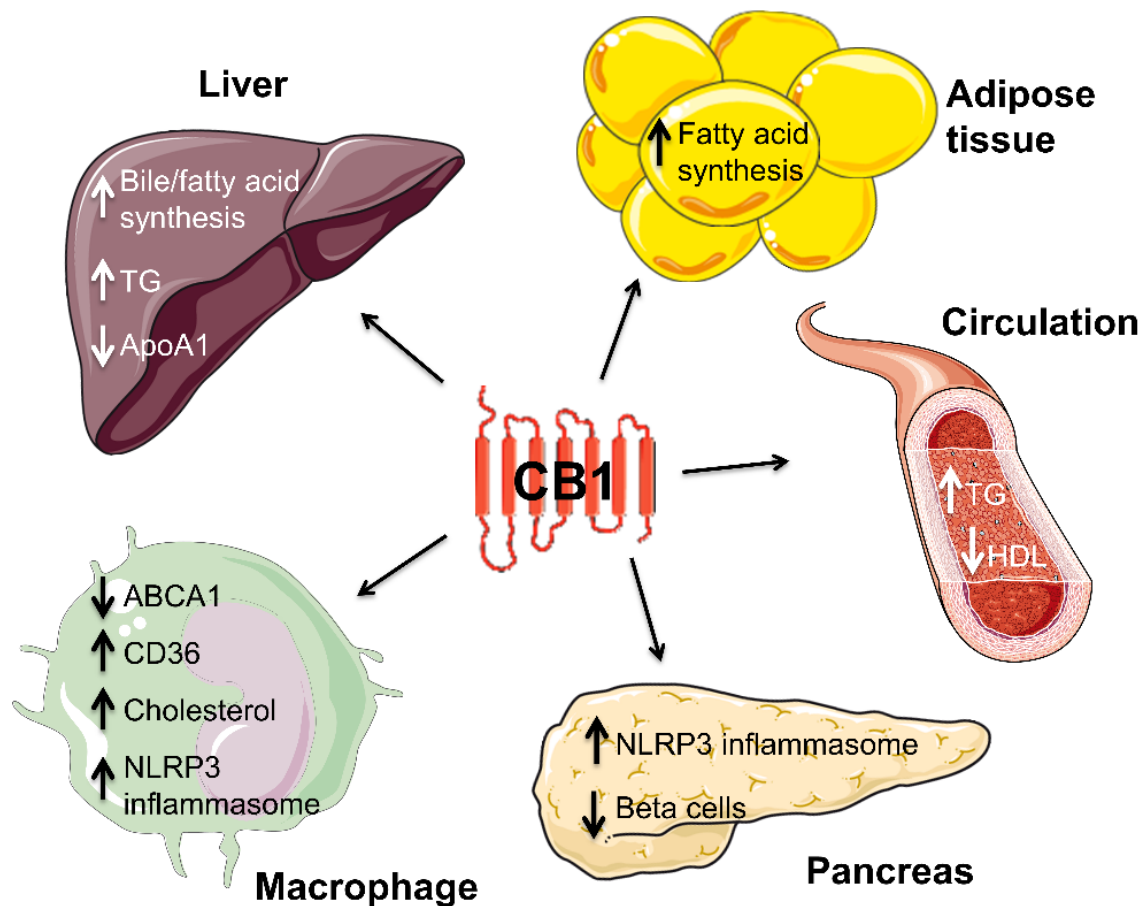


Figure 6: CB1 signaling: Peripheral metabolic effects.

CB1 signaling impacts multiple peripheral organs differently. In the liver, activating CB1 stimulates bile and fatty acid synthesis, causing triglyceride (TG) accumulation and reduced ApoA1 secretion. This lowers HDL and raises TG levels in the blood. It also promotes fatty acid synthesis in adipose tissue through CB1 activation. Stimulating CB1 receptors in macrophages enhances the uptake of CD36 while reducing ABCA1-mediated cholesterol efflux, resulting in the buildup of cholesterol within the cells. CB1 activation in infiltrating macrophages in the pancreas triggers NLRP3 inflammasome activation, resulting in β cell loss. CB1 signaling in podocytes in the kidney has been linked to glomerular and tubular dysfunction, as well as fibrosis. Adapted from Raquel Guillamat-Prats *et al* [3].

3.3.2 Pharmacological tools to activate or block CB1

Studies investigating the molecular signaling pathways and potential therapeutic benefit of CB1 modulation in atherosclerosis have mainly focused on the use of CB1 antagonists, which block CB1 activation [140, 141]. However, research has also explored the effects of CB1 agonists, which activate CB1, as potential treatments for atherosclerosis [142, 143]. There is ongoing development of selective CB1 modulators that aim to specifically target CB1 receptors in particular tissues, thus minimizing the unwanted side effects associated with non-selective CB1 modulation [134, 144, 145].

3.3.2.1 Globally active CB1 antagonists

AM281 is a small molecule that binds selectively and reversibly to the CB1 receptor, thereby blocking the action of endocannabinoids such as anandamide [146, 147]. AM281, a synthetic compound, exhibits a chemical structure resembling that of 2-arachidonoyl glycerol, a naturally occurring ligand for the CB1 receptor [148]. AM281 has been extensively employed in research to investigate the impact of CB1 inhibition on diverse physiological and pathological processes, such as memory deficit [149] systemic hemodynamics, and renal [150].

3.3.2.2 Peripherally active CB1 inhibitors

The development of CB1 inhibitors began in the early 2000s after the discovery of rimonabant, which was the first approved CB1 antagonist used as an anti-obesity medication. However, rimonabant was ultimately pulled from the market due to safety concerns, primarily arising from a heightened risk of psychiatric side effects [141, 151-154]. To tackle these safety concerns, the United States National Institute of Health and Jenrin Discovery collaborated in the development of antagonists with activity limited to the periphery, such as JD5037, a selective peripheral CB1 receptor inverse agonist [155]. Animal studies have demonstrated that CB1 antagonists exhibit promising effects in reducing food intake and body weight [156, 157].

3.3.2.3 CB1 activator ACEA

ACEA, which stands for arachidonyl-2'-chloroethylamide, is a synthetic agonist of the CB1 receptor (Figure 7) [1]. It has much higher and selective CB1 receptor binding affinity compared to endocannabinoids and was used as a research tool for studying the effects of CB1 activation on various physiological and pathological processes, including atherosclerosis [158]. When ACEA binds selectively and reversibly to the CB1 receptor, it activates downstream signaling pathways, involving an increase in p38 MAPK phosphorylation and a reduction in AMPK phosphorylation in ACEA-treated mice. [159]. ACEA, a synthetic

compound, shares a chemical structure resembling that of anandamide (Figure 7), a naturally occurring ligand for the CB1 receptor [134]. In animal models of atherosclerosis, the effects of ACEA treatment on plaque formation and progression have been complex and sometimes contradictory. Several studies have indicated that CB1 activation can aggravate atherosclerosis through mechanisms such as increased oxidative stress and inflammation, impairment of endothelial function, and promotion of lipid-rich plaque formation [137]. On the contrary, alternative studies have proposed that ACEA may exert a protective effect against neurological disease [160].

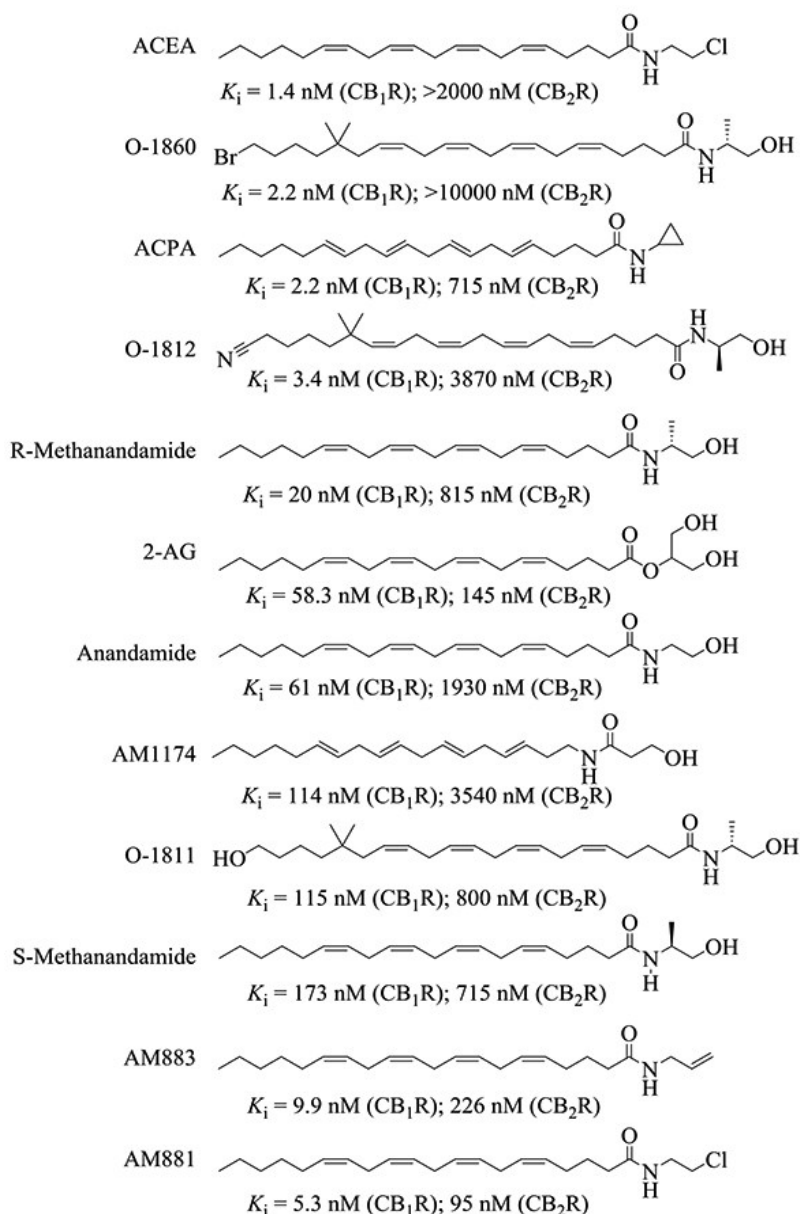


Figure 7: Representative long-chain endocannabinoids and their synthetic analogs.
Adapted from Yang JF *et al* [1].

3.4 Aim of the study

Atherosclerosis, a chronic inflammatory disease, stands as a primary contributor to morbidity and mortality on a global scale [161]. CB1 is involved in regulating immune responses and inflammation [47, 48]. Notably, myeloid cells, such as macrophages, have a significant impact on atherosclerosis development [162-164]. Previous research has indicated the involvement of CB1 in the progression of atherosclerosis [135, 165]. Nevertheless, a comprehensive understanding of the precise mechanisms connecting CB1 to this disease remains incomplete, and in particular, the specific *in vivo* role of macrophage CB1 in atherosclerosis has not been investigated so far [166-168]. Additionally, it is unclear if sex-specific differences exist in this context. Addressing these gaps in knowledge is crucial for identifying new therapeutic targets for effectively preventing and treating atherosclerosis. To address these knowledge gaps, the aim of this thesis was to investigate the involvement of CB1 in myeloid cells with a particular focus on macrophages and its impact on atherosclerosis progression in mouse models, including both males and females.

4. MATERIALS AND METHODS

4.1 Materials

4.1.1 Chemical and reagents

Table 2: Chemicals and reagents

Chemical /Reagents	Company
2-Methylbutane	Sigma-Aldrich Chemie GmbH, Munich, Germany
2-mercaptoethanol	Sigma-Aldrich Chemie GmbH, Munich, Germany
2-Propanol	Sigma-Aldrich Chemie GmbH, Munich, Germany
β -Estradiol	Sigma-Aldrich Chemie GmbH, Munich, Germany
ACEA	Tocris, Wiesbaden-Nordenstadt, Germany
Acetic acid (glacial) 100% anhydrous	Merck KGaA, Darmstadt, Germany
Acetone	Sigma-Aldrich Chemie GmbH, Munich, Germany
BSA \geq 98 %	Carl Roth GmbH + Co. KG, Karlsruhe, Germany
AM281	Tocris, Wiesbaden-Nordenstadt, Germany
Aniline blue	Sigma-Aldrich Chemie GmbH, Munich, Germany
AnnexinV	Invitrogen, Karlsruhe, Germany
AnnexinV binding buffer	Invitrogen, Karlsruhe, Germany
Antifade mounting medium	Vector Laboratories, Newark, United States
Antimycin A	Sigma-Aldrich Chemie GmbH, Munich, Germany
Biebrich Scarlet-Acid Fuchsin Solution	Sigma-Aldrich Chemie GmbH, Munich, Germany
Bouin`s solution	Sigma-Aldrich Chemie GmbH, Munich, Germany
Bradford 1x Dye Reagent	Bio-Rad, Hercules, USA
CFSE	Thermo Fisher Scientific, CA, USA
Citric Acid	Merck KGaA, Darmstadt, Germany
CountBright absolute counting beads	Thermo Fisher Scientific, CA, USA
Cycloheximide	Abcam, Berlin, Germany
Dihydrorhodamine 123	Cayman Chemical, Ann Arbor, USA
DMSO	Carl Roth GmbH + Co. KG, Karlsruhe, Germany
EDTA	Sigma-Aldrich Chemie GmbH, Munich, Germany
Embedding Medium Tissue-Tek OCT	Sakura Finetek, Torrance, USA
Eosin Y-solution	Sigma-Aldrich Chemie GmbH, Munich, Germany
Ethanol 99%	Klinikum der Universität München
Ethanol 99% (absolute)	VWR International, Radnor, USA

FCCP	Sigma-Aldrich Chemie GmbH, Munich, Germany
FeCl ₃	Sigma-Aldrich Chemie GmbH, Munich, Germany
Fetal Bovine Serum	Sigma-Aldrich Chemie GmbH, Munich, Germany
Halt™ Phosphatase Inhibitor Cocktail	Thermo Fisher Scientific, CA, USA
Halt™ Protease Inhibitor Cocktail, EDTA free (100x)	Thermo Fisher Scientific, CA, USA
Hanks Buffered Saline Solution (HBSS)	Sigma, Merck, Darmstadt, Germany
Hematoxylin solution according to Mayer	Sigma-Aldrich Chemie GmbH, Munich, Germany
HEPES solution 1 M	Sigma-Aldrich Chemie GmbH, Munich, Germany
Human Dil-Low Density Lipoprotein	Kalen Biomedical, Germantown, USA
Hydrochloric acid	Merck KGaA, Darmstadt, Germany
Immu Mount embedding medium	Thermo Fisher Scientific, CA, USA
Isopropanol	KMF Laborchemie, Lohmar, Germany
JD-5037	Hycultec GmbH, Beutelsbach, Germany
Kaiser's glycerol gelatine	Sigma-Aldrich Chemie GmbH, Munich, Germany
Ketamine	WDT eG, Garbsen, Germany
LPS	Sigma, Merck, Darmstadt, Germany
Mayer's hematoxylin solution	Sigma, Merck, Darmstadt, Germany
M-PERTM Mammalian Extraction Buffer	Thermo Fisher Scientific, CA, USA
Nile Red	Sigma-Aldrich Chemie GmbH, Munich, Germany
Oil Red O	Sigma-Aldrich Chemie GmbH, Munich, Germany
Oligomycin A	Sigma-Aldrich Chemie GmbH, Munich, Germany
Paraformaldehyde	Merck KgaA, Darmstadt, Germany
PBS (for cell culture)	gibco, Bleiswijk, Netherlands
PBS powder	Biochrom AG, Berlin, Germany
Penicillin-Streptomycin	Sigma-Aldrich Chemie GmbH, Munich, Germany
PeqGold Trifast	Peqlab Biotechnologie GmbH, Erlangen,
Permeabilization Buffer (10X)	Thermo Fisher Scientific, CA, USA
Phosphomolybdic acid hydrate	Sigma, Merck, Darmstadt, Germany
Phosphotungstic acid hydrate	Sigma, Merck, Darmstadt, Germany
Pifithrin-α	Cayman Chemical, Ann Arbor, USA
Potassium chloride	Sigma, Merck, Darmstadt, Germany
Propidium iodide	Invitrogen, Karlsruhe, Germany
Red blood cell Lysis/Fixation Solution (10x)	BioLegend, San Diego, USA

RLT Plus Buffer	Qiagen, Venlo, The Netherlands
RPMI-1640	gibco, Bleiswijk, Netherlands
QIAzol Lysis Reagent	Qiagen, Venlo, The Netherlands
Rotenon	Sigma-Aldrich Chemie GmbH, Munich, Germany
Roti-Histofix 4 %	Carl Roth GmbH + Co. KG, Karlsruhe, Germany
Seahorse XF 1.0 M glucose solution	Agilent, Santa Clara, USA
Seahorse XF 100 mM pyruvate solution	Agilent, Santa Clara, USA
Seahorse XF 200 mM glutamine solution	Agilent, Santa Clara, USA
Seahorse XF RPMI medium	Agilent, Santa Clara, USA
Sodium citrate tribasic dihydrate	Sigma-Aldrich Chemie GmbH, Munich, Germany
Sodium chloride 0.9%	B. Braun AG, Puchheim, Germany
Sodium chloride	Sigma, Merck, Darmstadt, Germany
TCL buffer 2x	Qiagen, Venlo, The Netherlands
Tissue-Tek O.C.T	Sakura Finetek Germany GmbH, Staufen,
TMB solution 1x	Thermo Fisher Scientific, CA, USA
Trypan blue dye	Bio-Rad, Hercules, USA
Tween 20	Sigma-Aldrich Chemie GmbH, Munich, Germany
Weigert's iron hematoxylin solution	Sigma-Aldrich Chemie GmbH, Munich, Germany
Xylazine	WDT eG, Garbsen, Germany
Xylene	Sigma-Aldrich Chemie GmbH, Munich, Germany

4.1.2 Buffers and solutions

Table 3: Buffers and solutions

Buffers and solutions	Composition
ACK lysis buffer	150 mM NH ₄ Cl, 10 mM KHCO ₃ , 0.1 mM Na ₂ EDTA, pH 7.4
Anesthesia	700 µl Ketamine (50 mg/ml), 500 µl Xylazine (20 mg/ml) with 4500 µl normal saline
Antigen retrieval buffer	1.4 mM citric acid, 5.74 mM sodium citrate tribasic dihydrate, 0.035 % (v/v) tween 20
Aortic digestion cocktail	10 mg/mL collagenaseIV, 20 U/mL DNase I in PBS
BSA-blocking buffer	1 % (w/v) albumin in PBS
Citrate buffer	630 mL ddH ₂ O, 12.6 mL solution A (2.101 g citric acid in 100 mL ddH ₂ O), 57.4 mL solution B (14.70 g sodium citrate in 500 mL ddH ₂ O), 320 µL Tween 20, pH 6.0.
ELISA reagent diluent	1.0 % BSA in PBS (pH 7.2-7.4)

ELISA substrate solution	1:1 mixture of Color Reagent A (H ₂ O ₂) and Color Reagent B (Tetramethylbenzidine)
ELISA wash solution	10 mM phosphate buffer pH 7.4, 150 mM NaCl, 0.05% Tween 20
ELISA stop solution	2 M H ₂ SO ₄ in ddH ₂ O
FACS buffer	0.5 % (w/v) albumin in PBS
ORO stock solution	0.5 % (w/v) ORO in 99 % 2-propanol
RPMI medium	RPMI1640 (10% FBS; 10% M-CSF; P/S)
PBS solution 1X	9.55g PBS Dulbeccos in 1L ddH ₂ O (pH 7.4)

4.1.3 Kits

Table 4: Kits

Kit	Company
AnnexinV/PI Apoptosis Detection Kit	BioLegend San Diego, USA
CFDA SE Cell Tracer Kit	Thermo Fisher Scientific, Eugene, USA
Cholesterol CHOP-PAP kit + Calibrator	Roche, Basel, Switzerland
ddPCR Supermix for Probes (No dUTP)	Bio-Rad, Hercules, USA
High Sensitivity RNA Analysis Kit	Agilent, Santa Clara, USA
Monocyte Isolation Kit mouse	Miltenyi Biotec, Bergisch Gladbach
Mouse IL1b DuoSet ELISA	R&D Systems, Inc., Minneapolis, USA
peqGOLD Total RNA kit	Peqlab Biotechnologie GmbH, Erlangen, Germany
PrimeScript RT Reagent Kit	Takara, Shiga, Japan
Probe qPCR master mix	Promega, Madison, USA
Qubit RNA High Sensitivity Assay Kits	Thermo Fisher Scientific, Eugene, USA
Qubit RNA IQ Assay Kits	Thermo Fisher Scientific, Eugene, USA
RNeasy Micro Kit	Qiagen, Venlo, The Netherlands

4.1.4 Primers

Table 5: Primers for qPCR analysis

Murine gene	5'-3' primer sequence or Assay ID
<i>Ccr1</i>	Mm00438260_s1
<i>Ccr5</i>	Fw AATATTTCTTGAAAGTATTTTTAGCCGT Rev TTAAAACTCTTTTGATTGAGAGTAAGCA Probe FAM-AGATGTTATG TCCAAGCATG CAGTTTCGGA-TAMRA

<i>Cd74</i>	Mm00658576_m1
<i>Chil3</i>	Fw GGA AGC CCT CCT AAG GAC AAA Rev GAA TGT CTT TCT CCA CAG ATT CTT Probe FAM-TGT TCT GGT GAA GGA AAT GCG TAA-TAMRA
<i>Cnr1</i>	Fw ATGCGAAGGGGTTCCCTC Rev ATGGTACGGAAGGTGGTATCT Probe FAM-TGGCACCTCTTTCTCAGTCACGTTGAGC-TAMRA
<i>Cnr1 (ddPCR)</i>	Fw ATGCGAAGGGGTTCCCTC Rev ATGGTACGGAAGGTGGTATCT Probe 5'6-FAM-TGGCACCTC/ZEN/TTTCTCAGTCACGTTGAGC-3IABkFQ
<i>Cx3cr1</i>	Mm02620111_s1
<i>Hprt</i>	Fw GACCGGTCCCGTCATGC Rev TCATAACCTGGTTCATCATCGC Probe VIC-ACCCGCAGTCCCAGCGTCGTG-TAMRA
<i>Hprt (ddPCR)</i>	Fw GACCGGTCCCGTCATGC Rev TCATAACCTGGTTCATCATCGC Probe 5HEX-ACCCGCAGT/ZEN/CCCAGCGTCGTG-3IABkFQ
<i>Ifng</i>	Mm01168134_m1
<i>Il1b</i>	Mm00434228_m1
<i>Il6</i>	Mm00446190_m1
<i>Il12a</i>	Mm00434165_m1
<i>Irf5</i>	Mm00496477_m1
<i>Mif</i>	Mm01611157_gH
<i>Ncor1</i>	Mm01333102_m1
<i>Ndufa6</i>	Mm01303455_g1
<i>Nos2</i>	Mm00440502_m1
<i>Tnf</i>	Mm00443258_m1

MWG-Biotech AG provided the self-designed primers and probes for qPCR, while Life Technologies supplied the TaqMan Gene Expression Arrays.

4.1.5 Antibodies

Table 6: Murine antibodies for flow cytometry

Antigen	Conjugation	Dilution	Reference	Provider
CCR1	PE	1:50	FAB5986P	R&D
CCR5	PE-Cy7	1:100	107017	Biolegend

CD3	FITC	1:500	555274	BD
CD11b	PB	1:500	101224	BioLegend
CD11b	APC	1:500	17-0112-82	invitrogen
CD11b	APC-Cy7	1:500	101225	Biolegend
CD11b	PerCP	1:500	101230	Biolegend
CD16/32	purified	1:1000	553142	BD
CD19	PE	1:500	12-0193-82	eBioscience
CD38	PE-Cy7	1:500	102717	Biolegend
CD45.2	APC	1:500	558702	BD
CD45.2	BV510	1:500	109837	Biolegend
CD45.2	FITC	1:500	553772	BD
CD80	PerCP/Cy5.5	1:200	104721	Biolegend
CD115	APC	1:500	17-115-282	eBioscience
F4/80	APC	1:500	123116	Biolegend
F4/80	PB	1:500	123123	Biolegend
Ki67	FITC	1:200	11-5698-82	eBioscience
Ly6C	BV510	1:500	128033	Biolegend
Ly6G	APC-Cy7	1:500	127623	Biolegend
Live/dead	Zombie NIR	1:400	423105	Biolegend
Mitotracker green	FITC	100nM	M7514	Invitrogen

Table 7: Antibodies used for immunohistochemistry

Antigen	Source	Dilution	Reference	Provider
CD68	Rat	1:400	MCA1957GA	Bio-Rad
Ki67	Rat	1:50	11-5698-82	eBioscience
Ly6G	Rat	1:100	551459	BD
NOS(pan)	Rabbit	1:100	2977	Cell Signaling
Phospho-p53	Rabbit	1:100	12571s	Cell Signaling

Table 8: Isotype controls for immunohistochemistry

Immunoglobulin	Reference	Provider
Normal rat IgG	6-001-A	RD system
Normal rabbit IgG	315-005-003	JIR
Rat IgG2a FITC	553929	BD

The working concentration of normal IgG for isotype control is similar to specific primary antibody.

Table 9: Secondary antibodies for immunohistochemistry

Antigen	Source	Conjugation	Dilution	Reference	Provider
anti-rat	donkey	Cy3	1:300	712-165-153	JIR
anti-rabbit	donkey	AF488	1:100	711-545-152	JIR

4.1.6 Enzymes

Table 10: Enzymes

Enzyme	Final concentration	Company
Collagenase I	0.45 U/ μ l	Worthington Biochemical Corp, Lakewood, USA
Collagenase IV	0.125 U/ μ l	Worthington Biochemical Corp, Lakewood, USA
Hyaluronuclease I	0.06 U/ μ l	Sigma-Aldrich Chemie GmbH, Munich, Germany
Deoxiribonuclease I	0.06 U/ μ l	Roche, Basel, Switzerland

4.1.7 Consumables

Table 11: Material

Material	Company
0.5 ml PD-Tips steril / RNase free	Brand, Wertheim, Germany
40 μ m cell strainer blue	BD Falcon, Eysins, Switzerland
70 μ m cell strainer white/grey	BD Falcon, Eysins, Switzerland
Cell culture flasks 75, 175cm ²	Corning, Taufkirchen, Germany
Centrifuge tubes 15, 50 ml	Corning, Taufkirchen, Germany
Cover glass 10 mm	VWR, Ismaning, Munich, Germany
Cover slips 24x60 mm	Menzel-gläser, Braunschweig, Germany
Cryomold embedding dish 10 x 10x 5 mm	Sakura Finetek, Torrance, USA
Cryotube, sterile, pointed, free-standing 1 ml, 2 ml	Corning, Taufkirchen, Germany
Disposable filtration system with 250ml bottle	Corning, Taufkirchen, Germany
Disposable filtration system with 500ml bottle	Corning, Taufkirchen, Germany
Disposable pipettes 5 to 25 ml	Corning, Taufkirchen, Germany
ELISA 96-well-plate	Brand, Wertheim, Germany
FACS tubes (5ml Polystyrene round bottom)	BD Falcon, Eysins, Switzerland

FACS tubes + blue cell strainer	BD Falcon, Eysins, Switzerland
Filter pipette tips	Starlab, Hamburg, Germany
PCR tubes	Nippon Genetics, Düren, Germany
Microcentrifuge tube 0.5 to 5 ml	Starlab, Hamburg, Germany
Microlance needles 23G	BD Falcon, Eysins, Switzerland
Microscope slides 25x75x1mm	Menzel-gläser, Braunschweig, Germany
Multiwell cell culture plates flat, sterile 6,12, 24 well	Corning, Taufkirchen, Germany
Pasteur pipettes, glass, 225mm	Brand, Wertheim, Germany
Pasteur pipettes, plastic, 2.5ml, 150mm	Brand, Wertheim, Germany
Petri dishes 100mm/20mm	Corning, Taufkirchen, Germany
qPCR clear seal	Nippon Genetics, Düren, Germany
qPCR 96 well plates	Nippon Genetics, Düren, Germany
Seahorse XFe24 FluxPak	Agilent, Santa Clara, USA
Sealing tape	Corning, Taufkirchen, Germany
Syringe sterile 1 to 10 ml	BD Falcon, Eysins, Switzerland
Tissue-tek	Sakura Finetek, Staufen, Germany

4.1.8 Equipment

Table 12: Equipment

Equipment	Company
Autoclave LTA 400	Zirbus technology GmbH, Bad Grund, Germany
Balance SE 203 LR	VWR International, Radnor, USA
Centrifuges Megafuge 1.0R	Heraeus, Hanau, Germany
Centrifuge 5418 R	Eppendorf AG, Hamburg, Germany
CO ₂ incubator CB 160	BINDER GmbH, Tuttlingen, Germany
Cryotome CM3050S	Leica Biosystems, Wetzlar, Germany
FACS Canto II flow cytometer	BD Bioscience, San Jose, USA
FACSAria III Cell Sorter	BD Bioscience, San Jose, USA
Hood HERAsafe	Heraeus, Hanau, Germany
Laboratory pH Meter 766	Knick GmbH, Berlin, Germany
LifeSep Magnetic Plate Holder 96F	Sigma-Aldrich Chemie GmbH, Munich, Germany
Leica DM6000 microscopes	Leica Biosystems, Wetzlar, Germany
Leica LMD7000 microscopes	Leica Biosystems, Wetzlar, Germany
Leica RM 2235 microtome	Leica Biosystems, Wetzlar, Germany

Leica CM 3050S cryostat	Leica Biosystems, Wetzlar, Germany
Nanodrop ND1000 Peqlab	VWR International, Radnor, USA
PCR Plate Spinners	VWR International, Radnor, USA
PCR Thermocycler Biometra Tpersonal	Biometra GmbH, Göttingen, Germany
QuantStudio 6 Real-Time PCR Systems	Thermo Fisher Scientific, Eugene, USA
TC20 Automated Cell Counter	Bio-Rad Laboratories GmbH, Feldkirchen, Germany
Tecan F200 PRO microplate reader	Tecan Group, Maennedorf, Switzerland
Thermomixer F1.5	Eppendorf AG, Hamburg, Germany
TissueLyser LT	Qiagen, Hilden, Germany
Vortex Mixer TX4	VELP Scientifica, Usmate, Italy
Water bath type 1004	Memmert WB14 (Memmert GmbH + Co. KG)
Water Purification System Milli-Q	Merck Millipore, Billerica, USA

4.1.9 Software

Table 13: Software

Software	Company
BD FACSDiva software	BD Bioscience, San Jose, USA
FlowJo v10.3	Tree Star, Inc., OR, USA
GraphPad Prism 9.00	GraphPad Software Inc, USA
LAS V4.3	Leica Biosystems, Wetzlar, Germany
Image J software	National Institutes of Health, USA
WAVE	Agilent, CA, USA
D&A 2.4 analysis	Thermo Fisher Scientific, CA, USA

4.2 Methods

4.2.1 Mouse model

To study the role of *Cnr1* in myeloid cells, the *Cnr1^{fllox/fllox}* mice [169] were crossbred with apolipoprotein E-deficient mice (*Apoe^{-/-}* mice, strain #002052, Jackson lab) background with transgenic mice bearing the lysozyme M promoter (*LysMCre*) for selective *Cre* expression in myeloid cells. By implementing this selective breeding approach, the targeted removal of *Cnr1* specifically in myeloid cells was successfully accomplished, leading to the production of mice possessing the intended deletion. With this genetic modification, targeted investigations into the role of *Cnr1* in this particular cell population can be conducted. Male and female mice, 8

weeks old, were categorized by their genotypes as follows: *Apoe*^{-/-}*LysMCre*^{+/-}, *Apoe*^{-/-}*Cnr1*^{flox/flox}, and *Apoe*^{-/-}*LysMCre*^{+/-}*Cnr1*^{flox/flox}. Mice were subjected to a western diet (WD; 0.2% cholesterol, Ssniff, TD88137) for durations of either 4 or 16 weeks [4]. In subsequent investigations, WD was administered to *Ldlr*^{-/-} mice for a duration of 4 weeks. Afterwards, the mice were partitioned into two sets. The initial set received JD5037 (3 mg/kg) via intraperitoneal injections once daily for a duration of 4 weeks. Meanwhile, the second group was given a vehicle mixture consisting of 10% DMSO, 40% PEG3000, 5% Tween-80, and 45% saline, administered over a period of four weeks. During this period, both groups consistently received the WD as their diet. The baseline organs were collected from 8-week-old mice, which were fed a standard chow diet, underwent organ phenotyping. Each mouse was housed individually in ventilated cages, with 4 to 6 mice per cage. They were kept in a carefully regulated environment that followed a 12-hour light-dark cycle. The temperature was maintained at 23°C, while the relative humidity was set at 60%. The mice had unrestricted access to food pellets and tap water. All animal experiments were approved by the local Ethics committee (District Government of Upper Bavaria; License Number: 55.2-1-54-2532-111-13 and 55.2-2532.Vet_02-18-114) and conducted in accordance with the institutional and national guidelines and following the ARRIVE guidelines.

4.2.2 Mouse dissection

At the end of each experiment, mice were anesthetized by intraperitoneal (i.p.) injection with ketamine (80 mg/kg) and xylazine (12 mg/kg) using a 1 mL insulin syringe with a 30 G needle. Unless described otherwise, blood was obtained via cardiac puncture using a 26 G microlance needle flushed with 0.5 M EDTA into an EDTA micro tube. For intermediate time points, blood samples were obtained via the tail vein. Flow cytometry and plasma analysis were performed on these samples to evaluate multiple parameters, such as cholesterol and triglyceride levels. In order to remove any remaining blood before organ harvest, 10 mL of phosphate-buffered saline (PBS) solution was used to perfuse the mice, followed by the collection of hearts, spleens, and femurs. The aortas were extracted from the aortic arch all the way down to the iliac bifurcation. When no particular directives were given, plasma was acquired by subjecting EDTA-anticoagulated blood to centrifugation at a speed of 3000xg for a duration of 10 minutes. This plasma was then utilized for cholesterol and triglyceride measurements, or preserved at -80 °C until further analysis. The heart tissues were conserved in Tissue-Tek and maintained at a temperature of -20 °C. In order to extract RNA, the organs were rapidly frozen using liquid nitrogen. For flow cytometry analysis, the organs were immersed in PBS and kept chilled on ice until they were prepared for subsequent procedures.

4.2.3 Plasma cholesterol and triglycerides measurement

Cholesterol levels in the plasma were assessed utilizing a colorimetric assay called CHOD-PAP (Roche). To prepare for analysis, the plasma samples underwent a dilution process of 1:9 in a 0.9% saline solution. In a similar manner, the evaluation of overall plasma triglyceride levels was measured employing a colorimetric assay (CPO-PAP, Roche) that required no dilution of the plasma samples. The calibration solution, containing the calibrator with a cholesterol concentration of 160 mg/dl and a triglycerides concentration of 130 mg/dl, was mixed with 3 mL of distilled water. To create the standard curve, the solution was diluted by serial dilutions in 0.9% saline. A precise volume of 5 μ L was transferred from each standard or the diluted plasma samples into a 96-well microtiter plate with a flat bottom and samples was measured in duplicates. Afterwards, the plates were treated with either CHOD-PAP CHOL reagent or CPO-PAP TG reagent, with a combined volume of 200 μ L. After incubating at room temperature for 30 minutes, the mixture was subjected to absorbance measurement at 450 nm using a Tecan Infinite F200 PRO microplate reader.

4.2.4 Plaque analysis in descending aorta

The descending aorta was surgically removed, carefully placed onto a slide, and then secured in position. The aorta with insect needles was subsequently fixed overnight at a temperature of 4°C using a 1% solution of paraformaldehyde (PFA). The following day, the aorta was cleaned from the adipose tissue. The tissue was subjected to Oil-red-O (ORO) staining by submerging it in a working solution of ORO at room temperature for a duration of 30 minutes. Afterward, the aortas underwent a thorough rinsing process using 60% isopropanol. To remove any undesired staining caused by non-specific binding of ORO from the endothelial surface. After a brief rinsing with tap water, the aortas were mounted in Kaiser's glycerol gelatin mounting media. Next, the lesions were examined under a DM6000B fluorescent microscope, and the LAS V4.3 software was employed to calculate the proportion of lesions in relation to the total surface area of the aorta.

4.2.5 Histology and immunofluorescence

For histology, mouse hearts were first isolated and perfused with PBS. The heart base including the valve level was collected by transverse sectioning and placed in a cryomold containing OCT. For freezing, the bottom part of the cryomold was exposed to 2-methylbutane, which was cooled by liquid nitrogen. Frozen blocks were stored in airtight closed bags at -20 °C until further processing. Using a Cryotome CM3050S, 5 μ m-thick serial sections were collected starting from the onset of the three aortic valves until they disappeared. Usually ten object slides containing eight serial sections were collected reflecting an area of 400 μ m. Half

of the sections were fixed in 4 % Roti-Histofix for 10 min and stored at RT, unfixed sections were kept at -20 °C. The arch region, was fixed overnight at a temperature of 4°C using a 1% solution of PFA. Afterward, the arch was carefully embedded in immunohistochemistry-grade paraffin and kept at room temperature.

4.2.5.1 ORO staining of aortic root

To evaluate the progression of lesion formation in the aortic root, cryosections of 5 µm thickness were utilized for ORO staining. Following a 5-minute rehydration period in PBS, the slides were air-dried for an additional 5 minutes. A freshly prepared ORO working solution was used to stain the lipids. To prepare the solution, 120 mL of the ORO stock solution were diluted by adding 80 mL of ddH₂O. After stirring for one hour, the mixture was filtered. The lipids were stained for 15 minutes using this solution. The slides underwent a brief rinse with flowing tap water, followed by the application of hematoxylin for nuclear counterstaining. Following the air-drying process, Immu-Mount was used to mount the slides. LAS V4.3 software was employed for lesion quantification, and the Leica DM6000B fluorescent microscope was utilized to capture images. Mean values were calculated based on eight serial sections stained with a 50 µm interval for each mouse heart.

4.2.5.2 Hematoxylin-eosin staining of arch

A microtome was employed to cut the arch into sections with a thickness of 5 µm. Arch lesion quantification was conducted by employing Hematoxylin-eosin (H&E) staining. The slides were subjected to a deparaffinization process involving a sequential treatment series comprising 2x xylene, followed by 100% ethanol, 95% ethanol, 70% ethanol, and 2x H₂O. Each treatment lasted for 2 minutes. The nuclei underwent a 5-minute exposure to Mayer's hematoxylin solution at room temperature. Subsequently, the slides were rinsed in running tap water for another 5 minutes. A staining process using Eosin Y-solution was then performed on the slides, lasting for 3 minutes. Subsequently, the slides underwent a dehydration process involving 95% ethanol, 100% ethanol, and xylene, with each step lasting for 2 minutes. After allowing the slides to dry naturally, they were then mounted using the antifade mounting medium. The Leica DM6000B fluorescent microscope was employed to capture the images, while the LAS V4.3 software was utilized for lesion size measurement. The lesion's size was assessed by computing the cumulative inner vessel area ratio. For each mouse, four sections were stained, with a 50 µm interval between each section. The average values were subsequently derived from these measurements.

4.2.5.3 Masson's trichrome stain

The frozen sections were washed with water and immersed in Bouin's solution at room temperature overnight. After cooling in tap water, the sections were thoroughly washed until the removal of the yellow color. The sections underwent staining using Weigert's iron hematoxylin solution for a duration of 5 minutes, after which they were rinsed for 5 minutes under running tap water. Afterward, the sections were stained using a solution of Biebrich scarlet acid fuchsin for a duration of 5 minutes, followed by rinsing with Milli-Q water. Next, the sections underwent treatment with a working solution of 1% of phosphotungstic/phosphomolybdic acid for a duration of 5 minutes. Subsequently, aniline blue solution was applied to the sections for an additional 5 minutes. Then, the sections were thoroughly rinsed in a 1% acetic acid solution for 1 minute, followed by dehydration using alcohol. Following that, the sections underwent a clearing process with xylene and were ultimately mounted using a resinous mounting medium.

4.2.5.4 Immunofluorescence staining

To perform immunohistochemistry analysis on the cryosections obtained from the aortic root, the following protocol was implemented. Initially, the sections were fixed by immersing them in pre-cooled acetone for 5 minutes. Then, the sections were subjected to rehydration in PBS through three consecutive 5-minute rinses. Following the aforementioned procedures, the sections were subjected to blocking by submerging them in a solution comprising 1% bovine serum albumin (BSA) in PBS (pH 7.4) for a duration of 30 minutes. Afterward, the sections were placed in an incubator at 4°C overnight, where they were exposed to specific antibodies targeting CD68, iNOS, Ki67, and Ly6G (Table 7). Prior to the incubation, the antibodies were appropriately diluted in the blocking solution. Corresponding isotype controls were utilized for the negative staining controls (Table 8). The sections underwent three consecutive washes of 5 minutes each with PBS. Afterward, the samples were placed in PBS at room temperature and incubated for 45 minutes with secondary antibodies. After conducting three consecutive 5-minute washes with PBS, the samples were subjected to nuclear counterstaining using Hoechst dye. Following this step, the sections were rinsed, sealed with Immu-Mount, and subsequently analyzed using either LAS V4.3 software or ImageJ software. The imaging was conducted utilizing a fluorescence microscope (DM6000B) linked to a monochrome digital camera (DFC365FX, Leica), equipped with Thunder technology to enhance computational image processing capabilities [4].

4.2.5.5 Macrophage co-staining with Nile Red

To examine the lipid content in plaque macrophages, 5 µm cryosections from the aortic root

underwent rehydration in PBS for a duration of 10 minutes, followed by blocking with a pH 7.4 solution containing 1% BSA in PBS for a period of 30 minutes. Overnight incubation at 4°C was performed with antibodies against CD68 (Table 7) diluted in blocking solution, while corresponding isotype controls were employed for negative staining. Following the incubation period, the sections underwent three consecutive 5-minute washes in PBS. Subsequently, the samples were positioned at room temperature and incubated for 45 minutes with secondary antibodies conjugated to anti-rat AF488 (Table 9). The necessary amount of antibodies was diluted in PBS. Following that, the sections were subjected to three rounds of PBS washing, each lasting 5 minutes. To visualize lipids, staining with Nile Red solution was performed, allowing it to incubate for 5 minutes. Distilled water was used for a 5-minute wash, followed by nuclear counterstaining with Hoechst dye. After 5 minutes washing with purified water, the samples were secured in place with Immu-Mount and analyzed utilizing either LAS V4.3 software or ImageJ software. The evaluation was performed utilizing a fluorescence microscope (DM6000B) that was linked to a monochrome digital camera equipped with Thunder technology [4].

4.2.5.6 TUNEL staining

In cryosections of the aortic root, TUNEL staining was carried out to evaluate macrophage apoptosis. This particular assay identifies and measures apoptosis by labeling DNA strand breaks. In order to accomplish this, the Roche in situ cell death detection kit was used. Initially, the sections underwent permeabilization by subjecting them to a 20-minute cooling step in a 0.1 M citrate buffer (pH 6). Afterwards, the sections underwent incubation with a newly prepared TUNEL reaction mixture, which consisted of a solution containing label and enzyme for 15 minutes in a dark and humidified chamber at 37 °C. To determine the percentage of TUNEL-positive macrophages, a calculation was conducted by calculating the number of TUNEL-positive cells per total number of plaque cells (stained with Hoechst). These counts were subsequently expressed as a fraction of the total macrophage count per plaque. Following this, the sections underwent thorough cleansing and were securely mounted using Immu-Mount. The sections were analyzed using either LAS V4.3 software or ImageJ software. Images were taken with a fluorescence microscope (DM6000B) connected to a monochrome digital camera (DFC365FX, Leica) equipped with Thunder technology.

4.2.6 *In situ* hybridization

To confirm the existence of CB1 in macrophages, a fluorescent *in situ* hybridization with a murine *Cnr1* probe (VB6-17606, Affymetrix) was performed. RNase-free slides treated with RNase ZAP, were employed for the collection of cryosections from the aortic root. During

every stage, stringent precautions were implemented to uphold RNase-free conditions, up to the post-hybridization procedure. The sections were treated with a 4% PFA solution at room temperature for 5 minutes. Afterward, the specimens underwent three rounds of PBS washing for 5 minutes each. Subsequent to this, the tissue slices were treated with proteinase K, previously warmed and diluted in PBS to achieve a concentration of 10 µg/ml. The treatment was performed at room temperature for a duration of 5 minutes. Next, sections were immersed in 100% ethanol for 1 minute to ensure fixation. Followed by three 10-minute washes with PBS. Afterwards, the sections were transferred into an RNase-free chamber. The ViewRNA™ Cell Plus Assay Kit by Invitrogen was used for the hybridization of the target probes. The sections were incubated at 40°C for 2 hours. To reach a concentration of 5 µg/ml, the hybridization probe was combined with the probe set diluent. Subsequently, the sections underwent three washes with wash buffer at room temperature, with each wash lasting 5 minutes. To enhance the signal, the sections were then subjected to signal amplification. The procedure involved placing them in the pre-amplifier mixture and allowing them to incubate at a temperature of 40°C for 30 minutes. Afterward, the sections underwent a washing step and were then placed in the amplifier mixture for an extra hour, maintaining a temperature of 40°C. After the washing process, the sections underwent a 1-hour incubation at 40°C, accompanied by the active label probe mix. Later, the sections were subjected to *in situ* hybridization, followed by subsequent rinsing and incubation with a blocking buffer. Afterwards, the specimens were stained using a CD68 antibody, along with secondary antibodies that were linked to anti-rat AF488. This was followed by Hoechst staining, performed according to the above described procedure. The segments were ultimately purified and secured using Immu-Mount. Following that, the specimens were examined using a fluorescence microscope (DM6000B) connected to a monochrome digital camera (DFC365FX, Leica) equipped with Thunder technology [4].

4.2.7 Laser capture microdissection (LCM)

Aortic root sections were prepared from male *Apoe^{-/-}LysMCre^{+/-}* and *Apoe^{-/-}LysMCre^{+/-}Cnr1^{flox/flox}* mice, which were collected after WD for 4 weeks. Each 8 to 10 sections, each measuring 10 µm in thickness were obtained per mouse heart. The POL FrameSlide from Leica Microsystems was utilized to collect these sections onto RNase-free membrane metal frame slides. Following deparaffinization in a sterile RNase free environment, the sections were dried. In order to achieve precise extraction of lesions, a combination of a laser microdissection system (CTR6000, Leica Microsystems) and a microscope (LMD7000, Leica Microsystems) was utilized. Subsequently, the obtained lesions were carefully transferred into the lysis buffer provided with the RNA isolation kit (PAXgene Tissue miRNA kit, PreAnalytix).

4.2.8 Monocyte adoptive transfer

A magnetic separation monocyte isolation kit (Miltenyi, 130-100-629) was used to extract monocytes from the bone marrow of two mouse strains: *Apoe^{-/-}LysMCre^{+/-}* and *Apoe^{-/-}LysMCre^{+/-}Cnr1^{flox/flox}*. Afterward, centrifugation was performed to obtain a dense cell pellet, which was then followed by aspiration to remove the supernatant. After incubating for 15 minutes at 37°C, the cells were reintroduced into pre-warmed PBS containing 10µM of carboxyfluorescein succinimidyl ester (CFSE). Following centrifugation, the cells underwent resuspension in pre-warmed medium and were subsequently incubated for a duration of 30 minutes prior to undergoing another round of washing. Cell counts were determined using the TC20 Automated Cell Counter, after which 2.5×10^6 cells were intravenously injected through the tail vein. Both the donor mice and the *Apoe^{-/-}* recipient mice were subjected to a WD for four weeks prior to the adoptive cell transfer procedure. After 48 hours, the aortas and hearts were collected after perfusion. Using fluorescence microscopy, the presence of CFSE+ monocytes within cryosections of the aortic root was assessed. Furthermore, the aortas were subjected to digestion using flow cytometry for further analysis detection of CFSE+ monocytes.

4.2.9 Flow cytometry

Flow cytometry was utilizing fluorescently-labeled antibodies ([Table 6](#)). Before adding specific antibodies, the cells were placed in a 50 µL fluorescence-activated cell sorting (FACS) buffer solution, supplemented with an anti-CD16/CD32 antibody to block unspecific binding to FC receptors. The incubation was carried out at room temperature for a period of 5 minutes. Afterwards, 50 µL of antibody master mix prepared in FACS buffer, was added into the solution. The samples were subsequently placed in the fridge and kept in darkness at a temperature of 4°C for a period of 30 minutes. After completing the washing procedure, the cells were subsequently suspended in 300 µL of FACS buffer. Prior to analysis utilizing a BD FACS Canto II flow cytometer and BD FACSDiva software. FlowJo v10.2 software was utilized to analyze the obtained data. Protein expression levels were assessed by determining the geometric mean fluorescence intensity (MFI), while total cell counts were obtained by measuring the acquisition volumes. The overall cell counts were determined by creating a standard curve using the CountBright absolute counting beads solution. This process involved conducting measurements at various time intervals and flow rates (low, medium, and high) using the BD FACS Canto II instrument. The calculation was facilitated by employing defined volumes for sample resuspension and acquisition at a specific flow rate and time.

4.2.9.1 Determination of myeloid and lymphoid cell subsets counts in blood and bone marrow

Flow cytometry was employed to assess the overall populations of myeloid and lymphoid cell subsets in blood and bone marrow. The femurs were used to obtain bone marrow cells, which were then transferred into a 1 mL pipette tip. And subsequently placed into a 2 mL tube. Next, the tube was subjected to centrifugation at 10,000 x g for a duration of 1 minute, and the resultant pellets were reconstituted using ammonium chloride potassium (ACK) buffer to induce erythrocyte lysis. Blood samples were subjected to the same ACK buffer treatment for a duration of 10 minutes at room temperature. Subsequently, the cell suspensions were subjected to a blocking procedure lasting 5 minutes, employing the Fc-CD16/CD32 antibody. Once the blocking step was completed, the cells were then incubated with the specified antibodies (Table 6) for 30 minutes at a temperature of 4°C. The objective of this staining procedure was to differentiate and recognize distinct subsets of myeloid and lymphoid cells. Following the application of singlet and CD45+ gating, the myeloid populations expressing CD11b were subsequently categorized as follows: CD115+Ly6G- cells were identified as monocytes, while CD115-Ly6G+ cells were recognized as neutrophils. These myeloid cell subsets were subjected to examination to determine the MFI of chemokine receptors CCR1, CCR5, and CXR2. Flow cytometry data was acquired utilizing a BD FACSCanto II flow cytometer and processed employing FlowJo v10.2 software.

4.2.9.2 Flow cytometric cell sorting

After performing red blood cell lysis and antibody staining procedures, a BD FACSAria III Cell Sorter was used to isolate CD19+ B cells, CD3+ T cells, CD115+ monocytes, and Ly6G+ neutrophils from blood samples of *Apoe*^{-/-} mice [4]. To prepare the sorted cells for further analysis using droplet digital PCR, the cells were initially preserved through deep freezing in 2x TCL buffer containing 1% beta-mercaptoethanol.

4.2.10 BMDMs were utilized in *in vitro* assays.

BMDMs were obtained from femur and tibia of mice aged of 8 weeks. The bones underwent meticulous detachment from the surrounding muscle tissue on ice. Careful dissection was performed on the femur and tibia using sterilized scissors to sever them at both ends. Afterward, the bones were replaced to a sterile tube equipped with a blue tip and subjected to centrifugation at 10,000 rpm (8600x g) for 1 minute at a temperature of 4 °C. In order to ensure complete mixing, the pellet was subsequently resuspended in 1 ml of sterile ACK buffer by employing gentle pipetting. The combined contents of the tube were then subjected to centrifugation at 1400 rpm (400x g) for 5 minutes at a temperature of 4 °C. After removing the

supernatant, the cells underwent a single wash using medium. Afterward, the combined BM cell pellet one mouse were suspended in a volume of 25 ml of cell culture medium. The medium consisted of RPMI-1640, 10% FCS, 1% penicillin (100 U/ml), streptomycin (100 µg/ml), and 10% filtered L-929 cell-conditioned medium containing M-CSF. The mouse cells were cultured in either 75 cm² cell culture bottles or divided into two sets of twelve-well plates, with 1 ml of medium added to each well. The cells were placed in a CO₂ incubator with a temperature of 37°C for cultivation. To ensure an optimal macrophage differentiation, the culture medium was renewed every 2–3 days. Experiments were conducted when BMDMs reached a confluence of over 75% after a period of 7-10 days. For immunostainings, sterile cover slips were placed in 24-well plates, and cells were seeded onto them. During specific experiments, different treatments were administered to BMDMs. These treatments included the following substances and concentrations: estradiol (10 µM), lipopolysaccharide (LPS; 10 ng/mL), CB1 agonist ACEA (1 µM), and CB1 antagonist AM281 (10 µM). In the experimental procedure involving the combination of LPS treatment and CB1 blockade, the administration of AM281 occurred 15 minutes before exposing the cells to LPS. To suppress p53 activity, the p53 inhibitor pifithrin-α (PFT-α; 25 µM) was added 5 minutes prior to stimulating the cells with ACEA or AM281 [4].

4.2.10.1 BMDM ROS production assay

The detection of reactive oxygen species (ROS) was carried out by treating BMDM with 2.5 µg/mL DHR123 for 20 minutes at 37°C. The experiment utilized RPMI 1640 medium, which included glutamine, supplemented with 0.1% BSA and 0.1 mM HEPES. To stop the reaction, ice-cold PBS was added. The cells are collected using a scraper and then subjected to centrifugation at 300 x g for 5 minutes at a temperature of 4°C. Afterward, the cells underwent a single wash using FACS buffer and were subsequently stained with antibodies to identify macrophages (CD11b+F4/80+). This staining process lasted for 15 minutes at a temperature of 4°C in the dark. To facilitate proper detection, the FACS staining panel was prepared without the FITC-conjugated antibody since DHR123 was measured in the FITC channel. Following FACS staining, a single wash with PBS was performed. Afterward, the cells were resuspended with 300 µL of FACS buffer. The FACSCanto II instrument was then used to promptly detect the cellular ROS levels as green fluorescent cells.

4.2.10.2 BMDM mitochondrial activity assay

Differentiated BMDM were collected and resuspended with a 1:1000 diluted solution of Zombie NIR™ dye. Following a 15-30 minutes incubation in the dark at room temperature, the cells underwent a single wash using 2 mL of FACS buffer. Subsequently, the cells were treated

with a combination of pre-warmed antibodies (CD11b+ F4/80+) and MitoTracker Green. Following the staining procedure, the cells underwent a meticulous wash with warm FACS buffer. Subsequently, they were centrifuged at 300xg for 5 minutes. The resulting supernatant was then discarded. Finally, the cells were reconstituted in 300 μ L of FACS buffer, and immediately used for flow cytometry analysis.

4.2.10.3 BMDM oxLDL uptaking assay

BMDM were rinsed once with warm PBS. Subsequently, BMDMs were subjected to a 30-minute incubation with 1 μ g/mL Dil-oxLDL in complete RPMI medium. Following the loading process, the cells underwent two additional washes using warm PBS. Next, a heated citrate buffer was added and allowed to incubate at a temperature of 37°C for 10 minutes. In order to achieve the best possible cell detachment, the solution was carefully pipetted up and down. Afterward, the cellular samples were collected into FACS tubes, and then 1 mL of FACS buffer was added. Afterward, the cells were thoroughly washed with 2 mL of FACS buffer. Following that, the cells were centrifuged and then resuspended in 300 μ L of FACS buffer. Finally, a FACS Canto-II was employed to assess the quantity of intracellular Dil-oxLDL in the PE channel.

4.2.10.4 BMDM proliferation rate assay

BMDM were rinsed once with warm PBS. Then, BMDMs were subjected to a 30-minute blocking step using Fc-blocking agents. Subsequently, anti-CD11b-APC and F4/80-PE antibodies were used to label BMDM for a duration of 30 minutes under dark conditions. Next, the cells were fixed by suspending them in 500 μ L of 4% Histofix at 4°C for 10-20 minutes in a dark environment. Then samples were subjected to a single rinse using 2 mL of FACS buffer. After centrifugation, the FACS buffer was discarded, and the cells were subsequently resuspended in permeabilization buffer diluted 1:10 with water. The cells were then incubated for 15 minutes. Finally, the cells were centrifuged again. Afterward, the cells underwent labeling with an anti-Ki67-FITC antibody at a temperature of 4°C for a duration of 30 minutes. Once the labeling was completed, the cells were subjected to two rounds of washing with permeabilization buffer. Afterward, they were immersed in 300 μ L of FACS buffer and analyzed using a BD FACS Canto II flow cytometer, utilizing the BD FACSDiva software [4].

4.2.10.5 BMDM apoptosis assay

BMDMs were treated with cycloheximide (10 μ M, ab120093, abcam) for a duration of 6 hours at a temperature of 37°C. The cells were subsequently stained using Annexin V-conjugated FITC and propidium iodide (PI) using the Apoptosis Detection Kit (eBioscience). The FACSCanto II instrument was utilized for flow cytometry analysis. To ensure accurate results,

unstained negative controls were included to account for background correction.

4.2.10.6 Murine IL1 β ELISA

IL1 β levels in BMDM supernatants were measured using the mouse IL1 β DuoSet® ELISA kit from R&D Systems, following the manufacturer's instructions. For preparation of a 96-well plate, 100 μ L of capture antibody was added, resulting in a final concentration of 4 μ g/mL. The plate was then incubated overnight at room temperature. Subsequently, the plate was washed three times with a washing buffer (0.05% Tween 20 in PBS, pH 7.2) and blocked with 300 μ L of blocking buffer (1% BSA in PBS, pH 7.2) for 1 hour at room temperature. Following the washing step, per well was added 100 μ L of either the supernatants or standard in reagent diluent. The standards utilized in this process were created using the recombinant mouse IL1 β standard provided in the kit. Serial dilutions were performed in a 2-fold manner, covering a concentration range of 15.6 pg/mL to 1000 pg/mL. Subsequently, the plate underwent incubation with both samples and standards for a duration of 2 hours at room temperature. Afterward, a washing procedure was carried out. In each well, a detection antibody was introduced, achieving a final concentration of 250 ng/mL. The mixture was then incubated for an additional 2 hours at room temperature. Following a meticulous washing process, Streptavidin-HRP was added, diluted at a ratio of 1:200. The plate was then incubated at room temperature for a duration of 20 minutes. Afterwards, the plate was washed and then subjected to 100 μ L of Tetramethylbenzidine (TMB) substrate solution (ThermoFisher Scientific) for an extra 20 minutes at room temperature. To stop the reaction, 25 μ L of stop solution (2N H₂SO₄) was added to each well. Following this, the optical density at 450 nm was measured using a Tecan Infinite F200 PRO microplate reader, with a reference wavelength of 550 nm. The sample values were then determined by interpolating within the standard curve. A fourth-order polynomial curve fitting mode was applied via nonlinear regression (GraphPad Prism 9).

4.2.10.7 BMDM p53 nuclear immunofluorescence staining

In order to identify the nuclear translocation of p53 in BMDM, sterile cover slips were placed into 24-well plates, and the BMDM were differentiated as describe above (section 4.2.10). Subsequently, the cells were exposed to ACEA, AM281, or a vehicle for 1 hour. Then, the cells were fixed using pre-cooled acetone for 5 minutes, followed by three rounds of rehydration in PBS for 5 minutes each. After immersing the sections in a PBS solution (pH 7.4) containing 1% BSA for 30 minutes, the samples were then placed in the refrigerator at 4°C for overnight incubation with a primary antibody that specifically targets phospho-p53. The blocking solution was used to dilute the primary antibody as required. As part of the experimental control, negative staining controls were conducted using corresponding

isotypes. The sections underwent a triple wash using PBS, with each wash lasting for 5 minutes. Subsequently, samples were exposed to anti-rabbit AF488 conjugated secondary antibodies for a duration of 45 minutes at room temperature. The sections underwent a washing process with PBS three times for a duration of 5 minutes each. Subsequently, nuclear counterstaining was carried out utilizing Hoechst. After final washing step, Immumount, a water-based mounting medium for samples with fluorescence, was used to mount them, and their examination was conducted using the DM6000B fluorescence microscope. A monochrome digital camera equipped with Thunder technology was linked to the microscope. The subsequent analysis of these images was performed using either the widely utilized LAS V4.3 software or ImageJ software, both specifically designed for image analysis tasks.

4.2.11 mRNA expression analysis

4.2.11.1 RNA isolation

Murine tissues or isolated cells were subjected to total RNA extraction. If immediate processing was not feasible, the samples were stored in a 2 mL microcentrifuge tube at -80 °C for preservation. For RNA extraction, 500 µL of peqGOLD TriFast was added and cells were lysed by up-and-down pipetting. For frozen tissue lysis, Qiagen TissueLyser steel beads, and 500 µL of peqGOLD TriFast was added. The tissues lysis process was carried out using a TissueLyser, wherein the mixture was subjected to tissue lysis for 2 minutes at a frequency of 50 Hz. After subjecting the lysates to centrifugation at maximum speed for 2 minutes, the samples were cautiously transferred to a new microcentrifuge tube. To facilitate RNA extraction, 100 µL of chloroform was added, and the tube was gently agitated for a duration of 30 seconds. After subjecting the sample to centrifugation at 12000 x g for 15 minutes at room temperature, the mixture underwent phase separation, dividing into three distinct layers. The lower phase appeared red and consisted of phenol-chloroform, which contained proteins. The interphase, which comprised the middle layer, contained the genomic DNA, while the upper phase, transparent in appearance, consisted of RNA and constituted the aqueous layer. To avoid genomic DNA contamination, a careful extraction process was employed to meticulously isolate the RNA, which was subsequently transferred to a new tube while ensuring no contact with the interphase. The peqGOLD Total RNA Kit from Peqlab Biotechnologie was employed for the RNA purification, in accordance with the manufacturer's guidelines. Afterward, an evaluation of the RNA's quantity and quality was performed using the Nanodrop 100 instrument.

4.2.11.2 Reverse transcription

The PrimeScript RT reagent kit (TaKaRa) was used to transcribe 1 µg of the extracted RNA into complementary DNA (cDNA), as indicated in [Table 14](#). The reverse transcription (RT)

reaction mix was pipetted as instructed.

Table 14: RT reaction mix

Reagent	Amount for 1 µg RNA
5x PrimeScript Buffer	2 µL
PrimeScript RT Enzyme mix I	0.5 µL
Oligo dt Primer (50 µM)	0.5 µL
Random6mers (100 µM)	2 µL
RNA	1 µg
Add with RNase-free H ₂ O	10 µL

The reverse transcription (RT) procedure utilized a PCR thermocycler, following the program outlined in [Table 15](#). Subsequently, the transcribed cDNA was diluted with RNase-free H₂O to achieve a concentration of 5 ng/mL.

Table 15: RT program

Temperature	Time
37 °C	15 min
85 °C	5 s
4 °C	∞

4.2.11.3 Quantitative real time polymerase chain reaction (qRT-PCR)

Gene expression variations across different sample groups were examined by conducting a quantitative real-time PCR analysis using the QuantStudio™ 6 Pro Real-Time PCR System, (ThermoFisher). The PCR reactions were carried out using the GoTaq Probe qPCR Master Mix (Promega) [4]. Amplification of the targeted genes was achieved by utilizing a combination of primers and probes. These primers and probes were either self-designed and acquired from MWG or pre-designed primer-probe mixes purchased from Life Technologies (refer to [Table 16](#) for further information).

Table 16: Primer-probe mix

Self-designed 4x primer-probe mix		Pre-designed 4x primer-probe mix	
Primer fwd (100µM)	4 µL	Primer-probe-Mix	0.5 µL
Primer rev (100µM)	4 µL	Nuclease-free H ₂ O	Ad 5 µL
Probe (100µM)	1 µL		
Nuclease-free H ₂ O	ad 250 µL		

After preparing the 4x primer-probe mix according to the specifications provided in [Table 16](#), the qPCR mix was then pipetted following the instructions outlined in [Table 17](#).

Table 17: qPCR reaction mix

Reagent	Amount
Master mix 2x	10 μ L
Primer-probe mix 4x	5 μ L
cDNA (5 ng/ μ L)	5 μ L
Total	20 μ L

Nuclease-free water was utilized as a negative control. Duplicate samples were meticulously pipetted onto a semi-skirted 96-well qPCR plate. The qPCR analysis was subsequently conducted using a QuantStudio 6 Pro system from Thermo Fisher Scientific. The qPCR FAST program, as outlined in [Table 18](#), was followed during the procedure.

Table 18: qPCR FAST program

Temperature	Time
95 °C	20 s
95 °C	1 s
60 °C	20 s

The analysis was conducted using D&A 2.4 analyze software. The endogenous control gene utilized for normalization was *Hypoxanthin-guanin-phosphoribosyltransferase (Hprt)*. The expression of the target gene was determined by normalizing it to the endogenous control, and the results were reported as fold change ($\Delta\Delta$ Ct method analysis). The fold change was computed using the following formulas:

$$dCt = Ct(\text{gene of interest}) - Ct(\text{endogenous control})$$

$$ddCt = dCt(\text{treated}) - \text{average } dCt(\text{untreated})$$

$$\text{fold change} = 2^{-ddCt}$$

4.2.11.4 Droplet digital PCR

The QX200 Droplet Digital PCR (ddPCR™) system (Bio-Rad) was utilized for the ddPCR procedure. To create the reaction mixture, the following components were combined: 2 \times ddPCR Mastermix (Integrated DNA Technologies) 20 \times primer and probes (with final concentrations of 900 nM and 250 nM, respectively), and the cDNA template in a total volume of 20 μ L. Subsequently, the ddPCR reaction mixture was transfected into the sample well of

an eight-channel disposable droplet generator cartridge (Bio-Rad) and 60 μ L of droplet generation oil (Bio-Rad) was added per channel. Then, the oil-containing cartridge was inserted into the droplet generator (Bio-Rad), and the resulting droplets were carefully gathered and transferred to a 96-well PCR plate [4]. The content in the 96-well PCR plate was amplified over 40 cycles. Following the amplification process, the plate was placed into the Bio-Rad droplet reader and the analysis was conducted using the QuantaSoft analysis software.

4.2.11.5 RNA-sequencing

Bulk RNA-sequencing was performed using the prime-seq protocol that can be found on protocols.io (dx.doi.org/10.17504/protocols.io.s9veh66) [170]. Briefly, BMDMs were lysed in 100 μ L of RLT+, 1% beta-mercaptoethanol and 50 μ L of lysate was used for RNA-sequencing. The samples were proteinase K and DNase I digested and then cDNA synthesis was performed using uniquely barcoded oligodT primers. Samples destined for the same library were pooled and pre-amplification was then performed using 11-14 cycles, depending on the initial input per library. The cDNA was quantified using the PicoGreen dsDNA assay kit (Thermo Fisher, P11496) and qualified using the Bioanalyzer HS DNA chip (Agilent, 5067-4626). Libraries were then constructed with the NEB Next Ultra II FS kit (E6177S, NEB) using the prime-seq specifications. The libraries were quantified and qualified using the HS DNA chip on the Bioanalyzer and sequenced on an Illumina HiSeq 1500 at an average depth of 12.7 million reads per sample.

Reads were demultiplexed using deML and then filtered, aligned to the mouse genome mm10 using STAR 2.5.2b with default settings. BAM files were indexed and filtered on MAPQ > 15 with SAMtools 1.3.1. Raw tag counts and RPKM (reads per kilo base per million mapped reads) values per gene were summed using HOMER2's analyzeRepeats.pl script with default settings and the -oadj or -rpkm options for raw counts and RPKM reporting, respectively. Datasets were filtered to select genes expressed in at least 10% of samples. Differential gene expression analysis was calculated by using DESeq2 (Version 1.37.4) Bioconductor package in R version 4.2.0 (2022-04-22) under Ubuntu 20.04.3 LTS system, based on the negative binomial distribution [171]. Size factors and dispersion of samples were estimated first, then Negative Binomial GLM fitting and Wald statistics calculation was performed by DESeq2. Differential expression genes were identified by criteria: adjusted P value < 0.10 and fold changes > 1.5, based on the calculation results of DESeq2. Gene ontology enrichment analysis was performed using the enrichplot (Version 1.17.2) Bioconductor package [172] with differential expression genes (only filtered by adjusted P value < 0.10). Heatmap was drawn by pheatmap package (Version 1.0.12). Volcano plot was drawn by ggplot2 package (Version

3.4.0). Cneplots and dotplots were drawn by enrichplot package (Version 1.17.2). The Gene set enrichment analysis (GSEA) was done on GSEA software v4.3.2 for Windows with M2 curated gene sets and M5 ontology gene sets from mouse collections and C2 gene sets from human collections [173, 174]. The permutation type was gene_set. The significant pathways were chosen by following criteria: normalized enrichment score (NES) < -1 or > 1, false discovery rate (FDR) < 25% and nominal P value < 0.05.

4.2.12 Phospho kinase array

BMDMs obtained from four donor mice underwent ACEA treatment for 60 minutes [4]. Following that, the samples were rinsed once with ice-cold PBS and subsequently lysed on ice for 15 minutes. The M-PER Mammalian Extraction Buffer was employed for the lysis process. Thermo Scientific's Halt Phosphatase Inhibitor and EDTA-free Halt Protease Inhibitor Cocktail, diluted at a 1:100 ratio, were added to the buffer to enhance its performance. After subjecting the lysates to centrifugation at 4°C and 16000 × g for 15 minutes, the protein concentration was determined using the Pierce™ Coomassie Plus (Bradford) Assay, according to the manufacturer's instructions. The samples were shipped to our collaborator Emiel Van der Vorst's lab for analysis. The PamChip® peptide Ser/Thr Kinase assay microarray systems, developed by PamGene International, were employed to investigate the Serine-Threonine kinases (STKs) on the PamStation®12 technology. The STK-PamChip® array includes a comprehensive set of 144 unique phosphorylation sites, ensuring in-depth analysis. In order to identify phosphorylated Ser/Thr residues, the array underwent treatment with a combination containing 1.0 µg of protein, 400 µM adenosine triphosphate (ATP), and a blend of antibodies. The intensity of each spot was measured and quantified using BioNavigator software version 6.3, which was developed by PamGene International. To account for the local background, necessary adjustments were implemented. The kinases were prioritized by employing the functional scoring method called Upstream Kinase Analysis (PamGene). The approach utilized in this method incorporated specificity scores derived from peptides associated with a particular kinase, sourced from six databases. These specificity scores were then combined with sensitivity scores obtained through treatment-control comparisons. The obtained rankings were employed to assess the relative importance of different kinases. The heatmap exhibits kinases with a median final score exceeding 1.2. Furthermore, the p-values have been adjusted for multiple comparisons using the False Discovery Rate (FDR) technique [4]. For further analysis, kinases that met the criteria of having a median final score above 1.2 and an adjusted p-value below 0.05 were selected after conducting differential expression analysis. Following this, pathway enrichment analysis was performed using the ReactomePA package in R [172]. A network plot was generated by

utilizing the Enrichplot R package (version 1.4.0) (DOI: 10.18129/B9.bioc.enrichplot) in order to visually represent the complexities of the intricate biological relationships among these kinases and their associations with numerous annotation categories. The network plot offers a holistic visual representation of the intricate interconnections and relationships present in the biological system.

4.2.13 Extracellular Flux Analysis

The XFe24 analyzer was utilized to examine the metabolic features and assess the mitochondrial performance of mouse BMDMs. By incorporating pH and oxygen sensors into this analytical device, it is possible to measure and quantify two crucial parameters: the extracellular acidification rate (ECAR), which gauges the rate of acidity increase outside the cells, and the oxygen consumption rate (OCR), which quantifies the rate at which cells utilize oxygen. This technique enables the measurement of glycolysis and mitochondrial oxidative metabolism levels. The Seahorse Cell Mito Stress Test (Agilent) was utilized for the evaluation of cellular respiration, with specific modifications being made to the original manufacturer's protocol. BMDM cells underwent a 7-day culture period to induce differentiation. Afterwards, the cells were subjected to different treatments: CB1 agonist ACEA (1 μ M), CB1 antagonist (AM281, 10 μ M), LPS (10 ng/mL), or a vehicle. Following the treatments, 4×10^5 cells were transferred to a 24-well Seahorse plate and incubated for 48 hours. For optimal assay preparation, the sensor cartridge was hydrated at least one day in advance by adding 200 μ L of the calibrant solution in per well of the utility plate. Next, the cartridge was incubated at 37 °C without CO₂. After overnight incubation, 50 mL of XF base medium at a temperature of 37 °C was used to prepare the assay medium. To achieve a concentration of 2 mM, 500 μ L of a 200 mM L-glutamine solution was added. Subsequently, the cell culture medium was replaced by Seahorse medium (XF RPMI medium, pH 7.4) to incubate. The cells were incubation at 37°C without CO₂ for a duration of 60 minutes before transferring them to the Seahorse Analyzer XFe24. The injection compounds include: mixtures should be prepared with the following concentrations: 1 μ M of oligomycin, 1 μ M of fluoro-carbonyl cyanide phenylhydrazone, 1 μ M of antimycin A, and 1 μ mol/L of rotenone.

4.2.14 Statistical analysis

Statistical analyses were performed utilizing GraphPad Prism version 9.0 (GraphPad Software, Inc.). The normality of the data was assessed using the D'Agostino-Pearson omnibus normality test, and outliers were detected using ROUT = 1. To compare two groups of data with a normal distribution and ensure that the variances were not significantly different, a Student's unpaired t-test was conducted. For more than two groups, the data underwent

comparison through either one-way or two-way analysis of variance (ANOVA). Subsequently, post hoc analysis was conducted to tackle multiple comparisons, employing the Sidak, Tukey, or Dunnett test. In addition, we conducted planned comparisons utilizing the Fisher Least Significant Difference test. The reported results include the mean values and their standard error of the mean. A $P < 0.05$ was considered as significant.

5. RESULTS

5.1 Reduced formation of early and advanced atherosclerotic plaques through inactivation of myeloid CB1

5.1.1 CB1 expression and mouse model establishment

Droplet digital PCR was employed to initially confirm the presence of the *Cnr1* gene, which encodes the CB1 receptor, in sorted murine blood leukocytes. Among these leukocytes, lymphocytes displayed the highest mRNA expression levels, while monocytes and neutrophils exhibited slightly lower levels (Figure 8A). Heightened expression levels of *Cnr1* were observed in BMDMs obtained from *Apoe*^{-/-} mice subsequent to inflammatory stimulation caused by LPS alone or LPS combined with oxLDL, in line with prior discoveries in macrophage cell lines (Figure 8B) [168, 175].

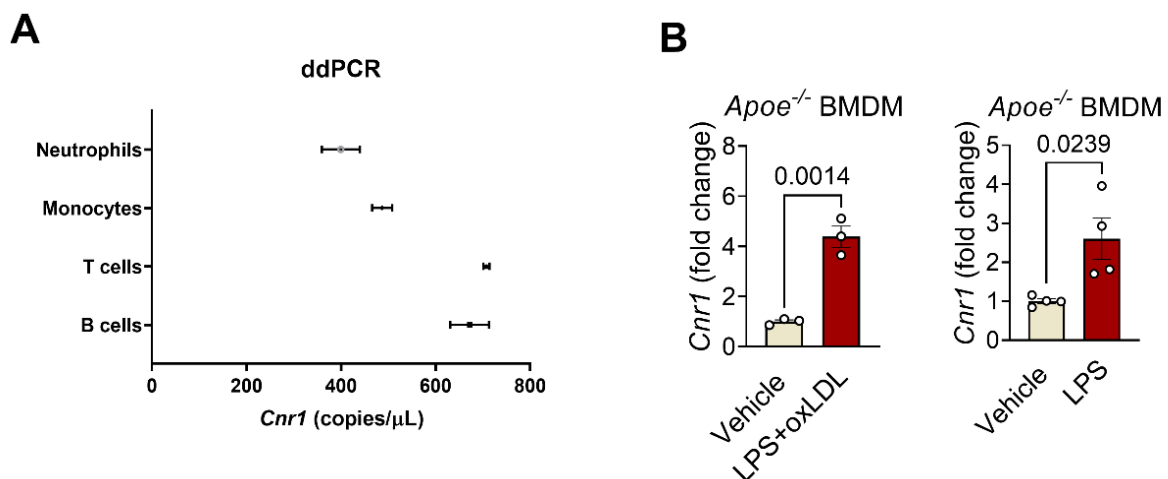


Figure 8: The expression of murine *Cnr1* in various myeloid cell subsets and BMDMs [4].

(A) Sorted myeloid cell subsets from murine blood were analyzed using ddPCR to assess *Cnr1* expression (n=3 mice). (B) The qPCR analysis was conducted on BMDMs collected from male *Apoe*^{-/-} mice (n=3-4 mice). The BMDMs underwent various treatments, such as vehicle, LPS administered at a concentration of 10 ng/mL, or oxLDL administered at a concentration of 1 μ g/mL. The data were displayed as mean \pm standard error of the mean (s.e.m.), and each dot on the graph represented an individual mouse. To calculate the P-value, a two-sided unpaired Student's t-test was utilized.

To study atherosclerosis, *Cnr1*^{flox/flox} mice were bred with *LysMCre*^{+/-} mice on an *Apoe*^{-/-} background. Aortic root sections from control mice (*Apoe*^{-/-}*LysMCre*^{+/-}) were examined to confirm the expression of *Cnr1* in plaque macrophages, which were identified using CD68+ immunofluorescence staining. This verification process involved the utilization of in situ hybridization. In contrast, the *Cnr1* signal was not detectable in plaque macrophages of mice with myeloid *Cnr1* deficiency (*Apoe*^{-/-}*LysMCre*^{+/-}*Cnr1*^{flox/flox}; Figure 9A), confirming an efficient knockdown. Additionally, the qPCR analysis of cultured BMDMs from *Apoe*^{-/-}*LysMCre*^{+/-}*Cnr1*^{flox/flox} mice showed a significant 50% decrease in *Cnr1* expression compared to the *Apoe*^{-/-}

$^{-}LysMCre^{+/-}$ control samples (Figure 9B). To ensure the preservation of *LysM* expression, heterozygous *LysMCre* mice were consistently employed throughout the entire study, thereby preventing the complete disruption caused by the insertion of Cre into the coding sequence of the lysozyme M gene [176].

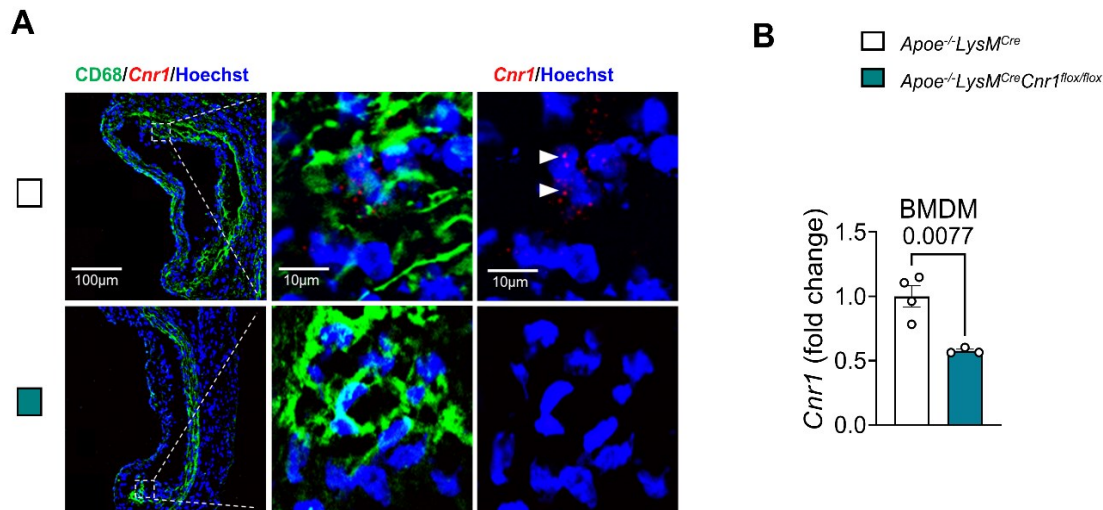


Figure 9: The expression of murine *Cnr1* in atherosclerotic plaques and BMDMs [4]. (A) Aortic root sections from *Apoe*^{-/-} mice, which were exposed to a 4-week WD, underwent fluorescence in situ hybridization. The sections were subjected to co-immunostaining for *Cnr1*, wherein CD68 was labeled in green and Hoechst33342 was used for blue nuclei staining. On the left, the scale bar was 100 μm, on the right 10 μm. (B) The expression of *Cnr1* in BMDMs from *Apoe*^{-/-}*LysMCre*^{+/-} mice and *Apoe*^{-/-}*LysMCre*^{+/-}*Cnr1*^{flox/flox} mice was analyzed using RT-PCR. The obtained results were compared, and a total of 3-4 mice were included in the analysis. The data were displayed as mean ± s.e.m., and each dot on the graph represented an individual mouse. To calculate the P-value, a two-sided unpaired Student's t-test was utilized.

5.1.2 The impact of CB1 receptor deficiency in myeloid cells on atherosclerosis progression

Following the establishment of the mouse model, the potential impact of CB1 depletion in myeloid cells on the initial phases of atherosclerotic plaque development was investigated. To ensure the atherosclerosis phenotype was not influenced by the *Cnr1*^{flox/flox} or *LysM*^{Cre} transgene insertion, two distinct control groups were initially employed. Throughout all subsequent experiments of the study, the control group consistently comprised *Apoe*^{-/-}*LysMCre*^{+/-} mice, ensuring that any potential influence of the *LysM*^{Cre} transgene insertion on the atherosclerosis phenotype was effectively eliminated. Male mice with myeloid *Cnr1* deficiency were subjected to a WD for four weeks. The mice exhibited reduced plaque sizes in the aortic roots when compared to the control groups, *Apoe*^{-/-}*Cnr1*^{flox/flox} or *Apoe*^{-/-}*LysMCre*^{+/-} (Figure 10A-D).

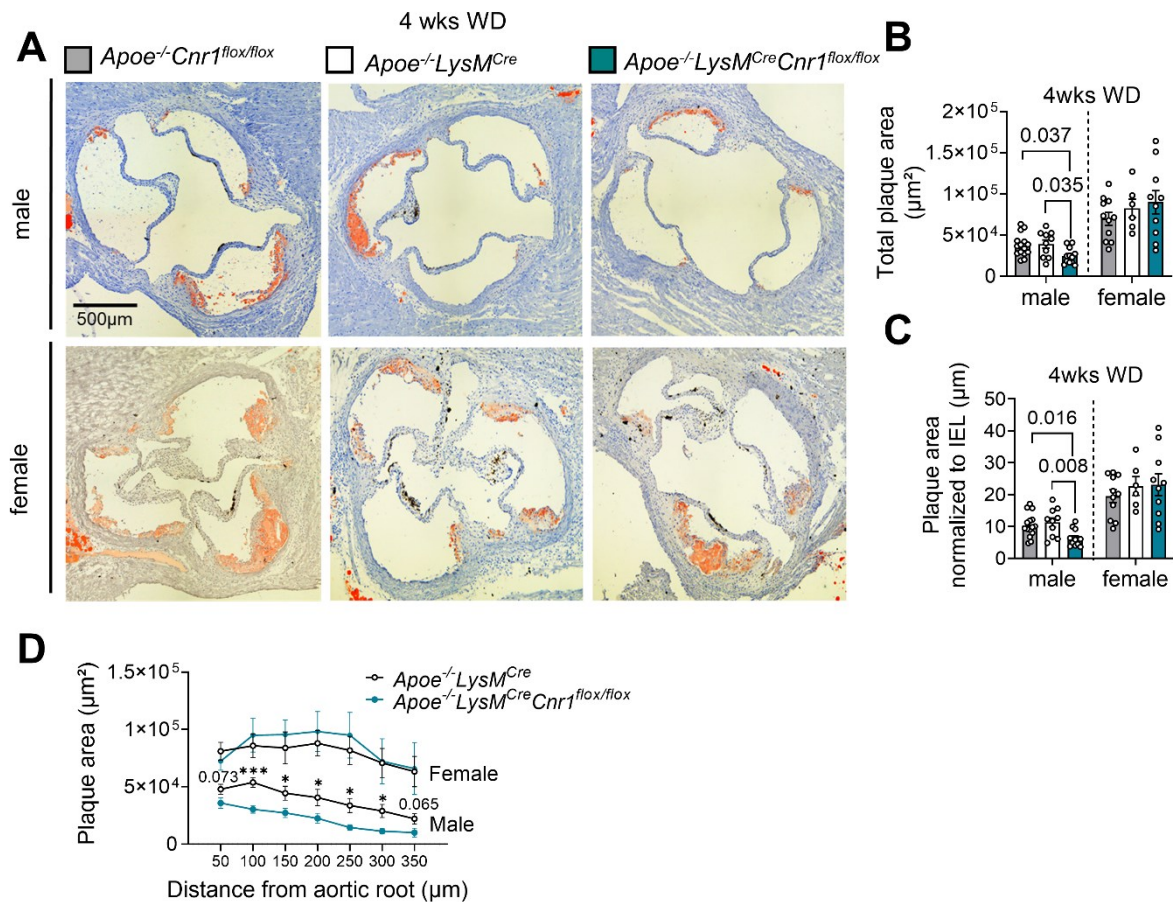


Figure 10: The influence of deficient CB1 receptors in myeloid cells on the development of atherosclerosis [4].

(A) Male and female mice lacking the *Apoe* gene (*Apoe*^{-/-}) and carrying either the *Cnr1*^{flox/flox}, *LysMCre*^{+/-}, or *LysMCre*^{+/-}*Cnr1*^{flox/flox} genotype were fed a WD for a duration of 4 weeks. Following the dietary intervention, the aortic roots of these mice were analyzed using ORO staining. The scale bar used in the analysis was 500 µm. (B) Measurement of the absolute size of the lesion area (n=6–15 mice) or (C) normalized to intimal endothelial layer (IEL) (n=6–15 mice). (D) Male (n=12–15 mice) and female (n=6–11 mice) *Apoe*^{-/-}*LysMCre*^{+/-} and *Apoe*^{-/-}*LysMCre*^{+/-}*Cnr1*^{flox/flox} mice were subjected to a WD for a duration of four weeks. Following the WD period, the plaque area per section of the aortic root was measured and analyzed. Each dot represents one biologically independent mouse sample and all data are expressed as mean ± s.e.m. Two-sided unpaired Student's t-test (D), one-way ANOVA followed by a post-hoc Tukey multi-comparison test (B-C) were used to determine the significant differences. Male and female were analyzed independently.

Contrarily, the absence of myeloid *Cnr1* in female mice did not result in any noticeable effect on early atherogenesis. Although a reduction in arterial macrophage buildup was linked to smaller plaque size in males, no comparable result was observed in females. Nevertheless, a decrease in the presence of inflammatory iNOS+CD68+ macrophages was observed in plaques of both males and females (Figure 11A-C). Notably, the deficiency of myeloid *Cnr1* did not influence the numbers of plaque neutrophils (Figure 11D-E).

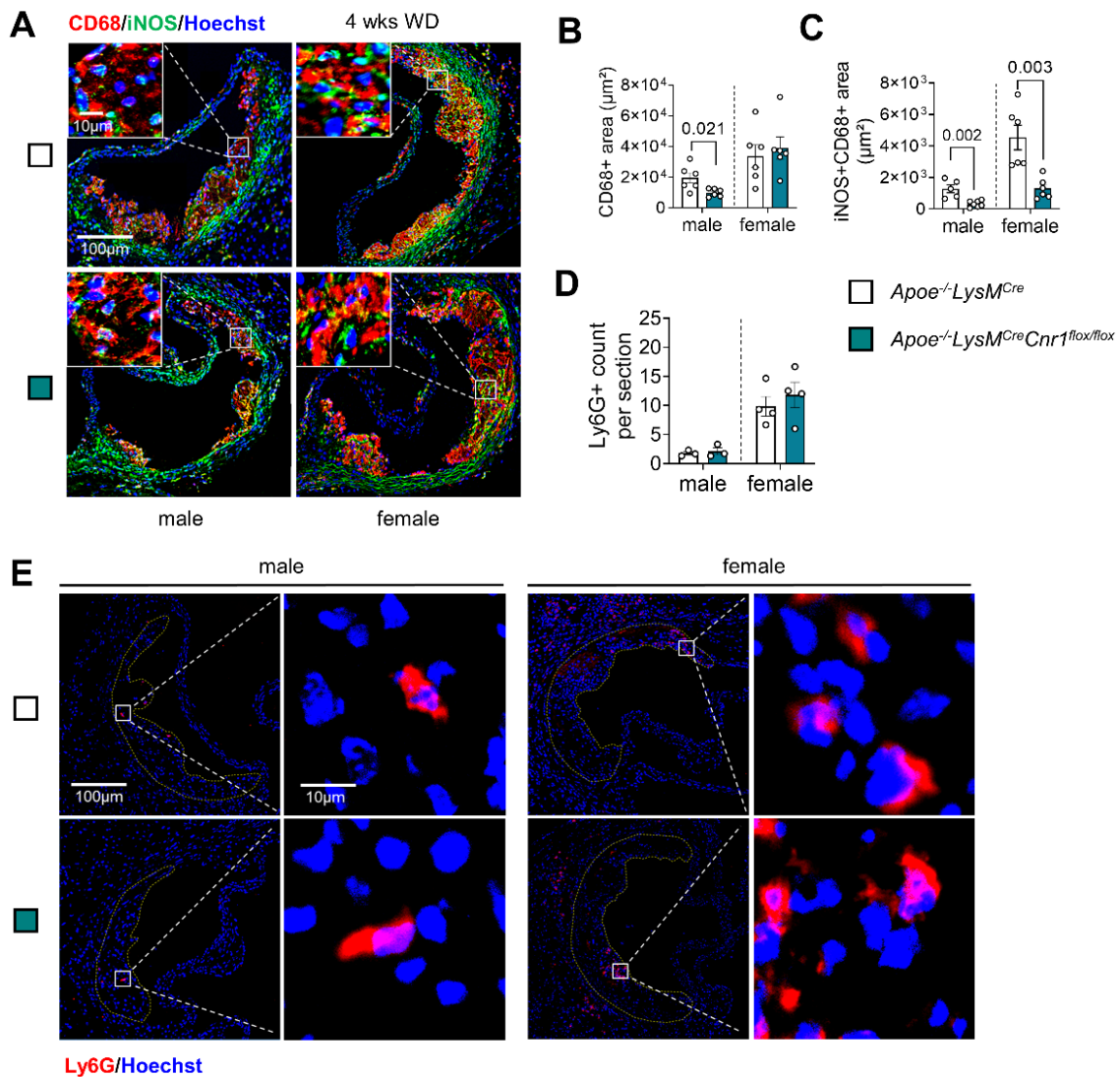


Figure 11: The influence of deficient CB1 receptors in myeloid cells on the advancement of arterial plaque [4].

(A) After a four-week period of consuming a WD, the aortic root lesions in male and female mice of the *Apoe*^{-/-}*LysM*^{Cre}^{+/+} and *Apoe*^{-/-}*LysM*^{Cre}^{+/+}*Cnr1*^{flox/flox} strains were examined by means of double immunostaining for iNOS (green) and CD68 (red). Additionally, the nuclei were counterstained with Hoechst 33342 (blue). The relative size of the lesions was indicated by the scale bar, with 10 μm (top) and 100 μm (bottom) being represented. (B) The numbers of lesional macrophages (n=6 mice) and (C) inflammatory macrophages (n=5–6 mice) were determined by conducting combined positive CD68 and iNOS staining. (D–E) Immunostaining was conducted on the aortic root sections of male and female mice, specifically using the *Apoe*^{-/-}*LysM*^{Cre}^{+/+} and *Apoe*^{-/-}*LysM*^{Cre}^{+/+}*Cnr1*^{flox/flox} strains (n=3–4 mice). Neutrophils were stained with an antibody against Ly6G, visualized in red. Following a 4-week period of consuming a WD, the cell nuclei were counterstained using Hoechst 33342, indicated by a blue color. The scale bar represents a size of 100 μm (left) and 10 μm (right). Each dot represents one biologically independent mouse sample and all data are expressed as mean \pm s.e.m. Two-sided unpaired Student's t-test was used to determine the significant differences. Male and female were analyzed independently.

5.1.3 The impact of CB1 deficiency in myeloid cells on plaque progression

Male mice with the *Apoe*^{-/-}*LysM*^{Cre}^{+/+}*Cnr1*^{flox/flox} genotype exhibited a smaller aortic root plaque

size after being fed a WD for 16 weeks in comparison to *Apoe*^{-/-}*LysMCre*^{+/-} control mice. This observed phenotype was also evident in the descending aortas of the male *Apoe*^{-/-}*LysMCre*^{+/-}*Cnr1*^{flox/flox} mice (Figure 12A-D).

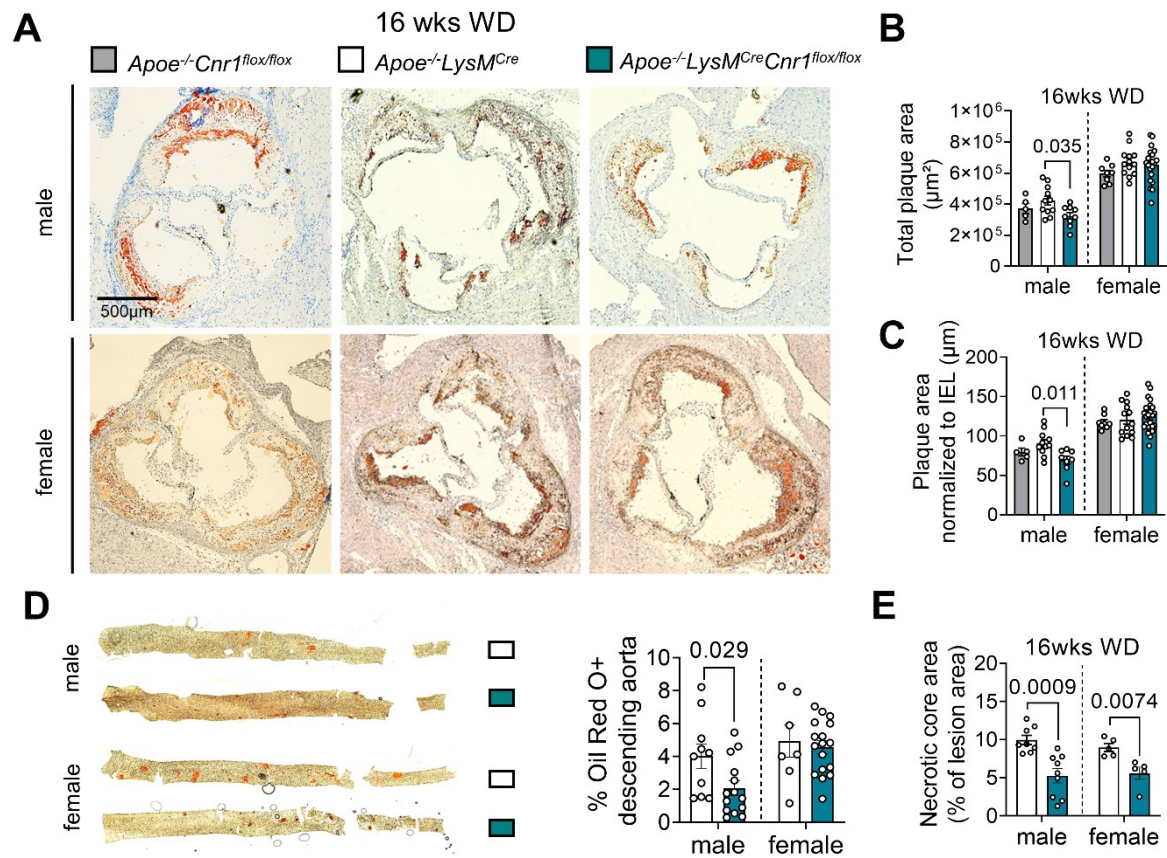


Figure 12: Examining the effect of myeloid CB1 deficiency on advanced atherosclerosis [4]. (A) Male and female mice with the genotypes *Apoe*^{-/-}*Cnr1*^{flox/flox}, *Apoe*^{-/-}*LysMCre*^{+/-}, and *Apoe*^{-/-}*LysMCre*^{+/-}*Cnr1*^{flox/flox} were subjected to a WD for a duration of 16 weeks. Subsequently, the aortic roots of these mice were analyzed using representative ORO stains. A scale bar measuring 500 µm was included for reference. Following a 16-week period of WD exposure, the extent of lesion area within aortic root sections was assessed using two approaches: (B) absolute quantification (n=5–21 mice) and (C) normalization to the IEL (n=5–21 mice). (D) After a 16-week consumption of a WD, the plaque percentage per total vessel area in the descending thoraco-abdominal aorta was assessed. The assessment involved examining en face preparations stained with ORO and utilized a sample size ranging from 7 to 17 mice. (E) After 16 weeks of a WD, masson trichrome-stained aortic root sections were analyzed to quantify the area of relative necrotic core (n=5–9 mice). Each dot in the graph represents a single sample, and the mean ± s.e.m. is displayed for each biologically independent mouse sample. To determine significant differences, independent analyses were conducted for males and females. Two-sided unpaired Student’s t-test (D-E) or one-way ANOVA followed by a post-hoc Tukey multi-comparison test (B-C) were used to determine the significant differences.

Both male and female mice with myeloid *Cnr1* deficiency demonstrated reduced sizes of necrotic cores in aortic sinus plaques (Figure 12E). Interestingly, there were no notable differences observed in the other components of the plaques, indicating overall a more stable plaque phenotype (Figure 13).

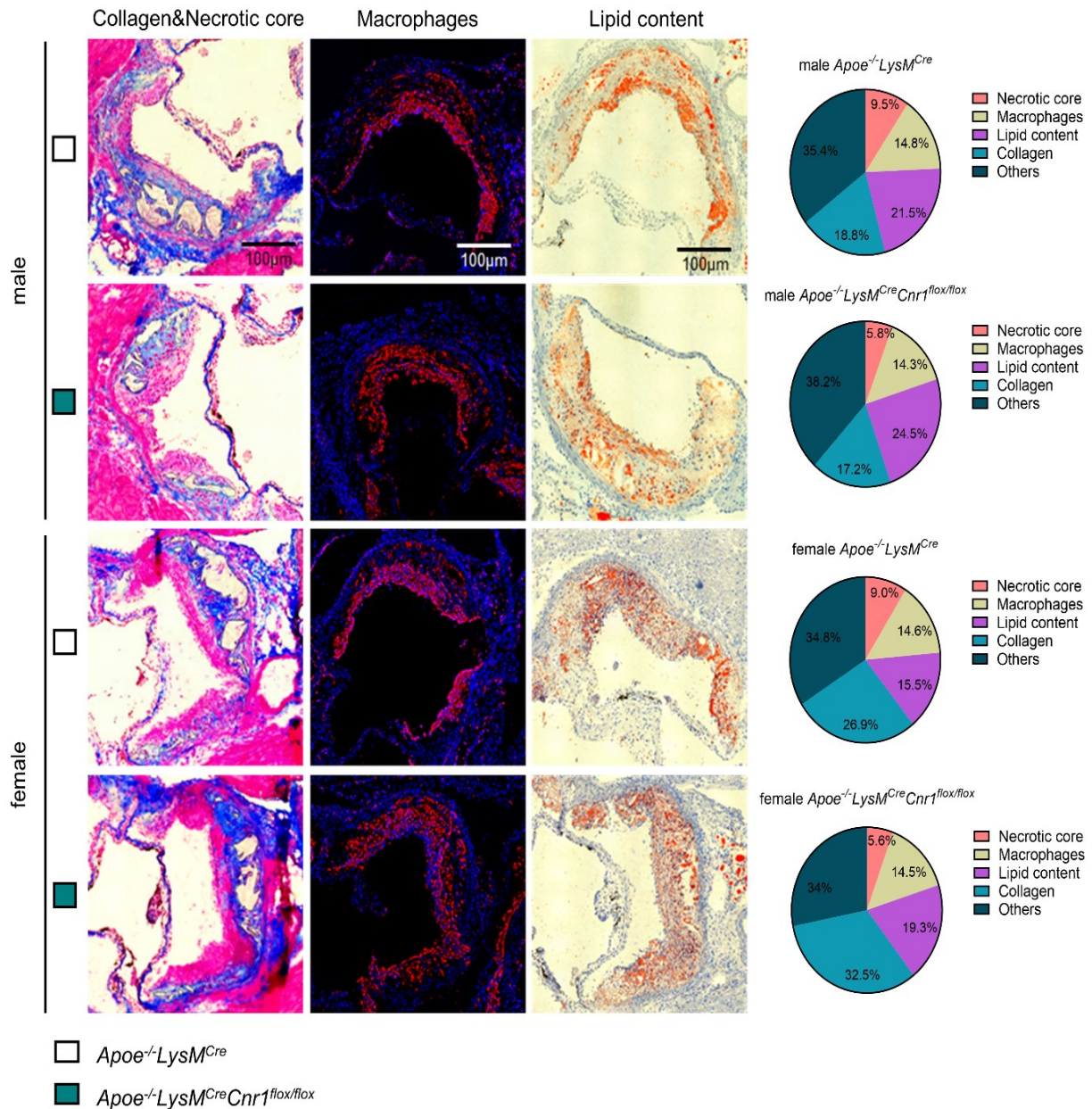


Figure 13: Impact of myeloid *Cnr1* deficiency on advanced plaque composition [4].

Representative aortic root plaque images stained with Oil-red-O and Masson staining's for lipid or collagen content, respectively, and quantification of the necrotic core area after 16 weeks WD. Scale bar: 100 μ m. Necrotic core and collagen content per total plaque area (n=6-10) were calculated. The accumulation of lesional macrophages was determined by CD68 staining (n=6-10)

Moreover, both male and female $Apoe^{-/-}LysM^{Cre}Cnr1^{flox/flox}$ mice exhibited a reduced proportion of plaque area in the aortic arches when compared to the control group (Figure 14A-B).

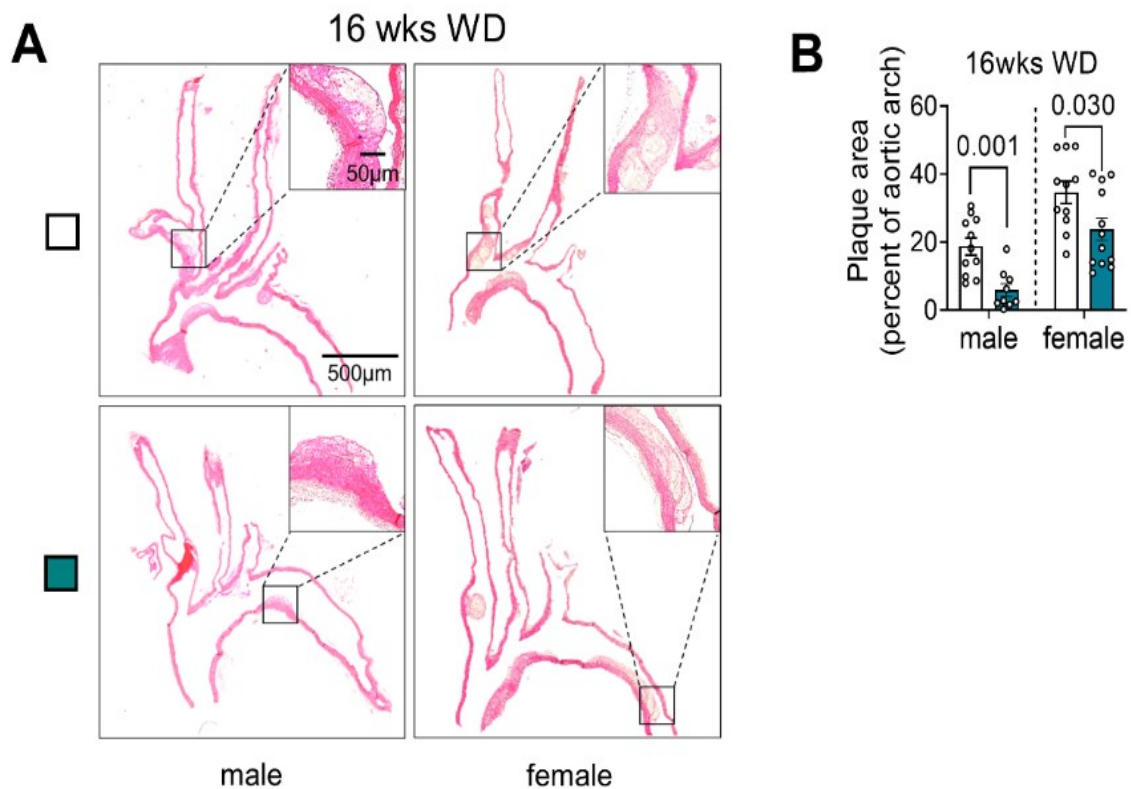


Figure 14: Examining the influence of myeloid CB1 deficiency on advanced of arterial arch plaque [4].

(A) Male and female mice with the genotypes *Apoe*^{-/-}*LysMCre*^{+/-} and *Apoe*^{-/-}*LysMCre*^{+/-}*Cnr1*^{fllox/fllox} were subjected to a WD for 16 weeks. Following this period, representative images of aortic arches were obtained using HE staining, with a scale bar of 500 μm. (B) A sample size of 9-12 mice was used to perform quantification of plaque area in aortic arch sections. Each dot in the graph represents an individual mouse sample, and the mean ± s.e.m. is displayed. Two-sided unpaired Student's t-test were used to determine the significant differences. Male and female were analyzed independently.

5.1.4 The effect of CB1 receptor deficiency in myeloid cells on metabolic parameters

The metabolic parameters significantly changed after a 16-week period of WD feeding when myeloid CB1 signaling was depleted. Interestingly, these effects were only observed in male mice and involved a lower body weight gain and less elevated plasma cholesterol levels (Figure 15A-D). In females, there was only a non-significant trend for less elevated plasma cholesterol levels. In summary, these discoveries indicate that the impact of myeloid *Cnr1* deficiency on plaque characteristics is affected by the biological sex and varies depending on the plaque stage and the affected vessel.

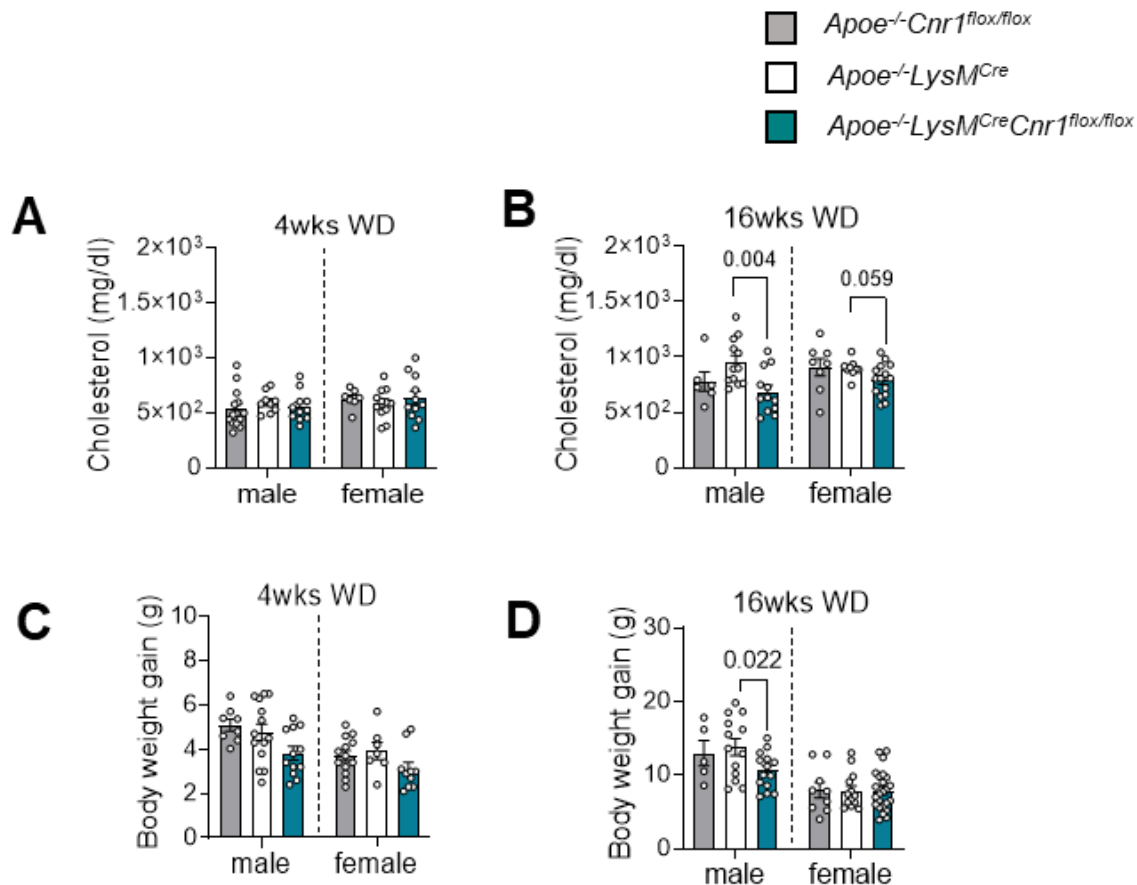


Figure 15: Effects of the absence of CB1 receptors in myeloid cells on metabolic parameters [4]. The cholesterol levels of mice with various genetic backgrounds, namely $Apoe^{-/-}Cnr1^{flox/flox}$, $Apoe^{-/-}LysM^{Cre}$, and $Apoe^{-/-}LysM^{Cre}Cnr1^{flox/flox}$, were assessed following a 4-week (A) and 16-week (B) exposure to a WD. The weight gain of mice with various genetic backgrounds, such as $Apoe^{-/-}Cnr1^{flox/flox}$, $Apoe^{-/-}LysM^{Cre}$, and $Apoe^{-/-}LysM^{Cre}Cnr1^{flox/flox}$, was evaluated following a WD for 4 weeks (C) and 16 weeks (D). The information is displayed in the format of mean \pm s.e.m., where each dot represents an independent mouse sample. One-way ANOVA was conducted to calculate the P-value, followed by a Tukey test (A-D).

5.2 Arterial monocyte recruitment is diminished due to a decrease in chemokine receptor expression in absence of myeloid CB1

5.2.1 The influence of CB1 deficiency in myeloid cells on the number of circulating leukocyte subsets

During the development of atherosclerosis, the primary origin of plaque macrophages arises from the recruitment of monocytes from the bloodstream [177]. Whether circulating myeloid counts would be affected by myeloid *Cnr1* deficiency was investigated in the following experiment. Figure 16A-D illustrates the increased levels of circulating monocytes and neutrophils in both male and female $Apoe^{-/-}LysM^{Cre}Cnr1^{flox/flox}$ mice at baseline or following a 4-week period on a WD. During the advanced stage of 12 to 16 weeks of WD, the effect was

inverted with higher monocyte and neutrophil counts in the *Apoe^{-/-}LysMCre^{+/-}* control group.

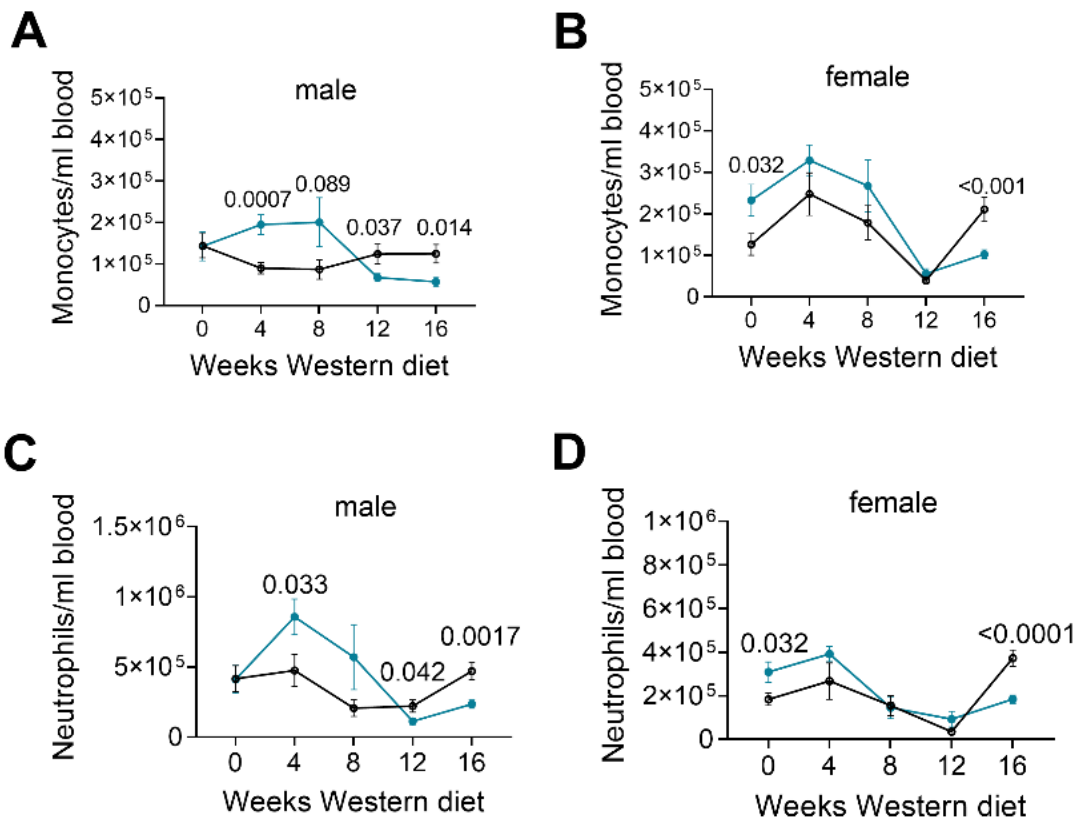


Figure 16: Myeloid CB1 deficiency impact on blood myeloid subset counts [4].

Flow cytometry was utilized to assess the levels of circulating monocytes and neutrophils in male and female mice at various time points (0, 4, 8, 12, and 16 weeks) during a WD intervention. The sample sizes for each time point and sex were as follows: 0 weeks: male (n = 9-10) and female (n = 9-10); 4 weeks: male (n = 18-19) and female (n = 6-10); 8 weeks: male (n = 10) and female (n = 5-10); 12 weeks: male (n = 7-8) and female (n = 5-6); 16 weeks: male (n = 14-15) and female (n = 15-23) (A-D). The mean value, along with the s.e.m. is displayed. Two-sided unpaired Student's t-tests was conducted separately for males and females.

Regardless of whether it was under baseline condition or following a WD, there were minor differences observed in myeloid cell counts within the bone marrow across the various genotypes (Figure 17A-D).

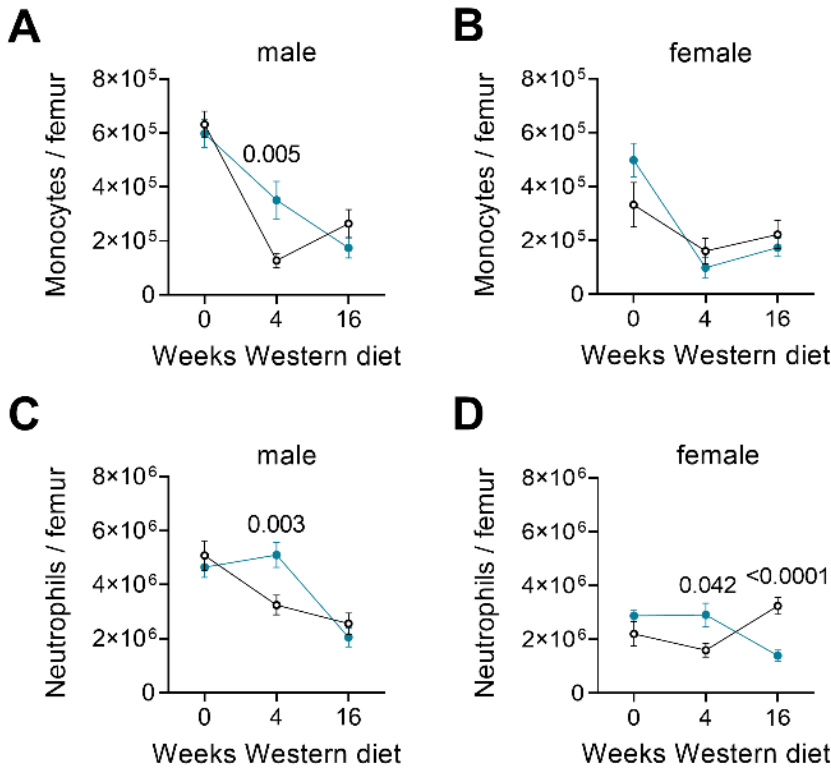


Figure 17: Myeloid CB1 deficiency impact on femur myeloid subset counts [4].

Flow cytometry was employed to evaluate the quantity of monocytes in the femur, classified as CD45+ CD11b+ CD115+ (**A** and **B**), as well as the number of neutrophils, categorized as CD45+ CD11b+ Ly6G+ (**C** and **D**), following 0, 4, and 16 weeks of WD. The mean value, along with the s.e.m. is displayed. Two-sided unpaired Student's t-tests was conducted separately for males and females.

Moreover, there were no discernible effects on lymphocyte blood counts among the various genotypes (**Figure 18A-B**). The findings suggest that the presence of CB1 receptors in myeloid cells plays a crucial role in their recruitment to arteries and lifespan regulation, while having no significant effect on their generation and release from the bone marrow.

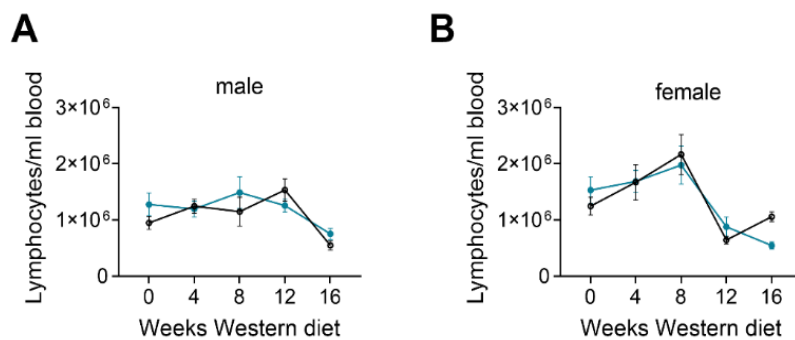


Figure 18: Myeloid CB1 deficiency impact on lymphocyte counts [4].

Lymphocyte counts were measured using flow cytometry at 0, 4, 8, 12, and 16 weeks of the WD in **A**) males and **B**) females. The mean value, along with the s.e.m. is displayed. Two-sided unpaired Student's t-tests was conducted separately for males and females.

5.2.2 Impact of CB1 deficiency in myeloid cells on the expression of growth factor and chemokine receptors

A pro-survival effect was evident as male *Cnr1*-deficient monocytes in circulation exhibited noticeably elevated surface levels of CD115, also known as colony stimulating factor 1 receptor (CSF1R) or macrophage colony-stimulating factor receptor (Figure 19A-B) [178, 179].

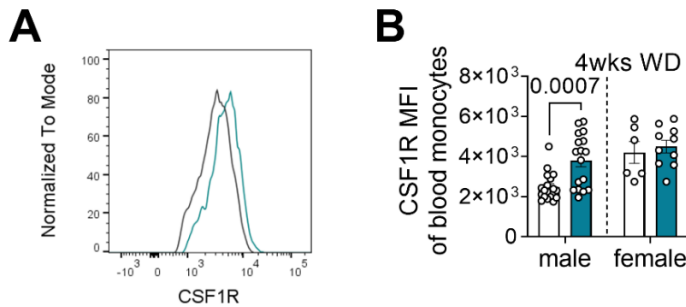


Figure 19: Myeloid CB1 deficiency impact on CSF1R expression [4].

(A-B) Flow cytometry was used to assess the expression levels of CSF1R on circulating monocytes after a 4-week period of WD, involving a total of 6-18 mice. For data analysis, a two-sided unpaired Student's t-test was executed, with separate analyses carried out for male and female data.

The presence of chemokine receptors CCR1 and CCR5 on circulating monocytes was investigated to determine their surface expression, as these receptors are crucial for the recruitment of monocytes to the plaque [180]. Male mice with the genotype *ApoE*^{-/-}*LysMCre*^{+/-}*Cnr1*^{flx/flx} displayed notably reduced receptor expression levels in their bloodstream when compared to *ApoE*^{-/-}*LysMCre*^{+/-} mice. On the other hand, no significant variance was observed among female mice (Figure 20A-D). The genotypes did not show any significant difference in neutrophil recruitment (Figure 10D), indicating that myeloid *Cnr1* deficiency does not impact this process. This observation is supported by comparable levels of CXCR2 on neutrophils between the different genotypes (Figure 20E).

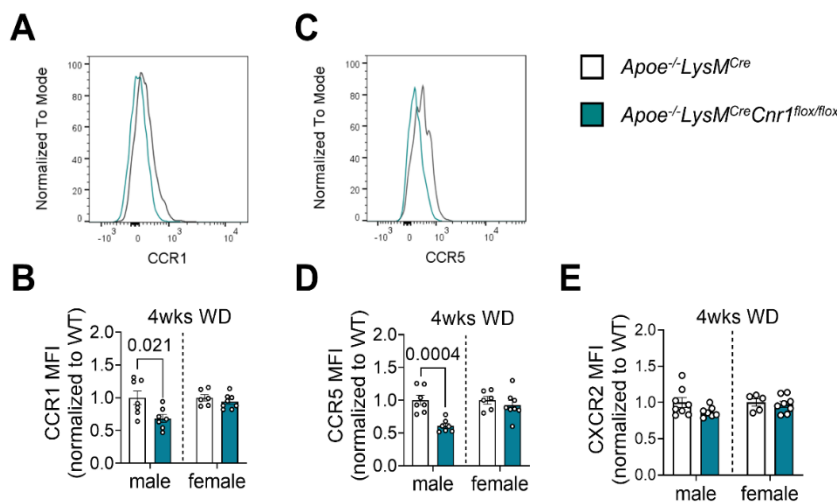


Figure 20: Myeloid CB1 deficiency's impact on chemokine receptor expression [4].

(A-D) A 4-week WD period (n=6–8 mice) was utilized to investigate the surface expression of CCR1 and CCR5 on circulating monocytes, employing flow cytometry. (E) After a four-week period of WD, flow cytometry was utilized to evaluate the surface expression of CXCR2 on circulating neutrophils. The analysis was conducted on a group of 5-8 mice. Each dot represents a mouse. The mean value and s.e.m. is shown. A two-sided unpaired Student's t-test (B, D and E) was executed, with separate analyses carried out for male and female data.

5.2.3 Arterial monocyte recruitment is impacted by the absence of CB1 in myeloid cells

An adoptive transfer experiment to test the hypothesis if lacking myeloid *Cnr1* decreases arterial monocyte recruitment was subsequently performed. *Apoe*^{-/-} recipients, previously treated with a WD for a duration of 4 weeks, were administered fluorescently labeled monocytes derived from either *Apoe*^{-/-}*LysMCre*^{+/-}*Cnr1*^{flox/flox} or *Apoe*^{-/-}*LysMCre*^{+/-} mice. Fluorescence microscopy analysis of aortic root sections showed a noticeably reduced number of plaque-infiltrated monocytes in mice receiving *Cnr1*-deficient monocytes compared to those receiving *Cnr1*-expressing monocytes from control mice. However, there was no significant trend observed in females (Figure 21A-B).

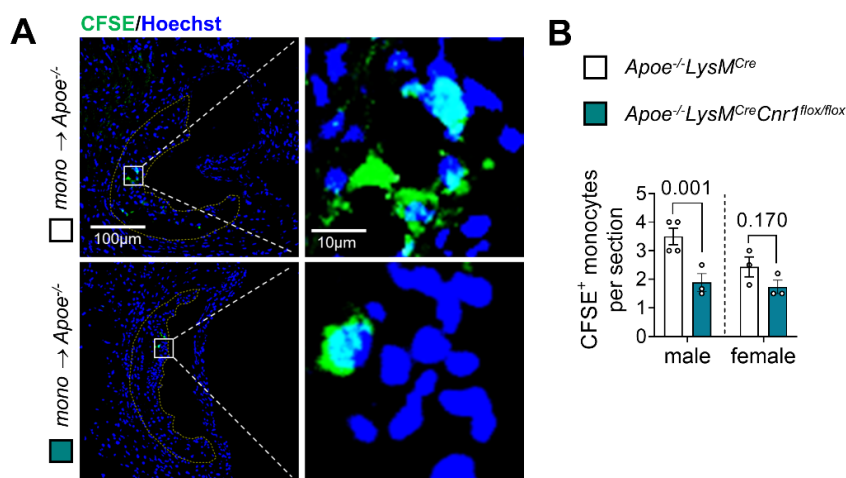


Figure 21: The impact of *Cnr1* deficiency in myeloid cells on the mobilization of arterial monocytes [4].

(A-B) Microscopy images were taken to quantify the migration of CFSE-labeled monocytes into aortic root lesions. The imaging was conducted 48 hours following the injection of these monocytes into male *Apoe*^{-/-} mice that were on a WD for a duration of 4 weeks. Hoechst 33342 was used to stain the nuclei, and scale bars indicating 100 μm (left) and 10 μm (right) were included in the provided images. The data obtained from male and female mice were analyzed separately. Each dot on the graph represents an independent sample from a mouse. The mean value and s.e.m of 3-4 mice per group are shown. To assess statistical significance, a two-sided unpaired Student's t-test was performed.

5.2.4 The regulation of chemokine receptor expression by CB1 signaling in BMDM

BMDMs derived from mice with the genotype *Apoe*^{-/-}*LysMCre*^{+/-}*Cnr1*^{flox/flox} or *Apoe*^{-/-}*LysMCre*^{+/-} were differentiated *in vitro* to examine the specific modulation of CCR1 and CCR5 expression through CB1 signaling. Male *Cnr1*-deficient BMDMs showed a reproducible reduction in CCR5 surface expression, whereas female BMDMs did not exhibit the same reduction (Figure 22A). Treatment with the potent estrogen receptor ligand estradiol at 10 nM concentration did not affect significantly the CCR5 surface expression in male BMDMs, indicating that the underlying mechanism of sex-specific CB1-dependent regulation of CCR5 cannot be fully explained by

differences in estrogen levels (Figure 22A). Male BMDMs lacking *Cnr1* showed decreased levels of *Ccr1* and *Ccr5* mRNA, as revealed by qPCR analysis (Figure 22B-C). BMDMs from male *Apoe*^{-/-} mice, when exposed to the synthetic CB1 agonist ACEA, exhibited elevated surface levels of CCR1 and CCR5. In contrast, the administration of the CB1 antagonist AM281 led to a reduction in the surface expression of CCR1 and CCR5 when compared to BMDMs treated solely with the vehicle (Figure 22D-E). In male *Apoe*^{-/-} BMDMs, Figure 22F illustrates that blocking CB1 with AM281 led to a reduction in the mRNA levels of *Ccr1* and *Ccr5*. This finding suggests that CB1 signaling plays a direct role in regulating these chemokine receptors, potentially through mechanisms involving transcriptional or post-transcriptional processes.

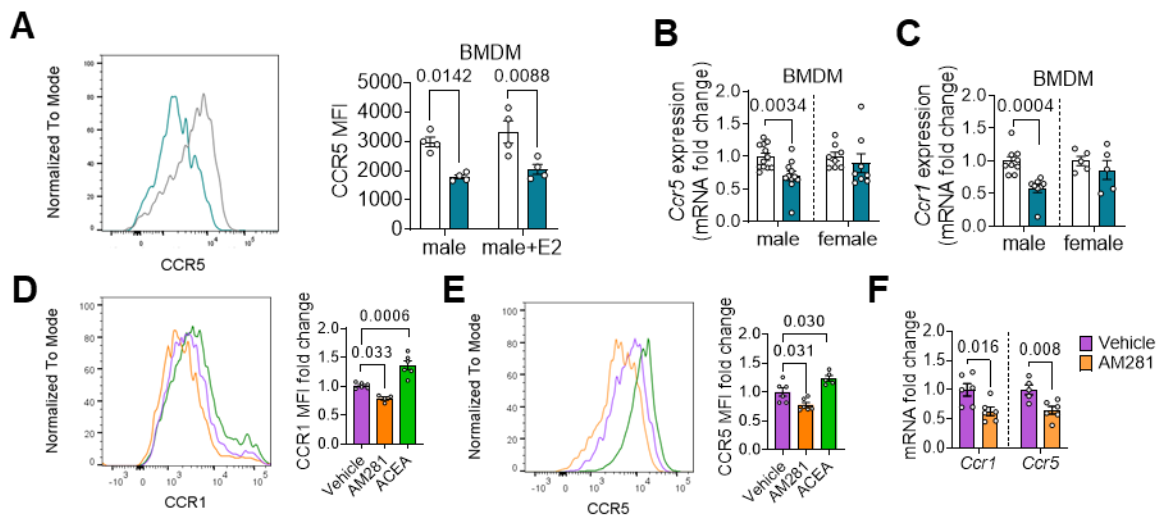


Figure 22: Impact of myeloid CB1 deficiency on chemokine receptors in BMDMs [4].

(A) Flow cytometry analysis was performed on male BMDM that were exposed to either a vehicle control or a 10 nM concentration of estradiol (E2) for a duration of 24 hours. The experiment was conducted using a sample size of 4 mice. (B, C) The gene expression levels in BMDMs without any treatment were assessed in a cohort of 5-12 mice. (D, E) For a 24-hour period, BMDMs obtained from *Apoe*^{-/-} mice were subjected to treatment with either a vehicle, 10 μ M AM281, or 1 μ M ACEA. The treated cells were then analyzed using flow cytometry, and this analysis was performed on a group of 4-6 mice. (F) After an 8-hour treatment with either a vehicle or 10 μ M AM281, the gene expression in BMDM from *Apoe*^{-/-} mice was evaluated. The study included a total of 5-6 mice. Data points are depicted as dots, with each dot representing an individual mouse sample. The mean \pm s.e.m. was utilized to present the data. Statistical analyses were conducted using various tests. For the comparison of groups B, C, and F, a two-sided unpaired Student's t-test was employed. Groups D and E were subjected to a one-way ANOVA with Tukey's test. Group A underwent a two-way ANOVA with Tukey's test. The male and female groups were separately analyzed for all groups (A-F).

5.3 Myeloid CB1 deficiency hampers macrophage growth by modulating p53 signalling

5.3.1 Impact of myeloid CB1 deficiency in macrophages proliferation

Macrophage numbers in the lesion depend on both recruitment and local proliferation [61]. In this study, *Apoe*^{-/-}*LysMCre*^{+/-}*Cnr1*^{fllox/fllox} mice displayed a reduced quantity of proliferating macrophages per section in their aortic roots when compared to *Apoe*^{-/-}*LysMCre*^{+/-} mice. This

analysis was based on co-immunostaining of macrophages and the proliferation marker Ki67 (Figure 23A-B). No observable genotype differences were found in females, but plaque macrophages in females generally showed lower proliferation rates compared to males (Figure 23A-B). The experiment was conducted *in vitro* using male and female BMDMs, and the results confirmed that male *Apoe*^{-/-}*LysMCre*^{+/-}*Cnr1*^{flox/flox} macrophages exhibited lower proliferation rates compared to *Apoe*^{-/-}*LysMCre*^{+/-} macrophages (Figure 23D). The impact of this was mitigated upon administering estradiol to male BMDMs (Figure 23D). Similarly, male *Apoe*^{-/-} BMDM proliferation was suppressed by CB1 antagonist AM281 treatment. In contrast, male *Apoe*^{-/-} BMDM proliferation was increased by the CB1 agonist ACEA treatment (Figure 23E). No difference between genotypes was detectable when performing similar experiments in female BMDMs.

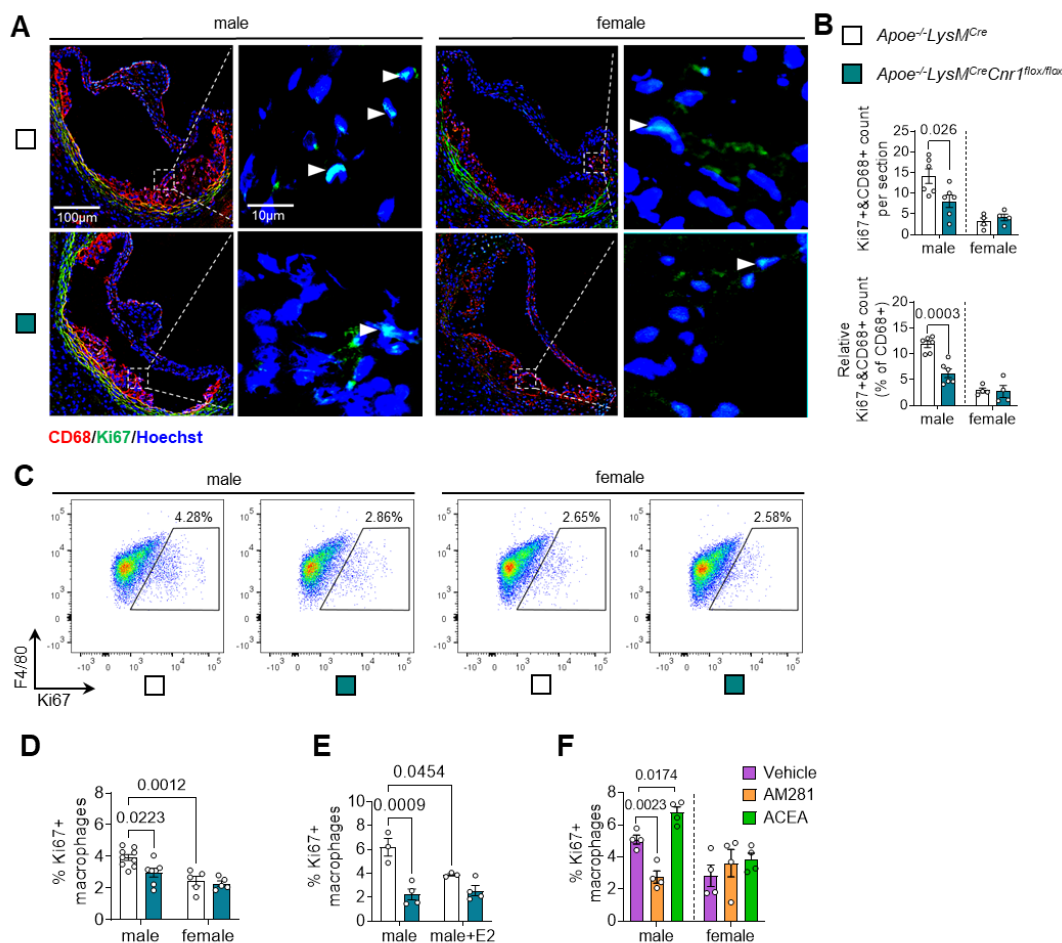


Figure 23: Impact of myeloid CB1 deficiency on macrophages proliferation [4].

(A) The provided images display proliferating macrophages in aortic root plaques after a 4-week period of consuming a WD. The image displays Ki67-positive macrophages, highlighted by white arrowheads in green, alongside CD68-positive macrophages, marked in red. The nuclei are stained with Hoechst 33342 in blue. Scale bars are provided for reference, measuring 100 μ m (left) and 10 μ m (right). (B) The proliferating plaque macrophages were calculated both as absolute numbers and relative to the overall cell counts (n=4-6 mice). (C, D) Flow cytometric analysis of proliferation rates in untreated male and female BMDM isolated from *Apoe*^{-/-}*LysMCre* and *Apoe*^{-/-}*LysMCreCnr1*^{flox/flox} mice (n=5-9 mice). (E) Proliferation rates in male BMDM treated with vehicle or 10 nM estradiol for 24 h (n=3-4 mice). (F) Four mice lacking the *Apoe* gene (*Apoe*^{-/-}) were subjected to treatment with either a vehicle control, 10 μ M AM281, or 1 μ M ACEA for a duration of 24 hours. Following the treatment, the proliferation of BMDMs was evaluated. The data was presented using the mean \pm s.e.m, where each dot represented an individual mouse. Statistical analyses were conducted using various tests. For the comparison of groups B, a two-sided unpaired Student's t-test was employed. Groups F were subjected to a one-way ANOVA with Tukey's test. Group D and E underwent a two-way ANOVA with Tukey's test. For comparisons B, the male and female groups were analyzed separately.

5.3.2 The activation of CB1 receptors influences kinase activity and promotes the translocation of p53 into the nucleus

Chip-based kinase activity profiling was employed to examine the signaling pathways implicated in CB1-dependent regulation of cell proliferation. Male BMDMs obtained from *Apoe*^{-/-} mice were treated with ACEA, a CB1 receptor agonist, which resulted in a notable decreased activity of kinases involved in of p53 signaling and cyclin-dependent pathways involved in controlling the cell cycle (Figure 24A-C).

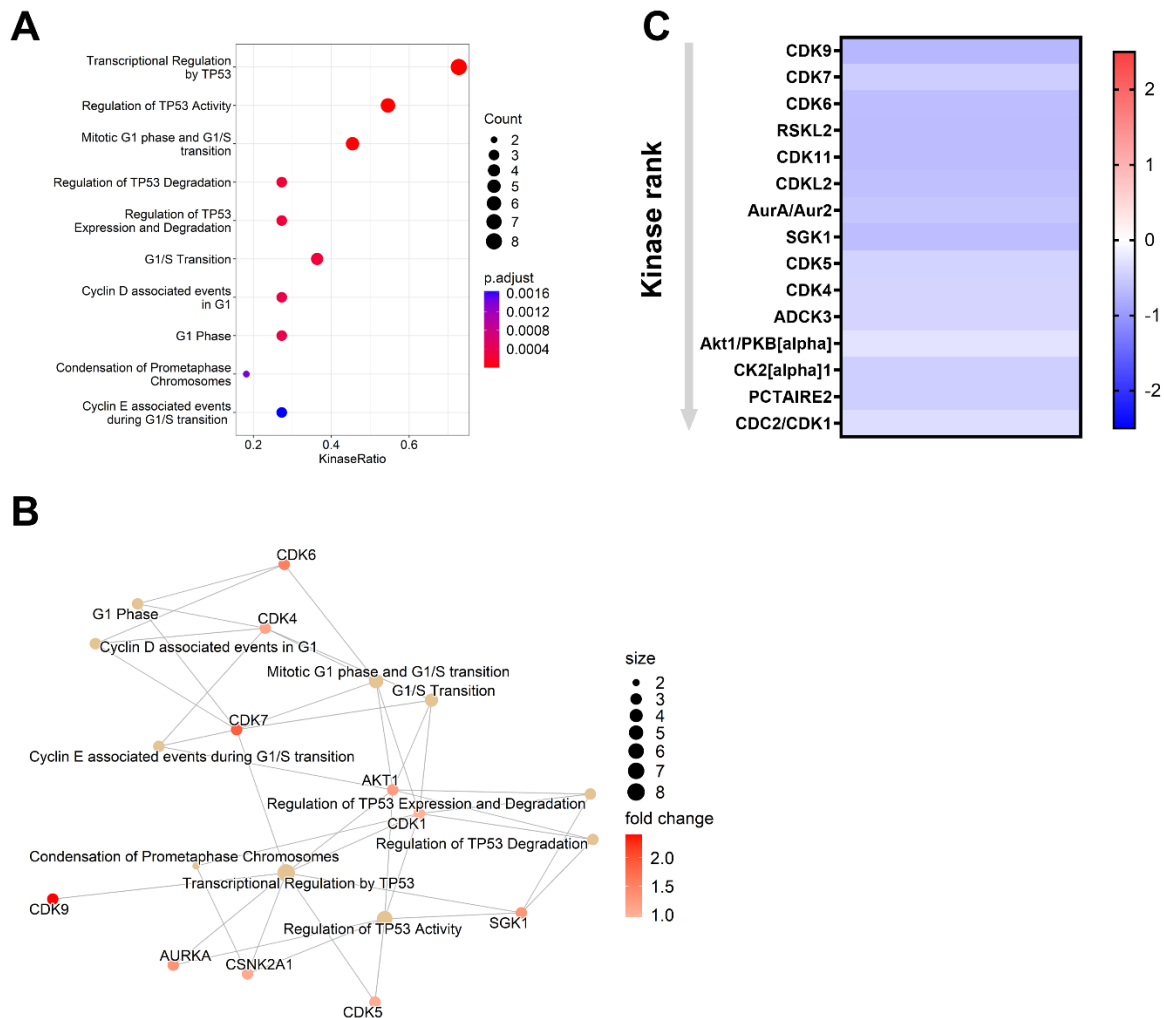


Figure 24: The effects of stimulating CB1 on kinase activity [4].

(A) Identification of the top 10 affected kinase pathways enriched in ACEA-stimulated BMDMs derived from male mice (n=4), following a 60-minute treatment with either the vehicle or 1 μ M ACEA. (B) The interaction map of BMDMs stimulated by ACEA highlights the affected pathways and related kinases. (C) The heatmap illustrates the significantly downregulated kinases in *Apoe*^{-/-} BMDMs after 60-minute treatment with 1 μ M ACEA compared to vehicle treated. The displayed statistics indicate the average kinase values, and only kinases with a median final score above 1.2 considered as significant are included.

To explore the impact of p53 activation on CB1-dependent cell proliferation regulation, BMDMs were first pre-exposed to the p53 inhibitor PFT α before administering the CB1 antagonist AM281. This pretreatment prevented the inhibition of cell proliferation when CB1

was blocked, indicating that p53 activation is involved in CB1-mediated control of cell proliferation. (Figure 25A). Moreover, the use of the CB1 antagonist AM281 led to an increased translocation of phosphorylated p53 into the nucleus. Conversely, the CB1 agonist ACEA showed noteworthy decreased effect on the levels of nuclear p53 (Figure 25B-C).

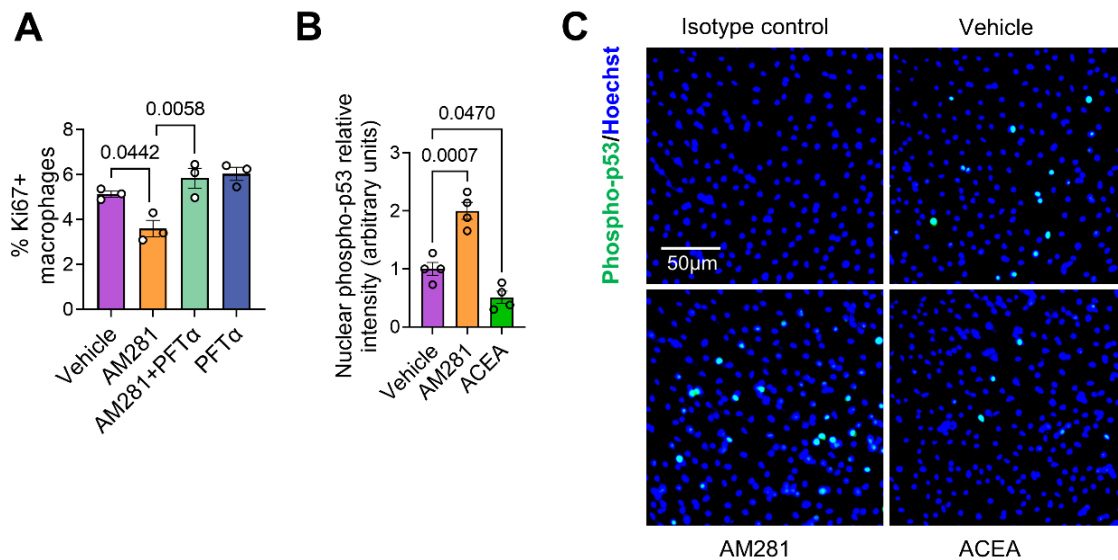


Figure 25: The effects of stimulating CB1 on the translocation of p53 to the nucleus [4].

(A) The growth of BMDM was assessed to determine their proliferation rates after 24 hours of exposure to various substances, such as the vehicle, AM281 (10 μ M), and p53 inhibitor (PFT- α ; 25 μ M). The experiment involved three mice as donors. (B) Immunostaining demonstrated the nuclear translocation of phosphorylated p53 in BMDM following a one-hour treatment with either the vehicle, AM281 (10 μ M), or ACEA (1 μ M). This experiment was conducted on four mice. (C) Phospho-p53 (shown in green) was visualized using immunostaining in *Apoe*^{-/-} BMDM cells after treatment with either the vehicle, 1 μ M ACEA, or 10 μ M AM281 for 60 minutes. The nuclei were stained using Hoechst 33342 (depicted in blue). The scale bar represents a length of 50 μ m. Each dot represents a mouse, with the data represented as the mean \pm s.e.m. The statistical analysis performed consisted of a one-way ANOVA followed by a Tukey test (A and B).

5.4 Myeloid CB1 deficiency reduces pro-inflammatory macrophage phenotype

5.4.1 The involvement of CB1 in macrophage polarization and the uptake of oxLDL

Both male and female mice of the *Apoe*^{-/-}*LysMCre*^{+/-}*Cnr1*^{flox/flox} strain exhibited decreased inflammatory macrophage phenotype in the aortic roots, as revealed by immunostaining analysis of plaques (Figure 11A and C). Further investigations were carried out using male BMDMs in additional *in vitro* experiments. Male *Apoe*^{-/-}*LysMCre*^{+/-}*Cnr1*^{flox/flox} BMDMs showed reduced pro-inflammatory markers (*Irf5*, *Nos2*) and increased expression of anti-inflammatory markers (*Cx3cr1*, *Chil3*) compared to *Apoe*^{-/-}*LysMCre*^{+/-} BMDMs, based on qPCR transcriptomic profiling (Figure 26A). Following LPS stimulation, the surface expression of pro-inflammatory macrophage activation markers (CD38 and CD80) was found to be diminished

in *ApoE*^{-/-}*LysMCre*^{+/-}*Cnr1*^{fllox/fllox} BMDMs, as evidenced by flow cytometry, when compared to *ApoE*^{-/-}*LysMCre*^{+/-} BMDMs (Figure 26B-C). The levels of pro-inflammatory cytokines in *Cnr1*-deficient BMDMs were less elevated following LPS stimulation, indicating a reduced inflammatory phenotype (Figure 26D). IL1 β , a key pro-atherogenic factor, was additionally confirmed at the protein level (Figure 26E). A similar downregulation of inflammatory genes was found in male peritoneal macrophages from *ApoE*^{-/-}*LysMCre*^{+/-}*Cnr1*^{fllox/fllox} mice collected after four weeks of a WD. Conversely, peritoneal macrophages of female mice showed only a minor reduction in IL1 β expression, which did not reach statistical significance (Figure 26F).

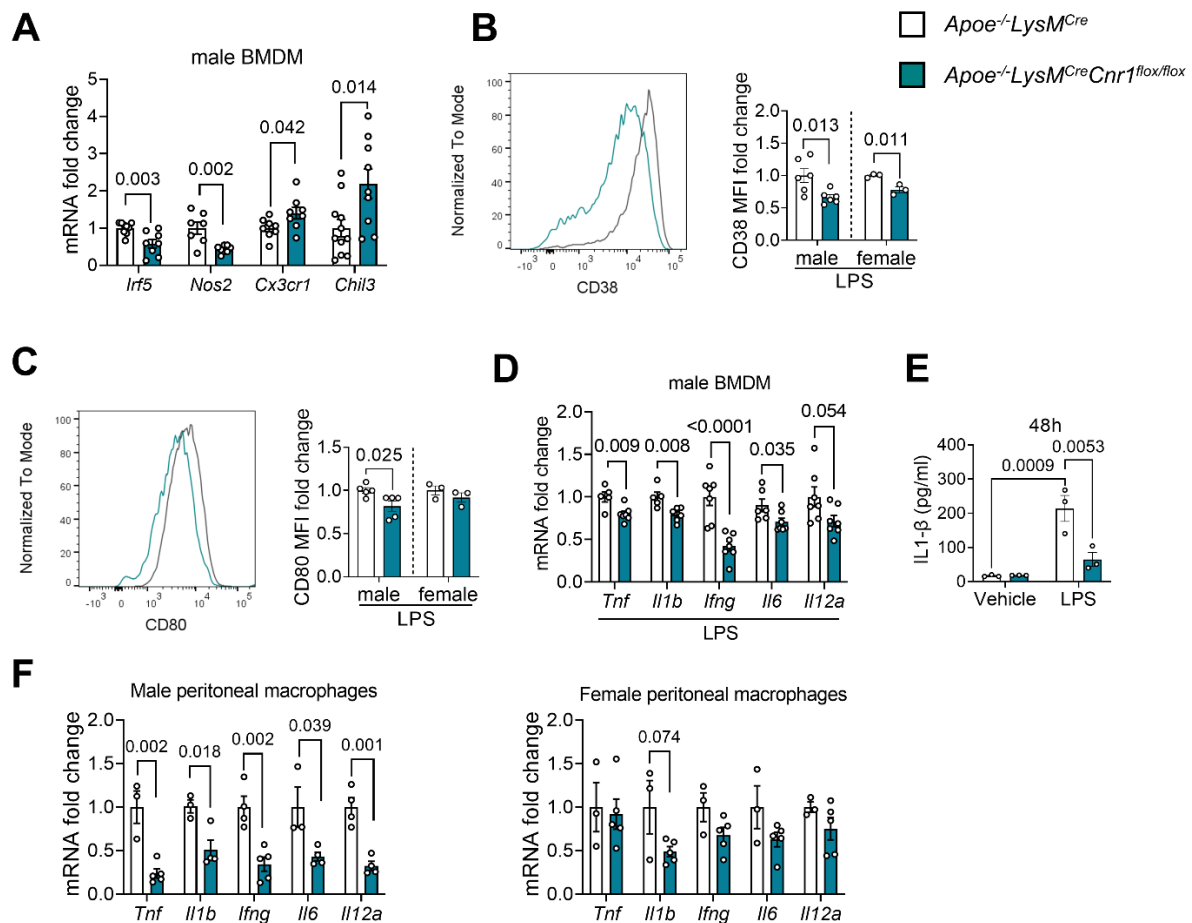


Figure 26: The role of CB1 in macrophage polarization [4].

A) The expression levels of macrophage polarization markers were determined in unstimulated BMDMs isolated from *ApoE*^{-/-}*LysMCre*^{+/-} and *ApoE*^{-/-}*LysMCre*^{+/-}*Cnr1*^{fllox/fllox} mice using qPCR analysis (n=7-12 mice). Flow cytometry analysis was conducted to assess the surface expression of CD38 (**B**) and CD80 (**C**) on BMDMs following a 48-hour stimulation with LPS (10 ng/mL). The study included a sample size of 3-6 mice. (**D**) The levels of pro-inflammatory cytokine gene expression were evaluated using qPCR in BMDMs that were stimulated with LPS for a duration of 8 hours, with a sample size of 5-7 mice. (**E**) IL-1 β secretion by BMDMs was quantified following a 48-hour stimulation with LPS, using a sample size of 3 mice. (**F**) The pro-inflammatory gene expression levels were assessed in peritoneal macrophages from both *ApoE*^{-/-}*LysMCre*^{+/-} and *ApoE*^{-/-}*LysMCre*^{+/-}*Cnr1*^{fllox/fllox} mice (n=3-5 mice) following a four-week period of WD. Every dot symbolizes a distinct mouse sample, and the data are expressed as the mean \pm s.e.m., and statistical analyses were conducted using a two-sided unpaired Student's t-test for **A-D** and **F**, and a two-way analysis of variance (ANOVA) followed by a Tukey test for **E**.

Furthermore, the *Apoe*^{-/-}*LysMCre*^{+/-}*Cnr1*^{fllox/fllox} BMDMs demonstrated a decrease in oxLDL uptake when compared to *Apoe*^{-/-}*LysMCre*^{+/-} BMDMs (Figure 27A). The decrease in oxLDL uptake seen in *Apoe*^{-/-}*LysMCre*^{+/-}*Cnr1*^{fllox/fllox} BMDMs after four weeks of WD were in accordance with the reduced lipid content detected in plaque macrophages in the aortic roots of male *Apoe*^{-/-}*LysMCre*^{+/-}*Cnr1*^{fllox/fllox} mice (Figure 27B-C). This evidence confirms the involvement of CB1 in the regulation of macrophage cholesterol uptake and metabolism in atherosclerosis.

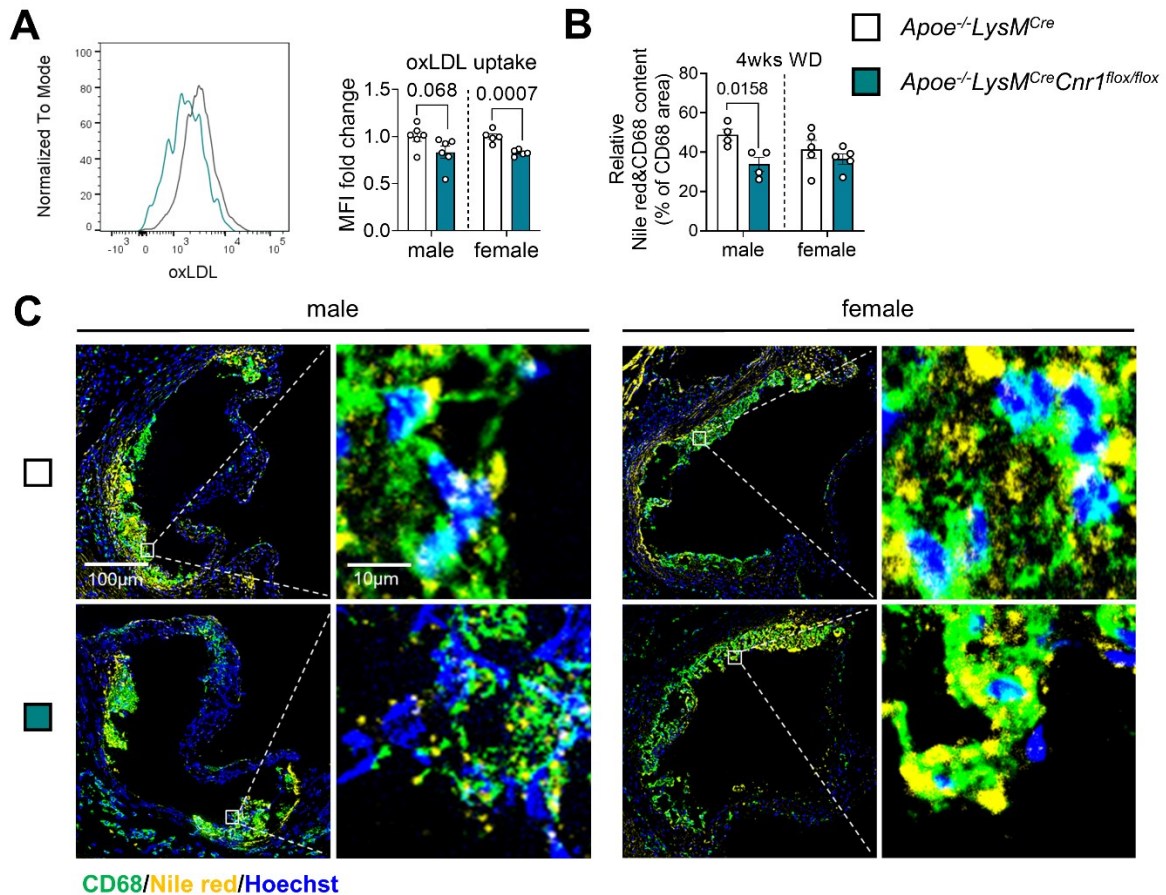


Figure 27: The role of CB1 in macrophage oxLDL uptake [4].

(A) Flow cytometric analysis was performed to assess the uptake of labelled dil-oxLDL by BMDMs (n=5-6 mice). (B-C) Following a 4-week period of WD, Nile Red staining revealed the lipid droplets within the macrophages of aortic root plaques, appearing as yellow. Additionally, CD68 staining was utilized to highlight the macrophages, shown here in green. Double immunostaining was conducted on aortic root lesions obtained from male and female mice of the *Apoe*^{-/-}*LysMCre*^{+/-} and *Apoe*^{-/-}*LysMCre*^{+/-}*Cnr1*^{fllox/fllox} strains (n=4-5 mice). The measurement of lipid droplet accumulation in macrophages was determined by analyzing the CD68 and Nile Red staining. Nuclei were counterstained with Hoechst 33342, appearing as blue. The scale bar denotes 100 µm (left) and 10 µm (right). Every dot symbolizes a distinct mouse sample, and the data are expressed as the mean ± s.e.m.. Statistical analyses were conducted using a two-sided unpaired Student's t-test for A-B. The male and female groups were analyzed separately.

5.4.2 Impact of myeloid CB1 deficiency on macrophage apoptosis

Atherosclerotic plaque development is closely associated with macrophage apoptosis. TUNEL staining of apoptotic macrophages in the aortic roots of male *Apoe^{-/-}LysM^{+/-}CreCnr1^{flox/flox}* mice demonstrated a tendency for fewer apoptotic macrophages per section compared to *Apoe^{-/-}LysMCre^{+/-}* mice, however, no discernible variation was observed between the genotypes in females (Figure 28A-B). The decrease trend was observed in male and female BMDMs *in vitro*, validating that *Apoe^{-/-}LysM^{+/-}CreCnr1^{flox/flox}* macrophages had tendency for fewer apoptotic macrophages in comparison to *Apoe^{-/-}LysM^{+/-}* macrophages (Figure 28C-D).

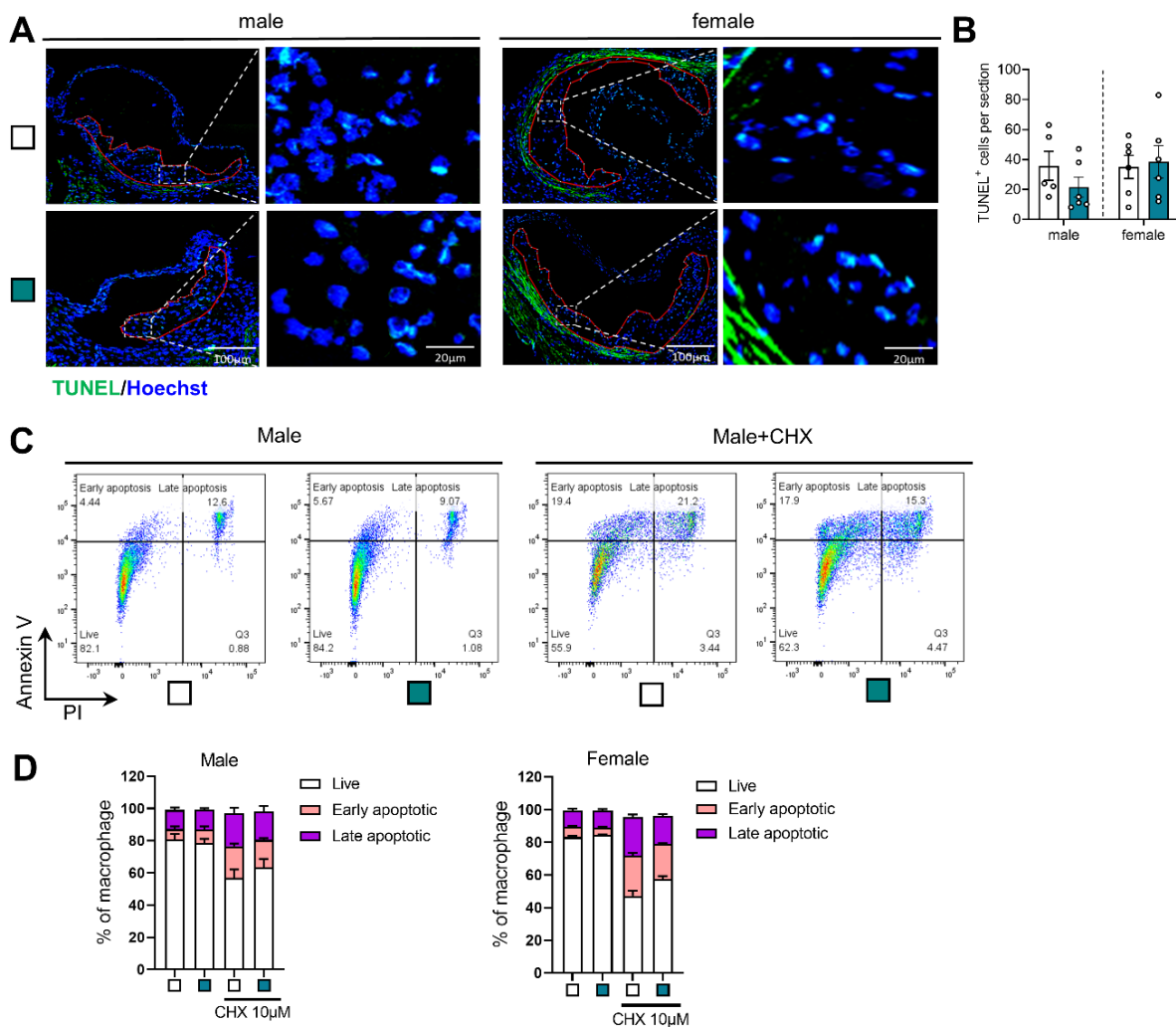


Figure 28: Effects of myeloid CB1 deficiency on plaque macrophage apoptosis [4].

(A) After a duration of 4 weeks on a WD, aortic root plaques display apoptotic macrophages, distinguished by a green marker (TUNEL+). The nuclei are subsequently stained in blue using Hoechst 33342. In the accompanying images, the scale bar is positioned at 100 μ m on the left image and 20 μ m on the right image. (B) Apoptotic plaque macrophage counts per section (n=6 mice). (C, D) Utilizing flow cytometry, the apoptotic rates in male and female BMDM obtained from *Apoe^{-/-}LysMCre^{+/-}* and *Apoe^{-/-}LysMCre^{+/-}Cnr1^{flox/flox}* mice were analyzed, with a sample size of three mice per group.

5.4.3 Macrophage inflammatory reprogramming is regulated by CB1 signaling

When male or female *Apoe*^{-/-} BMDMs were treated with the CB1 agonist ACEA, an increase in CD38 surface expression was observed. This finding adds further evidence to support the direct role of CB1 signaling in the reprogramming of macrophage inflammation (Figure 29A), whereas AM281, a CB1 antagonist, suppressed LPS-induced CD38 and CD80 upregulation. (Figure 29B-C). CB1 antagonism using AM281 also suppressed LPS-induced pro-inflammatory cytokine mRNA expression (Figure 29D).

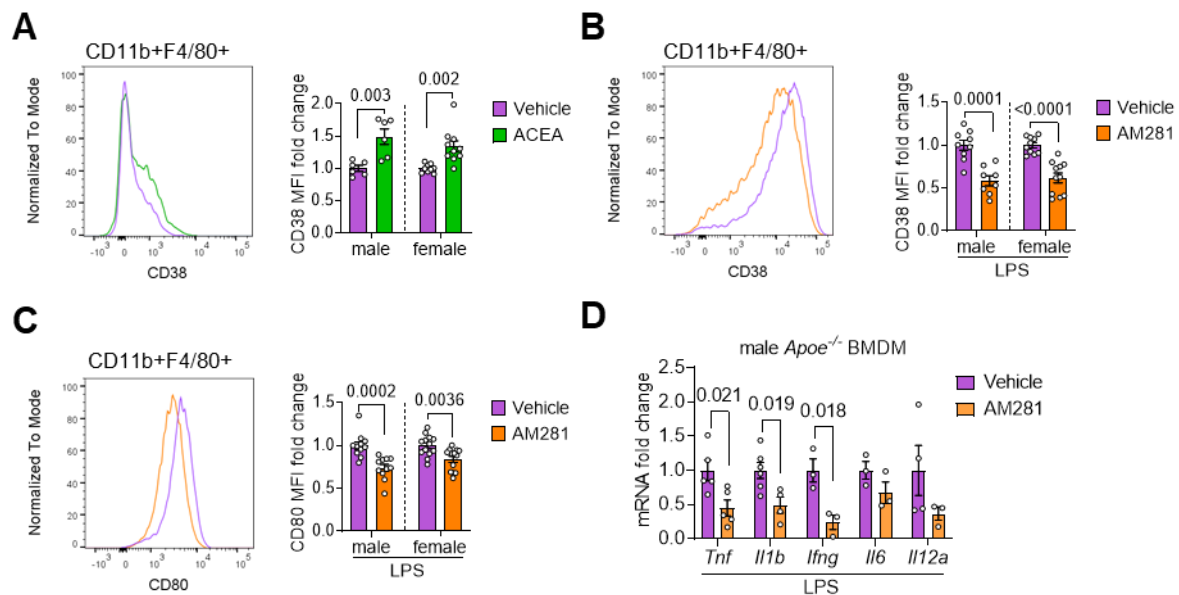


Figure 29: CB1-dependent regulation of macrophage inflammatory reprogramming [4].

BMDMs were isolated from *Apoe*^{-/-} mice and subjected to either (A) treatment with 1 μ M ACEA or vehicle for 24 hours, with CD38 surface expression analyzed (n=6-10 mice), or (B) stimulation with LPS for 24 hours in the presence of 10 μ M AM281 or vehicle, with CD38 surface expression analyzed (n=8-12 mice). (C) CD80 surface expression on 24 h LPS-stimulated BMDMs in presence of 10 μ M AM281 or vehicle (n=8-12). (D) The measurement of gene expression levels of pro-inflammatory cytokines was conducted in *Apoe*^{-/-} BMDMs, which were stimulated with LPS for 8 hours. This was done under two conditions: one group was treated with 10 μ M AM281, while the other group served as the vehicle control. The experiment was performed using a sample size of 3-5 mice. Every dot on the graph represents an individual mouse sample that is biologically independent. The data is presented as the mean \pm s.e.m. To compare groups (A-D), two-sided unpaired Student's t-tests were performed. Male and female samples were analyzed separately (A-C).

5.5 CB1 profoundly regulates the transcriptional, translational, and metabolic profiles of BMDMs

5.5.1 CB1 stimulation significantly influences the transcriptomic profile of BMDMs

To enhance our understanding of the molecular pathways triggered by CB1 activation in macrophages, an untargeted RNA sequencing approach was utilized for transcriptomic analysis of ACEA-stimulated *Apoe*^{-/-} BMDMs. Gene ontology analysis demonstrates that CB1

predominantly impacts crucial biological processes and molecular functions linked to the regulation of transcription, chromatin, and histone modification (Figure 30A-C and Figure 31A-B).

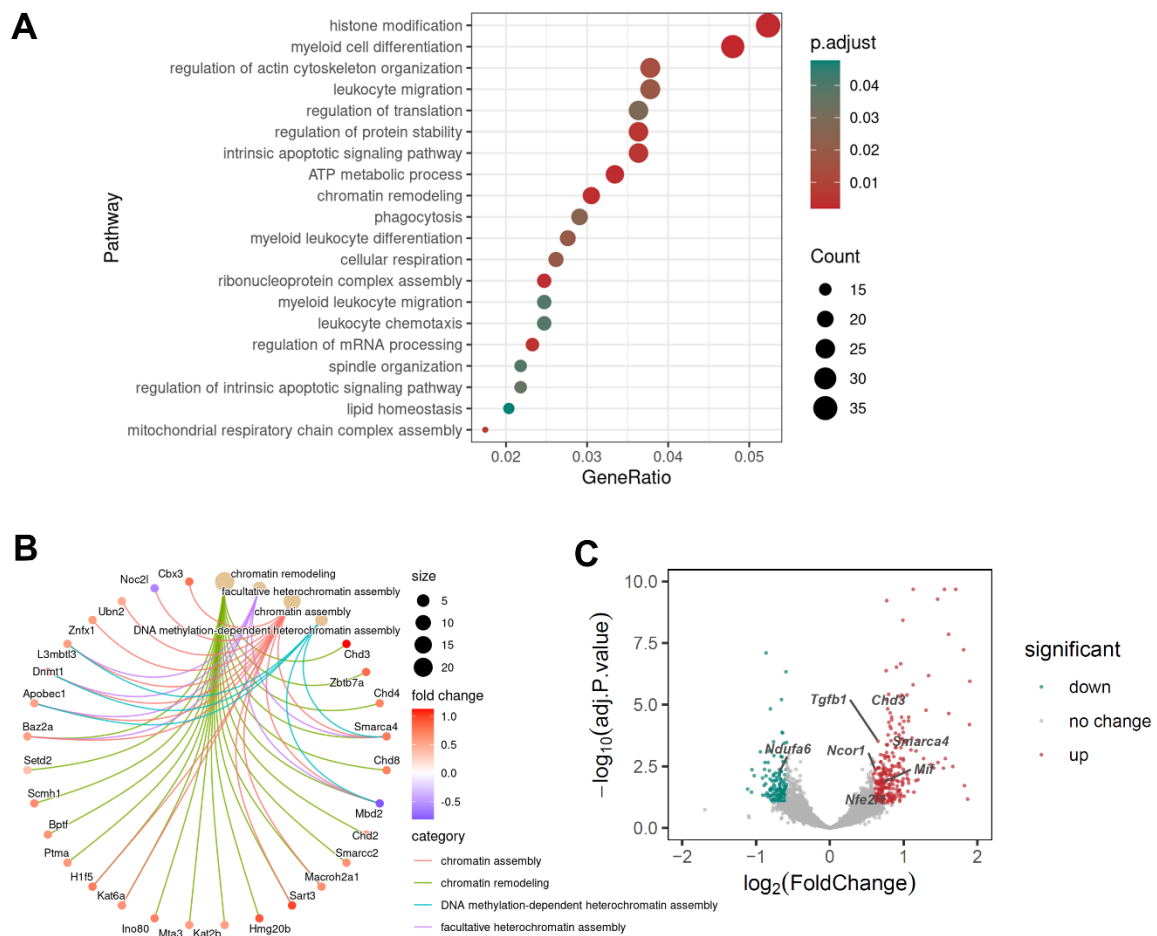


Figure 30: The effects of stimulating CB1 on the transcriptomic profile of BMDM [4]. (A) Determine the principal regulated biological processes. (B) Perform network analysis on pathways related to chromatin modification and examine the associated differentially expressed genes (DEGs) in male BMDMs treated with 1 μ M ACEA for 24 hours, comparing it to the treatment with the vehicle. (C) Volcano plot of bulk RNA-seq data showing DEGs in male *Apoe*^{-/-} BMDMs stimulated with 1 μ M ACEA for 24 h versus vehicle (n=5 separate BMDM donor mice).

The discoveries indicate that CB1 might play a role in regulating transcriptional processes by means of epigenetic alterations. The analysis of BMDMs stimulated by ACEA in the transcriptome unveiled several pathways associated with myeloid differentiation, leukocyte migration, mRNA processing, spindle organization, and actin cytoskeletal organization. The data in the mouse model with myeloid *Cnr1* deficiency reinforce these observations, as the gene set enrichment analysis (GSEA) revealed noteworthy associations with inflammatory response, cholesterol transport, and efflux (Figure 31C).

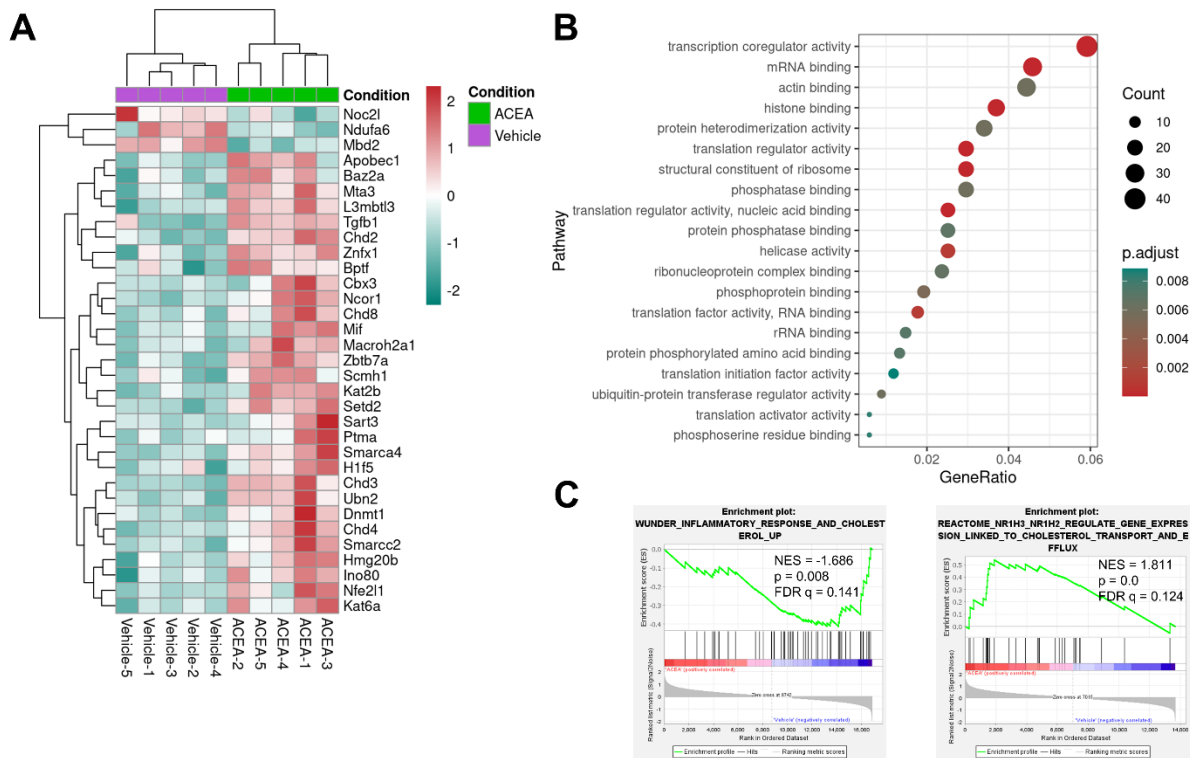


Figure 31: Transcriptomic profile of BMDMs after CB1 agonist stimulation [4].

(A) Heat map showing chromatin modification pathway-related DEGs and selected genes highlighted in (Figure 26C). (B) Pathway analysis showing top molecular functions regulated in CB1-stimulated BMDM. (C) GSEA identifies CB1-regulated gene sets associated with inflammatory response and cholesterol. Enrichment plots of significantly enriched gene sets with normalized enrichment score (NES), nominal P value and false discovery rate (FDR) q-value are shown.

5.5.2 Validation of the key regulated genes in BMDMs and plaques of *Cnr1*-deficient mice

CB1 stimulation revealed the upregulation of *Mif*, an atypical chemokine with established involvement in atherosclerosis (Figure 30C and Figure 31A) [181]. *Ndufa6* functions as a supplementary component of mitochondrial complex I, which is an integral part of the mitochondrial membrane's respiratory chain. It encodes the NADH:ubiquinone oxidoreductase subunit A6 protein, which has a vital role. Additionally, GO analysis indicates its potential involvement in regulating ATP metabolic processes (Figure 30A). *Ndufa6* and *Mif* were confirmed as two significant differentially expressed genes through qPCR analysis, showing their downregulation in *Apoe*^{-/-}*LysMCre*^{+/-}*Cnr1*^{fllox/fllox} BMDMs (Figure 32A). In order to reinforce the regulatory function of CB1 in the specific key targets identified *in vivo*, LCM was conducted with plaque sections collected after a duration of 4 weeks WD. The qPCR analysis of reverse transcribed RNAs isolated from LCM samples unveiled a noteworthy decrease in *Mif* expression within the plaques of *Apoe*^{-/-}*LysMCre*^{+/-}*Cnr1*^{fllox/fllox} mice. However, the reduction in *Ndufa6* levels observed in the LCM plaques did not reach a statistically significant level (Figure

32B). Within 30 minutes, a rapid increase in *Ndufa6* mRNA levels was observed when BMDMs were treated with 1 μ M CB1 agonist ACEA in subsequent experiments. Unlike other conditions, *Mif* displayed notable upregulation following 8 hours of ACEA stimulation (Figure 32D). The *Mif* promoter has key transcription factor binding sites, including one for p53 [182], which was recognized as a CB1 target through kinase activity profiling (Figure 23A). Pretreatment with the p53 inhibitor PFT α hindered the initial increase in *Ndufa6* mRNA levels within 30 minutes upon ACEA stimulation. Despite inhibiting p53, *Mif* upregulation remained unchanged. Surprisingly, the inhibition of p53 actually intensified *Mif* upregulation, as observed in Figure 32E. This enhancement may be attributed to post-transcriptional mechanisms such as mRNA processing and stability.

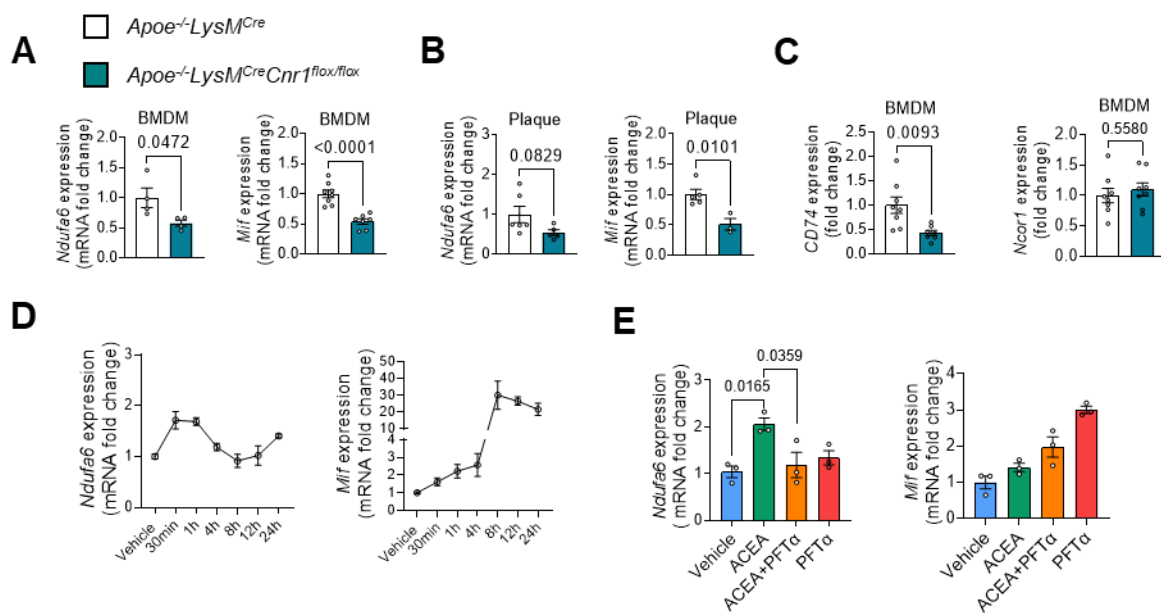


Figure 32: The effect of CB1 signaling in macrophages gene expression and mitochondrial function [4].

BMDMs were obtained from *Apoe*^{-/-}*LysM*^{Cre}^{+/-} and *Apoe*^{-/-}*LysM*^{Cre}^{+/-}*Cnr1*^{flox/flox} mice (A-C) or *Apoe*^{-/-} mice (D-E). (A and C) qPCR analysis was conducted on BMDMs obtained from baseline male mice (n=4-8) as well as on BMDMs derived from laser capture microdissected (B) plaques of aortic root sections from male mice (n=3-6) that were exposed to a 4-week WD. (D) Gene expression levels of male *Apoe*^{-/-} BMDMs were analyzed using qPCR at specified time points following stimulation with 1 μ M ACEA. The expression levels were normalized to the vehicle control at time point 0. (E) BMDMs (n=3 mice) were treated with 1 μ M ACEA for 30 minutes, either alone or in the presence of the p53 inhibitor (PFT- α), and subjected to gene expression analysis using qPCR. The data are displayed as mean \pm s.e.m., and each dot corresponds to an individual mouse sample. A two-sided unpaired Student's t-test was utilized to compare groups in A to C, while a one-way analysis of variance (ANOVA) followed by a Tukey test was employed for comparisons between groups in D and E.

5.5.3 CB1 signaling in macrophages influences mitochondrial function

Following the GO pathway analysis hinting to an involvement of CB1 in mitochondrial oxidative respiration regulation, additional studies were undertaken to explore the impact of CB1 signaling on the control of mitochondrial function. Male and female *Apoe*^{-/-}*LysM*^{Cre}^{+/-}*Cnr1*^{flox/flox} BMDMs exhibited significantly higher mitotracker staining intensity compared to *Apoe*^{-/-}

LysMCre^{+/-} BMDMs, indicating increased mitochondrial content as measured by flow cytometry (Figure 33A). *Cnr1*-deficient BMDMs showed reduced ROS levels, indicating improved mitochondrial function (Figure 33B). Using the Seahorse metabolic flux analyzer, we found no discernible variation in maximum respiration between *Apoe*^{-/-}*LysMCre*^{+/-}*Cnr1*^{fllox/fllox} and *Apoe*^{-/-}*LysMCre*^{+/-} BMDMs under homeostatic conditions. However, despite the lack of full preservation of OCR in *Cnr1* deficiency, it led to significantly higher maximum respiration rates compared to LPS-treated controls after being stimulated with LPS (Figure 33C-D). *Apoe*^{-/-} BMDMs exhibited significantly lower maximum respiration rates after ACEA treatment. The decline in OCR induced by LPS was partially prevented by AM281 (Figure 33E-F).

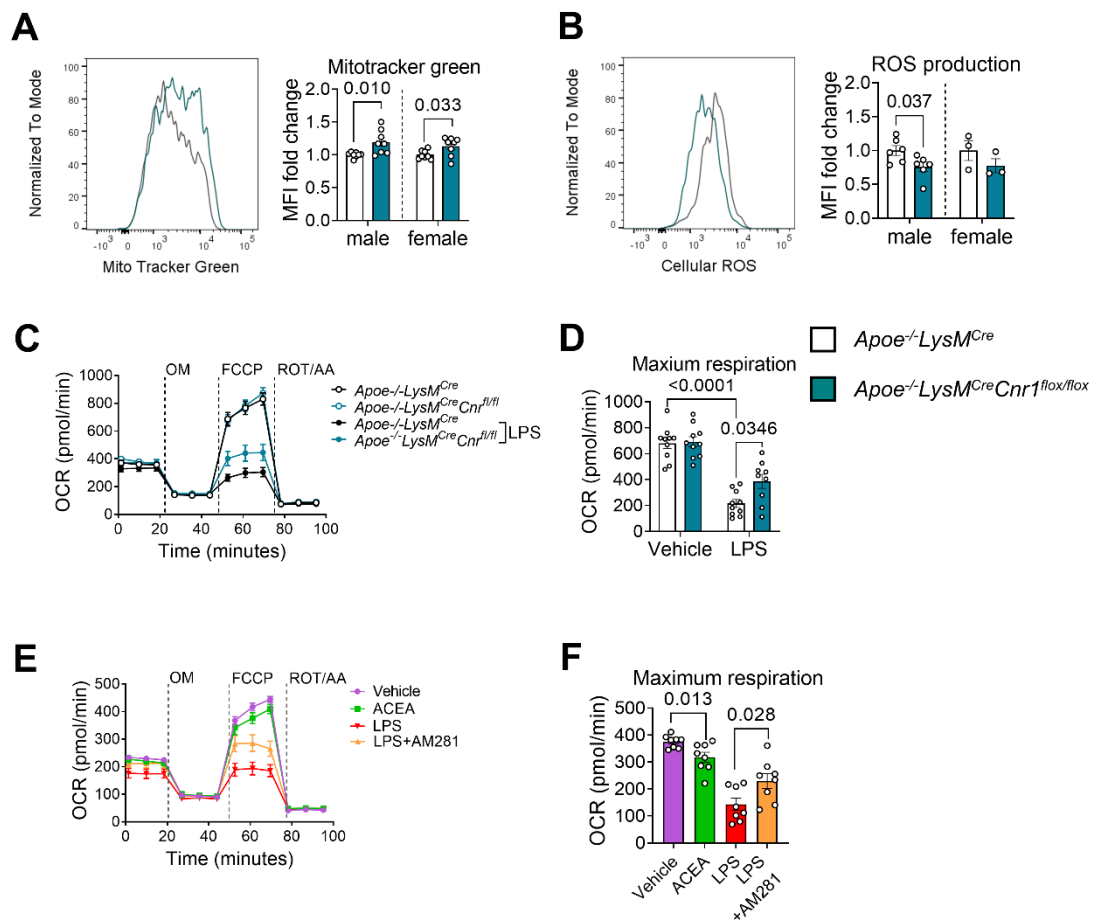


Figure 33: The influence of CB1 signaling in macrophages mitochondrial function [4].

BMDMs were isolated from *Apoe*^{-/-}*LysMCre* and *Apoe*^{-/-}*LysMCreCnr1*^{fllox/fllox} mice (A-D) or *Apoe*^{-/-} (E-F). (A) Mitochondrial content in BMDMs was assessed using flow cytometric analysis, where staining with MitoTracker™ green was employed (n=8 mice). (B) ROS levels were assessed by conducting flow cytometric analysis using DHR123 staining on a sample size of 3-6 mice. (C-F) To assess mitochondrial respiration in BMDMs (n=8-10 mice), OCR measurement was performed. This involved a stepwise injection of oligomycin (OM), carbonyl cyanide 4-(trifluoromethoxy) phenylhydrazine (FCCP), and a combination of rotenone (ROT) and antimycin A (AA). Each point on the graph corresponds to a distinct mouse sample, and the data is presented as the average value along with the standard error of the mean. To perform statistical analyses, a two-sided unpaired Student's t-test was employed for A and B, a one-way ANOVA was conducted, followed by a Tukey test for F, and a two-way ANOVA was performed, followed by a Tukey test for D.

5.6 Plaque progression in atherosclerosis is inhibited by peripheral CB1 antagonism

5.6.1 Metabolic parameters after treatment with peripheral antagonist

In a final experiment, the therapeutic possibilities of blocking peripheral CB1 receptors was studied. The *Ldlr*^{-/-} mouse model was selected over the *Apoe*^{-/-} model due to its closer resemblance to the human cholesterol profile [121]. Following a continuous four-week administration of the peripheral CB1 antagonist JD5037, male and female groups receiving the antagonist exhibited decreased plasma cholesterol levels. Additionally, males displayed reduced plasma triglyceride levels, and only males witnessed a notable decrease in the rate of body weight gain, as anticipated (Figure 34A-D).

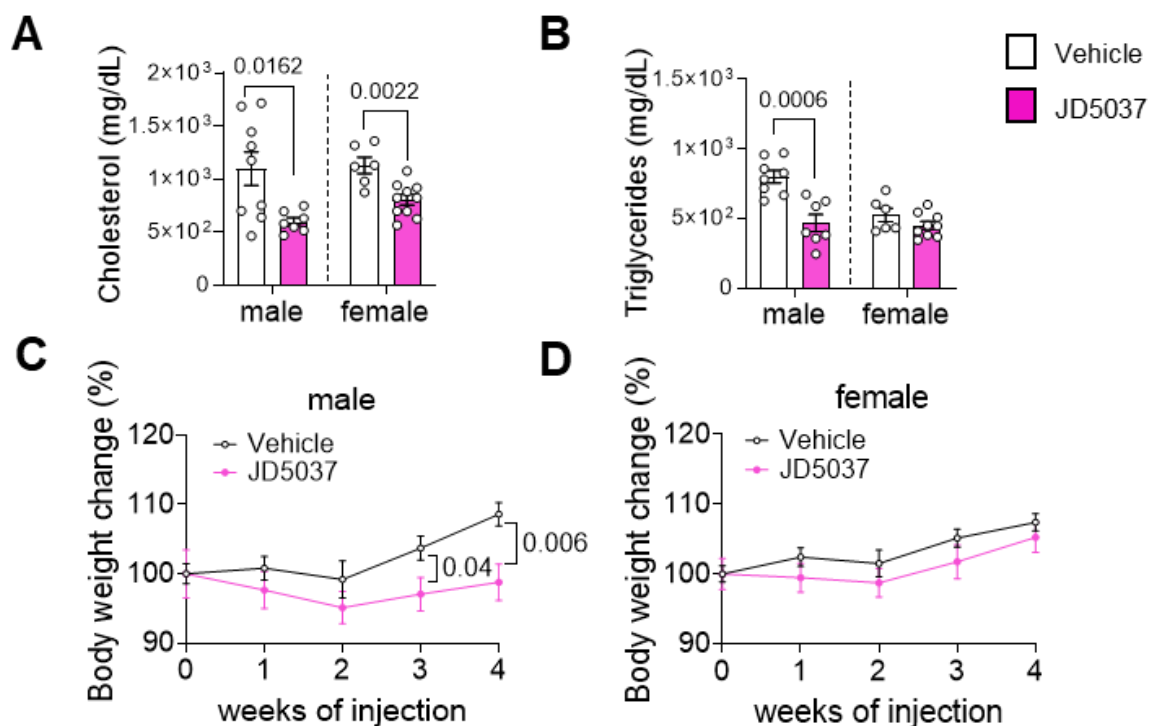


Figure 34: Peripheral CB1 antagonism's impact on metabolic parameters [4].

Cholesterol and triglyceride levels (A-B), as well as body weights (C-D), were assessed in male and female *Ldlr*^{-/-} mice (n=6-10 mice) after 8 weeks on a WD. Over the course of the final four weeks of the diet, the mice were administered daily injections of either JD5037, a peripheral CB1 antagonist, or a vehicle. The dataset includes multiple dots, each representing a mouse. The data is displayed as the mean ± s.e.m. Statistical analysis for groups A-D was performed using a two-sided unpaired Student's t-test. The male and female groups were analyzed separately.

5.6.2 Effect of peripheral CB1 antagonism impact on plaque progression

The early-stage progression of plaque in the aortic roots and arches of male mice was suppressed by administering the peripheral CB1 antagonist JD5037 for a period of 4 weeks. Remarkably, the administration of JD5037 to female mice did not result in any significant difference in plaque size compared to the control group (Figure 35A-F).

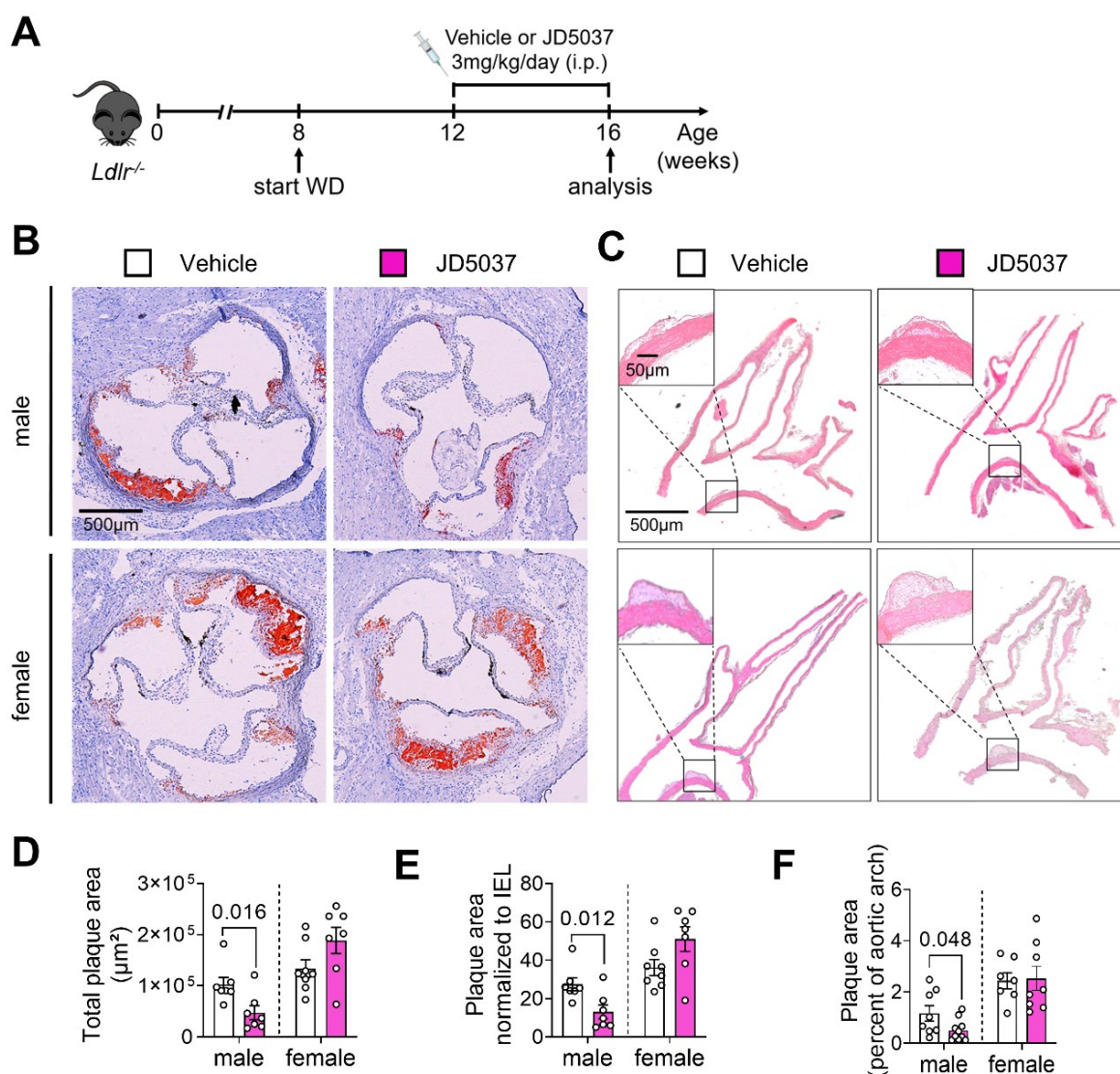


Figure 35: Peripheral CB1 antagonism's impact on plaque progression [4].

(A) During the last 4 weeks of the 8-week WD, *Ldlr*^{-/-} mice in the experimental setup were given daily intravenous injections of JD5037 (3 mg/kg) or a vehicle. (B) Representative ORO-stained images of aortic root cross-sections. (C) Representative HE-stained images of longitudinal sections of the aortic arch. The area of lesions within the aortic roots was measured in 7-8 mice, either presented in absolute terms (D) or adjusted to the IEL (E). (F) A sample size of 7-8 mice was used to quantify the plaque area in sections of the aortic arch. The graph depicts each mouse as a dot, symbolizing its representation. The data is displayed as mean values accompanied by the standard error of the mean. To assess the comparisons between groups D-F, two-sided unpaired Student's t-tests were employed. Separate analyses were conducted for both male and female groups.

In male individuals, a diminished presence of iNOS and CD68-positive plaque macrophages suggested a link between decreased plaque growth and reduced accumulation, proliferation, and inflammatory polarization of macrophages in the aortic roots (Figure 36A-E). The utilization of JD5037 resulted in a decrease in CD80 expression on peritoneal macrophages in both male and female mice, indicating a shift towards a more moderate inflammatory profile (Figure 36F). There are two possible explanations for the variations in the impact of peripheral

CB1 antagonism on plaque and peritoneal macrophages. The first reason is the elevated concentrations of JD5037, which may be specifically existent at the location of peritoneal injection. The second reason is the diverse transcriptomic profiles detected in macrophages derived from different tissues [183].

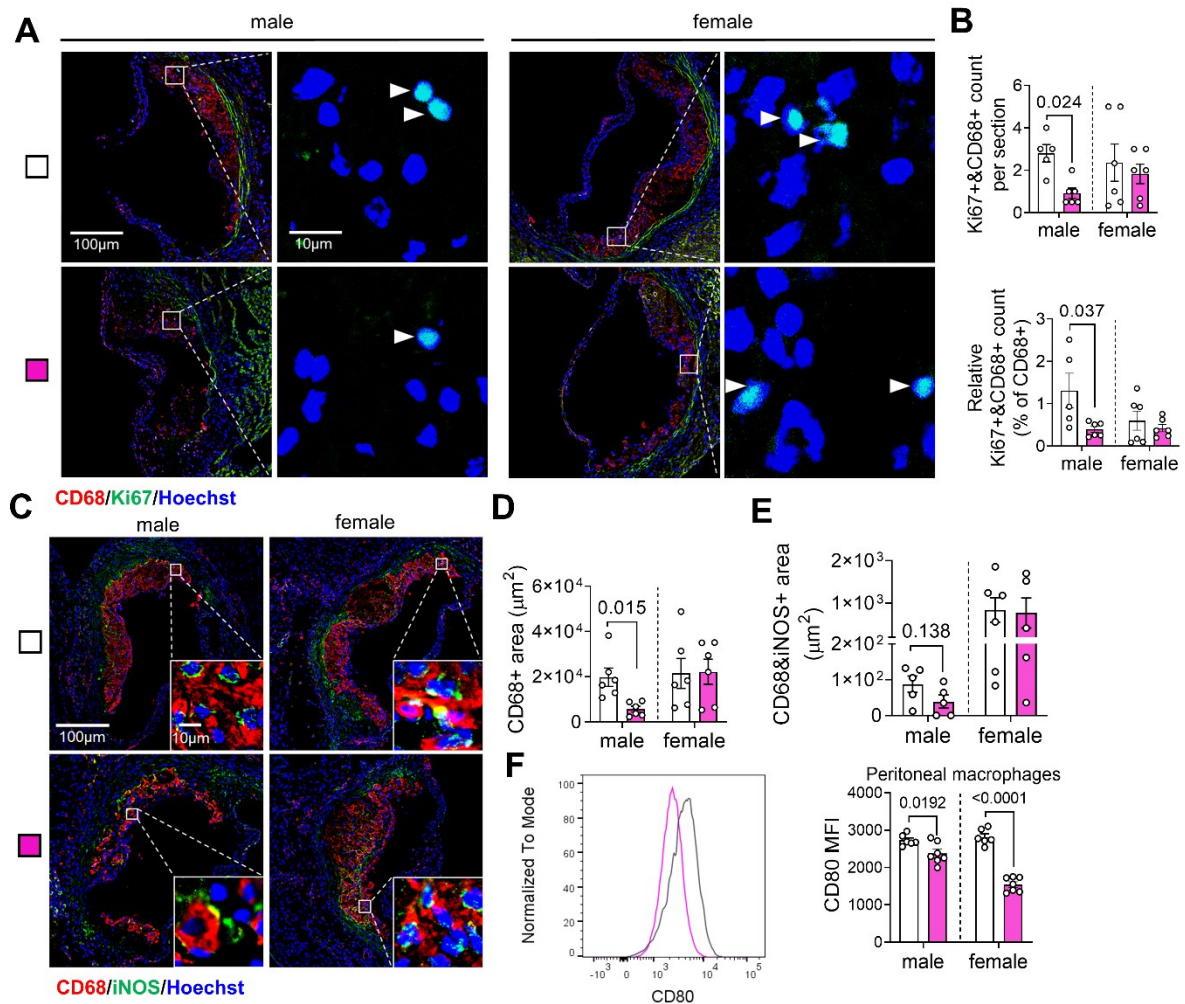


Figure 36: Peripheral CB1 antagonism impact on the advancement of arterial plaque [4].

(A) The provided figures display representative images of macrophages actively proliferating within aortic root plaques. The white arrowheads highlight Ki67+ cells, indicating their role as actively dividing cells, while the CD68+ cells represent macrophages. Nuclei were stained using Hoechst, and scale bars indicating measurements are included: 100 μm (on the left) and 10 μm (on the right). (B) In a subset of five to six mice, the overall and proportional counts of plaque macrophages undergoing proliferation were evaluated. (C-E) Immunostaining was utilized to identify and quantify the presence of iNOS (green) and CD68 (red) macrophages within aortic root lesions of male and female *Ldlr*^{-/-} mice (n=5-6) treated with either a vehicle or JD5037. The nuclei were stained using Hoechst 33342 (blue). The scale bar corresponds to 100 μm (left) and 10 μm (right). (F) The assessment of CD80 expression on peritoneal macrophages was conducted at the study endpoint, involving a sample size of 6-7 mice. The graph depicts each mouse as a dot, symbolizing its representation. The data is displayed as mean values accompanied by the standard error of the mean. To assess the comparisons between groups B, D, E, F and F, two-sided unpaired Student's t-tests were employed. Separate analyses were conducted for both male and female groups.

6. DISCUSSION

6.1 Pleiotropic effects of myeloid cell CB1 signaling in atherosclerosis

In this study, the contribution of myeloid cell CB1 signaling in the context of atherosclerosis has been elucidated, taking advantage of recent progress in targeted genetic depletion and pharmacological blocking techniques. CB1 signaling exhibits pleiotropic effects in various cell types, including circulating monocytes, plaque macrophages, peritoneal macrophages, and *in vitro* cultured BMDMs, thereby exerting a diverse range of actions relevant to atherosclerosis pathophysiology. The processes regulated in monocytes and macrophages encompass recruitment, chemotaxis, proliferation, production of inflammatory cytokines, uptake of oxLDL, and regulation of mitochondrial oxidative respiration. The molecular regulation of this phenomenon seems complex, including p53-dependent transcriptional control, chromatin accessibility, and potentially post-transcriptional mechanisms. The absence of myeloid CB1 in male mice exhibited more pronounced atheroprotective benefits, especially during the initial phases of the disease. Female mice showed a notably smaller advanced-stage plaque, but this distinction was only noticeable in the aortic arch. These findings suggest that the relevance of CB1 signaling on the atherosclerotic phenotype varies with disease stage, arterial location, and sex. Different cellular key players and biological processes are likely to exert distinct influences on the various stages of the disease, exhibiting gender-specific effects that may involve the modulation of sex hormones and other factors. In the initial phases of atherogenesis, the development of plaques is primarily influenced by the recruitment of monocytes and their differentiation into foam cells. In the later stages, the growth of arterial plaques includes macrophage proliferation, apoptosis, the elimination of apoptotic cells, and necroptosis [184, 185]. In this study, female macrophages have been observed to exhibit a slower rate of proliferation compared to male macrophages, possibly due to the suppressive effects of the female sex hormone estradiol on cellular proliferation. This phenomenon has been previously observed in other cell types, including monocytic leukemia cells and vascular smooth muscle cells [186, 187].

6.2 Regulation of cellular cholesterol metabolism and proliferation by CB1

The GSEA findings indicate that signaling of CB1 is involved in the metabolism of cellular cholesterol, which is closely linked to cellular proliferation [188, 189]. The assertion is reinforced by the significant influence of genetic mutations in receptors responsible for cholesterol uptake or efflux on the proliferation of myeloid cells [189, 190]. The bioGRID

repository (<https://orcs.thebiogrid.org/Gene/12801>) contains compelling evidence from CRISPR/Cas screens that substantiates the association between *CNR1* and cell proliferation in human cell lines [191]. In a previous laboratory study conducted *in vitro*, it was observed that synthetic cannabinoids decreased the expression of ABCA1, which is a transporter responsible for the efflux of cholesterol, while simultaneously increasing the expression of CD36, a scavenger receptor responsible for the uptake of modified LDL, in RAW264.7 cells. Pre-treatment with the CB1 antagonist/inverse agonist AM251 significantly inhibited this phenomenon [175]. A causal variant in the *CNR1* promoter associated with high-density lipoprotein cholesterol levels has been discovered through human genetic studies [192]. CB1 signaling has a complex impact on cholesterol metabolism. In this study, male mice lacking the CB1 receptor in macrophages showed a decreased uptake in oxLDL *in vitro* and fewer plaque macrophages containing lipids in the aortic roots after WD *in vivo*. These findings suggest that CB1 regulates macrophage cholesterol metabolism in atherosclerosis.

6.3 Regulation of inflammation, apoptosis and plaque stability by CB1

Furthermore, the production of IL1 β was dampened in BMDMs lacking the CB1 receptor, suggesting a decrease in inflammasome activation. This is consistent with a prior investigation that established a connection between CB1 signaling and the activation of inflammasomes in macrophages within the pancreas [193]. The decreased buildup of cholesterol in plaque macrophages might play a role in promoting a less inflammatory and more stable plaque phenotype. This is because an excessive accumulation of cholesterol hinders macrophages' ability to effectively remove apoptotic cells [37, 194]. The results from the GSEA analysis provide evidence supporting the connection between CB1 activation in macrophages and the upregulation of genes associated with inflammation and cholesterol. The formation of a necrotic core is influenced by compromised removal of apoptotic cells by plaque macrophages, resulting in secondary necrosis, as well as the buildup of extracellular lipids [195]. Advanced lesions can exacerbate inflammation and facilitate the destabilization of plaques through processes known as necroptosis, pyroptosis, and secondary necrosis [196]. The reduced inflammation seen in *Cnr1*-deficient macrophages corresponds to smaller necrotic plaques in *ApoE*^{-/-}*LysMCre*^{+/-} *Cnr1*^{flox/flox} mice.

6.4 The absence of myeloid *Cnr1* is linked to changes in p53 and cyclin dependent kinase activity

In response to CB1 agonist stimulation *in vitro*, the kinase profiling array revealed changes in the function of p53 and several cyclin-dependent kinases. These kinases are well-known for

their involvement in the control of the cell cycle. [197]. This suggests that p53 might act as a transcriptional regulator for these genes, influencing their expression levels and consequently affecting cell cycle progression [198, 199]. Furthermore, modulation of nuclear translocation through CB1 agonism or antagonism had an additional impact on the transcriptional regulation of these target genes, implying a potential crosstalk between the p53 pathway and the endocannabinoid system. An earlier experimental investigation on diet-induced hepatic steatosis reported an association between CB1 and p53 function [200]. In our mouse model lacking myeloid *Cnr1*, p53-mediated transcriptional regulation and epigenetic mechanisms could play a crucial role. Prior research connects p53 to macrophage recruitment and proliferation, as well as reducing necrotic core size [201-203]. Additionally, recent discoveries have revealed that clonal hematopoiesis mediated by TP53 increases the risk for the development of atherosclerotic disease [204]. At the same time, the identified target genes relevant to CDK and cell cycle regulation hold promise as potential therapeutic targets for conditions where dysregulated cell cycle progression is a hallmark, including cancer as well as cardiovascular disease [205, 206].

6.5 CB1 regulates the expression of chemokines and chemokine receptors

The here provided evidence obtained from protein and mRNA analysis strongly supports a direct CB1-mediated regulation of CCR1 and CCR5 chemokine receptor expression. CB1 agonist stimulation was used to validate the regulation of *Ccr5* by CB1 through bulk RNA sequencing of bone marrow-derived macrophages. *Mif* and *Cd74* were prominent DEGs regulated by CB1, with CD74 being a cognate MIF receptor. MIF is an inflammatory cytokine and an atypical chemokine that differs from conventional chemokines due to the absence of conserved cysteines and a characteristic chemokine molecular structure [181]. In the context of atherosclerosis, increased MIF expression contributes to the augmentation of leukocyte recruitment and vascular inflammation by interacting with specific chemokine receptors. These receptors include CXCR2, CXCR4, CD74, and ACKR3, which collectively facilitate the enhanced recruitment of atherogenic leukocytes and contribute to the inflammatory process within the vasculature [181]. CD74, also referred to as the MHC class II invariant chain, plays a crucial role in various immunological processes, impacting cancer cell proliferation through its interaction as a high-affinity receptor for MIF [207].

6.6 Role of macrophage CB1 in mitochondrial regulation and metabolism

The GO analysis revealed changes in mitochondrial ATP production, which were validated

through metabolic measurements. Pro-inflammatory macrophage polarization reduces oxidative respiration [208], while CB1 antagonism partially counteracts this effect. This suggests that LPS triggers an acute release of endocannabinoids by the macrophages, which activate their own CB1 receptors [209]. However, in comparison to LPS, the impact of the synthetic CB1 agonist ACEA on macrophage mitochondrial respiration is relatively moderate. This implies that the exogenous stimulation of CB1 alone is inadequate to trigger metabolic reprogramming in macrophages, suggesting that the exogenous agonist exerts a less important influence on mitochondrial metabolism in comparison to the endogenous ligands generated as a result of LPS stimulation. In this context, it is interesting to highlight that there exists a connection between CB1 receptors found in the mitochondria of neurons and the regulation of energy metabolism in these cells [210]. However, the lack of specific antibodies currently hampers the detection of CB1 protein, raising the question of whether mitochondrial CB1 signaling affects macrophage metabolism. Further studies are needed to address this issue.

6.7 Long-term treatment with a peripheral CB1 antagonist suppresses plaque macrophage build-up, proliferation, and inflammatory polarization

In a mouse model of atherosclerosis, the pharmacological inhibition of CB1 receptors in peripheral tissues had various anti-inflammatory and metabolic effects. The anti-atherogenic effects are likely diverse and cannot be exclusively attributed to their impact on myeloid cells. The observed protective effects could be partly ascribed to the reduction in cholesterol levels and its potential impact on other crucial cellular factors implicated in the advancement of atherosclerosis. The current study focused on the effects of prolonged administration of a peripheral CB1 antagonist on cellular outcomes in atherosclerotic mice. In agreement with the findings in the myeloid cell-specific genetic *Cnr1* deficiency model, pharmacological antagonism of peripheral CB1 receptors could replicate the suppressive effects on the accumulation, proliferation, and inflammatory polarization of plaque macrophages.

6.8 Inverse correlation between *CNR1* and crucial cellular pathways in the pathophysiology of human atherosclerosis

An intriguing discovery arose during the regression analysis conducted on the transcriptomic plaque data obtained from patients who underwent CEA. An intriguing and noteworthy inverse correlation was found between the expression of *CNR1* and multiple markers linked to cell proliferation, oxidative phosphorylation, and diverse inflammatory genes. The presence of these connections suggests a strong link between CB1 and vital cellular pathways associated

with the formation of human plaque, implying a noteworthy correlation. Contrary to expectations, the mouse model and *in vitro* experiments conducted with murine BMDMs revealed unexpected inverse associations. These findings challenge the assumed CB1-dependent mechanism that was anticipated to promote macrophage proliferation and the emergence of an inflammatory phenotype. It is important to highlight that the assessment of *CNR1* transcript levels in human plaques relied on the analysis of bulk RNAseq data from the entire plaque. Therefore, depending exclusively on this approach might not yield an accurate representation of *CNR1* expression in macrophages. The expression levels of *CNR1* in the plaque are ultimately shaped by a collective influence from different cell types, such as endothelial cells and smooth muscle cells, thereby determining the overall *CNR1* expression profile [211, 212]. Moreover, it is conceivable that continual activation of CB1 receptors in inflamed plaques could suppress gene expression, potentially resulting from receptor desensitization induced by prolonged elevation of endocannabinoid levels. Extended inhibition of the metabolizing enzyme monoacylglycerol lipase has been observed to cause this phenomenon in mice [213]. Furthermore, an extensive investigation exploring the human genome has brought to light a notable modification within a fundamental DNA component called a single nucleotide polymorphism [214]. The majority of genomic alteration data related to the ECS pertains to the CB1 receptors, with various polymorphisms identified in *CNR1*, including but not limited to rs10498963, rs884647, rs75205693, rs6933130, rs147997421, and rs202070651, among a total of over 10,000 [215]. Numerous studies have investigated the involvement of various SNPs in *CNR1* across multiple disorders. For instance, an examination of regular cigarette smokers indicated that the C allele variant of rs2023239 exhibited reduced nicotine reinforcement, implying the significance of this SNP in the context of nicotine dependence [216]. A compelling instance involves a study that examined SNPs in *CNR1* in relation to personality traits, linking rs806372 and rs2180619 to extraversion [217]. These genetic variations have been associated with the phenomenon of DNA methylation [214].

6.9 Limitations of this study

Our main research focus involved studying the molecular effects of CB1 in monocytes and macrophages, without considering the potential involvement of CB1 signaling in neutrophils. Therefore, the observed atheroprotective properties seen in our mouse model, in which myeloid *Cnr1* is inhibited, may be ascribed, to some extent, to the absence of CB1 signaling in neutrophils. In mice lacking myeloid CB1, no changes were detected in the surface presentation of CXCR2 on neutrophils. After four weeks of WD, the immunostaining analysis of plaque-associated neutrophils showed no discernible difference between the various genotypes examined. Additional investigation is required to further explore the sex-specific

differences in macrophage phenotypes, as evident in experimental atherosclerosis studies and *in vitro* studies involving BMDMs. Furthermore, it is imperative to conduct thorough investigations in order to comprehend the intricate mechanisms behind sex differences, including whether male estrogen receptor expression is affected by CB1. At the same time, to clearly confirm that estrogen is involved in this sex difference, experiments should be performed in ovariectomized mice, whose phenotype should shift toward a male phenotype. To adequately investigate this, a possibility is to engage in the examination of suitable experimental models, such as the mouse model known as the "four core genotypes" (FCG) [218]. In the future, it is crucial to allocate greater focus to the examination of sex-specific dimorphism in clinical research. In our *in vitro* studies, we did not use human blood or macrophages differentiated from human blood, but instead used BMDMs from mice. This is another limitation of our thorough *in vitro* studies.

6.10 Conclusion and future perspectives

To summarize, the inhibition of CB1 signaling in monocytes and macrophages has demonstrated several beneficial effects in the prevention of atherosclerosis. Some benefits of this approach comprise the following: diminished recruitment of monocytes to atherosclerotic plaques, limiting proliferation of plaque macrophages, decreased secretion of inflammatory cytokines and uptake of oxLDL, and improved mitochondrial oxidative respiration through the inhibition or genetic depletion of CB1 receptors. The biological function of CB1 signaling in murine macrophages reveals sex-specific disparities, suggesting that myeloid CB1 receptors play a more prominent role in promoting atherosclerosis in male mice, while their impact appears to be less significant in female mice. Considering biological sex as a significant factor in preclinical studies holds utmost importance. Further investigation is required to fully understand the clinical importance of the potential sex-specific influence of CB1 signaling in monocytes and macrophages.

7. REFERENCES

1. Yang, J.F., et al., *Binding Modes and Selectivity of Cannabinoid 1 (CB1) and Cannabinoid 2 (CB2) Receptor Ligands*. ACS Chem Neurosci, 2020. **11**(20): p. 3455-3463.
2. Cahill, P.A. and E.M. Redmond, *Vascular endothelium - Gatekeeper of vessel health*. Atherosclerosis, 2016. **248**: p. 97-109.
3. Guillamat-Prats, R., et al., *Endocannabinoid Signalling in Atherosclerosis and Related Metabolic Complications*. Thromb Haemost, 2019. **119**(4): p. 567-575.
4. Yong, W., et al., *Loss of myeloid cannabinoid CB1 receptor confers atheroprotection by reducing macrophage proliferation and immunometabolic reprogramming*. BioRxiv preprint, 2023.
5. Tavafi, M., *Complexity of diabetic nephropathy pathogenesis and design of investigations*. Journal of renal injury prevention, 2013. **2**(2): p. 59.
6. Kume, N., M. Cybulsky, and M. Gimbrone, *Lysophosphatidylcholine, a component of atherogenic lipoproteins, induces mononuclear leukocyte adhesion molecules in cultured human and rabbit arterial endothelial cells*. The Journal of clinical investigation, 1992. **90**(3): p. 1138-1144.
7. Steinbrecher, U.P., et al., *Modification of low density lipoprotein by endothelial cells involves lipid peroxidation and degradation of low density lipoprotein phospholipids*. Proceedings of the National Academy of Sciences, 1984. **81**(12): p. 3883-3887.
8. Rafieian-Kopaei, M., et al., *Atherosclerosis: process, indicators, risk factors and new hopes*. Int J Prev Med, 2014. **5**(8): p. 927-46.
9. WHO, *Cardiovascular diseases (CVDs)*. Retrieved March 21, 2023.
10. Libby, P., P.M. Ridker, and G.K. Hansson, *Progress and challenges in translating the biology of atherosclerosis*. Nature, 2011. **473**(7347): p. 317-25.
11. Frostegård, J., *Immunity, atherosclerosis and cardiovascular disease*. BMC Med, 2013. **11**: p. 117.
12. Libby, P., et al., *Atherosclerosis*. Nat Rev Dis Primers, 2019. **5**(1): p. 56.
13. Zaragoza, C., et al., *Animal models of cardiovascular diseases*. J Biomed Biotechnol, 2011. **2011**: p. 497841.
14. Tsang, H.G., et al., *Large animal models of cardiovascular disease*. Cell

- Biochem Funct, 2016. **34**(3): p. 113-32.
15. Wu, M.Y., et al., *New Insights into the Role of Inflammation in the Pathogenesis of Atherosclerosis*. Int J Mol Sci, 2017. **18**(10).
 16. Zhang, C., C.L. Franklin, and A.C. Ericsson, *Consideration of Gut Microbiome in Murine Models of Diseases*. Microorganisms, 2021. **9**(5).
 17. Fernandez, D.M. and C. Giannarelli, *Immune cell profiling in atherosclerosis: role in research and precision medicine*. Nat Rev Cardiol, 2022. **19**(1): p. 43-58.
 18. Shen, X., et al., *Gut Microbiota and Atherosclerosis-Focusing on the Plaque Stability*. Front Cardiovasc Med, 2021. **8**: p. 668532.
 19. Williams, J.W., et al., *Single Cell RNA Sequencing in Atherosclerosis Research*. Circ Res, 2020. **126**(9): p. 1112-1126.
 20. Eberhardt, N. and C. Giannarelli, *How Single-Cell Technologies Have Provided New Insights Into Atherosclerosis*. Arterioscler Thromb Vasc Biol, 2022. **42**(3): p. 243-252.
 21. Li, J., et al., *Intravascular Imaging of Atherosclerosis by Using Engineered Nanoparticles*. Biosensors (Basel), 2023. **13**(3).
 22. *2019 ESC/EAS guidelines for the management of dyslipidaemias: Lipid modification to reduce cardiovascular risk*. Atherosclerosis, 2019. **290**: p. 140-205.
 23. Lee, Y.T., et al., *Mouse models of atherosclerosis: a historical perspective and recent advances*. Lipids Health Dis, 2017. **16**(1): p. 12.
 24. Mozaffarian, D., et al., *Heart Disease and Stroke Statistics-2016 Update: A Report From the American Heart Association*. Circulation, 2016. **133**(4): p. e38-360.
 25. Lusis, A.J., *Atherosclerosis*. Nature, 2000. **407**(6801): p. 233-41.
 26. Brinks, J., et al., *Lifestyle Modification in Secondary Prevention: Beyond Pharmacotherapy*. Am J Lifestyle Med, 2017. **11**(2): p. 137-152.
 27. Tavakol, M., S. Ashraf, and S.J. Brener, *Risks and complications of coronary angiography: a comprehensive review*. Glob J Health Sci, 2012. **4**(1): p. 65-93.
 28. Wang, T. and J. Butany, *Pathogenesis of atherosclerosis*. Diagnostic histopathology, 2017. **23**(11): p. 473-478.
 29. Sandoo, A., et al., *The endothelium and its role in regulating vascular tone*. Open Cardiovasc Med J, 2010. **4**: p. 302-12.

30. Mussbacher, M., et al., *More than Just a Monolayer: the Multifaceted Role of Endothelial Cells in the Pathophysiology of Atherosclerosis*. *Curr Atheroscler Rep*, 2022. **24**(6): p. 483-492.
31. Schwartz, S.M., R. Virmani, and M.E. Rosenfeld, *The good smooth muscle cells in atherosclerosis*. *Current atherosclerosis reports*, 2000. **2**(5): p. 422-429.
32. Bennett, M.R., S. Sinha, and G.K. Owens, *Vascular Smooth Muscle Cells in Atherosclerosis*. *Circ Res*, 2016. **118**(4): p. 692-702.
33. Allahverdian, S., et al., *Smooth muscle cell fate and plasticity in atherosclerosis*. *Cardiovasc Res*, 2018. **114**(4): p. 540-550.
34. Swirski, F.K. and M. Nahrendorf, *Leukocyte behavior in atherosclerosis, myocardial infarction, and heart failure*. *Science*, 2013. **339**(6116): p. 161-6.
35. Osterud, B. and E. Bjorklid, *Role of monocytes in atherogenesis*. *Physiol Rev*, 2003. **83**(4): p. 1069-112.
36. Kunjathoor, V.V., et al., *Scavenger receptors class A-I/II and CD36 are the principal receptors responsible for the uptake of modified low density lipoprotein leading to lipid loading in macrophages*. *J Biol Chem*, 2002. **277**(51): p. 49982-8.
37. Moore, K.J., F.J. Sheedy, and E.A. Fisher, *Macrophages in atherosclerosis: a dynamic balance*. *Nat Rev Immunol*, 2013. **13**(10): p. 709-21.
38. Glass, C.K. and J.L. Witztum, *Atherosclerosis: the road ahead*. *Cell*, 2001. **104**(4): p. 503-516.
39. Lewis, G.F. and D.J. Rader, *New insights into the regulation of HDL metabolism and reverse cholesterol transport*. *Circulation research*, 2005. **96**(12): p. 1221-1232.
40. Nissen, S.E., et al., *Effect of recombinant ApoA-I Milano on coronary atherosclerosis in patients with acute coronary syndromes: a randomized controlled trial*. *Jama*, 2003. **290**(17): p. 2292-2300.
41. Cabral-Pacheco, G.A., et al., *The Roles of Matrix Metalloproteinases and Their Inhibitors in Human Diseases*. *Int J Mol Sci*, 2020. **21**(24).
42. Ley, K., Y.I. Miller, and C.C. Hedrick, *Monocyte and macrophage dynamics during atherogenesis*. *Arterioscler Thromb Vasc Biol*, 2011. **31**(7): p. 1506-16.
43. Koltsova, E.K., C.C. Hedrick, and K. Ley, *Myeloid cells in atherosclerosis: a delicate balance of anti-inflammatory and proinflammatory mechanisms*. *Curr Opin Lipidol*, 2013. **24**(5): p. 371-80.

44. Chistiakov, D.A., et al., *The role of monocytosis and neutrophilia in atherosclerosis*. J Cell Mol Med, 2018. **22**(3): p. 1366-1382.
45. Tedgui, A. and Z. Mallat, *Cytokines in atherosclerosis: pathogenic and regulatory pathways*. Physiol Rev, 2006. **86**(2): p. 515-81.
46. Ait-Oufella, H., et al., *Recent advances on the role of cytokines in atherosclerosis*. Arterioscler Thromb Vasc Biol, 2011. **31**(5): p. 969-79.
47. Ilhan, F. and S.T. Kalkanli, *Atherosclerosis and the role of immune cells*. World J Clin Cases, 2015. **3**(4): p. 345-52.
48. Chistiakov, D.A., et al., *Immune-Inflammatory Responses in Atherosclerosis: The Role of Myeloid Cells*. J Clin Med, 2019. **8**(11).
49. Kang, H., et al., *The Entry and Egress of Monocytes in Atherosclerosis: A Biochemical and Biomechanical Driven Process*. Cardiovasc Ther, 2021. **2021**: p. 6642927.
50. Hilgendorf, I., F.K. Swirski, and C.S. Robbins, *Monocyte fate in atherosclerosis*. Arterioscler Thromb Vasc Biol, 2015. **35**(2): p. 272-9.
51. Randolph, G.J., *The fate of monocytes in atherosclerosis*. J Thromb Haemost, 2009. **7 Suppl 1**(Suppl 1): p. 28-30.
52. Wolf, A.A., et al., *The Ontogeny of Monocyte Subsets*. Front Immunol, 2019. **10**: p. 1642.
53. Mehu, M., C.A. Narasimhulu, and D.K. Singla, *Inflammatory Cells in Atherosclerosis*. Antioxidants (Basel), 2022. **11**(2).
54. Moore, K.J., et al., *Macrophage Trafficking, Inflammatory Resolution, and Genomics in Atherosclerosis: JACC Macrophage in CVD Series (Part 2)*. J Am Coll Cardiol, 2018. **72**(18): p. 2181-2197.
55. Lorey, M.B., K. Öörni, and P.T. Kovanen, *Modified Lipoproteins Induce Arterial Wall Inflammation During Atherogenesis*. Front Cardiovasc Med, 2022. **9**: p. 841545.
56. Gui, Y., H. Zheng, and R.Y. Cao, *Foam Cells in Atherosclerosis: Novel Insights Into Its Origins, Consequences, and Molecular Mechanisms*. Front Cardiovasc Med, 2022. **9**: p. 845942.
57. Arango Duque, G. and A. Descoteaux, *Macrophage cytokines: involvement in immunity and infectious diseases*. Front Immunol, 2014. **5**: p. 491.
58. Shapouri-Moghaddam, A., et al., *Macrophage plasticity, polarization, and function in health and disease*. J Cell Physiol, 2018. **233**(9): p. 6425-6440.

59. Tong, Y., et al., *The Research Progress of Vascular Macrophages and Atherosclerosis*. Oxid Med Cell Longev, 2020. **2020**: p. 7308736.
60. Farahi, L., S.K. Sinha, and A.J. Lusis, *Roles of Macrophages in Atherogenesis*. Front Pharmacol, 2021. **12**: p. 785220.
61. Robbins, C.S., et al., *Local proliferation dominates lesional macrophage accumulation in atherosclerosis*. Nat Med, 2013. **19**(9): p. 1166-72.
62. Tang, J., et al., *Inhibiting macrophage proliferation suppresses atherosclerotic plaque inflammation*. Sci Adv, 2015. **1**(3).
63. Flynn, M.C., et al., *Monocytes, Macrophages, and Metabolic Disease in Atherosclerosis*. Front Pharmacol, 2019. **10**: p. 666.
64. Rosales, C., *Neutrophil: A Cell with Many Roles in Inflammation or Several Cell Types?* Front Physiol, 2018. **9**: p. 113.
65. Lehman, H.K. and B.H. Segal, *The role of neutrophils in host defense and disease*. J Allergy Clin Immunol, 2020. **145**(6): p. 1535-1544.
66. Gencer, S., et al., *Inflammatory Chemokines in Atherosclerosis*. Cells, 2021. **10**(2).
67. Irwandi, R.A., et al., *The Roles of Neutrophils Linking Periodontitis and Atherosclerotic Cardiovascular Diseases*. Front Immunol, 2022. **13**: p. 915081.
68. Mittal, M., et al., *Reactive oxygen species in inflammation and tissue injury*. Antioxid Redox Signal, 2014. **20**(7): p. 1126-67.
69. Döring, Y., O. Soehnlein, and C. Weber, *Neutrophil Extracellular Traps in Atherosclerosis and Atherothrombosis*. Circ Res, 2017. **120**(4): p. 736-743.
70. Thålin, C., et al., *Neutrophil Extracellular Traps: Villains and Targets in Arterial, Venous, and Cancer-Associated Thrombosis*. Arterioscler Thromb Vasc Biol, 2019. **39**(9): p. 1724-1738.
71. Ding, Y., N. Song, and Y. Luo, *Role of bone marrow-derived cells in angiogenesis: focus on macrophages and pericytes*. Cancer Microenviron, 2012. **5**(3): p. 225-36.
72. Shi, C. and E.G. Pamer, *Monocyte recruitment during infection and inflammation*. Nat Rev Immunol, 2011. **11**(11): p. 762-74.
73. Xu, H., et al., *Vascular Macrophages in Atherosclerosis*. J Immunol Res, 2019. **2019**: p. 4354786.
74. Björkegren, J.L.M. and A.J. Lusis, *Atherosclerosis: Recent developments*. Cell, 2022. **185**(10): p. 1630-1645.

75. Frangie, C. and J. Daher, *Role of myeloperoxidase in inflammation and atherosclerosis (Review)*. Biomed Rep, 2022. **16**(6): p. 53.
76. Nilsson, J., G.K. Hansson, and P.K. Shah, *Immunomodulation of Atherosclerosis: Implications for Vaccine Development—ATVB In Focus*. Arteriosclerosis, thrombosis, and vascular biology, 2005. **25**(1): p. 18-28.
77. Hansson, G.K., *Inflammation, atherosclerosis, and coronary artery disease*. New England journal of medicine, 2005. **352**(16): p. 1685-1695.
78. Bentzon, J.F., et al., *Mechanisms of plaque formation and rupture*. Circ Res, 2014. **114**(12): p. 1852-66.
79. Olzmann, J.A. and P. Carvalho, *Dynamics and functions of lipid droplets*. Nat Rev Mol Cell Biol, 2019. **20**(3): p. 137-155.
80. Nadkarni, S.K., et al., *Measurement of fibrous cap thickness in atherosclerotic plaques by spatiotemporal analysis of laser speckle images*. J Biomed Opt, 2006. **11**(2): p. 021006.
81. Libby, P., *Inflammation during the life cycle of the atherosclerotic plaque*. Cardiovasc Res, 2021. **117**(13): p. 2525-2536.
82. Guyton, J.R. and K.F. Klemp, *Development of the lipid-rich core in human atherosclerosis*. Arterioscler Thromb Vasc Biol, 1996. **16**(1): p. 4-11.
83. Thim, T., et al., *From vulnerable plaque to atherothrombosis*. J Intern Med, 2008. **263**(5): p. 506-16.
84. Martinet, W., D.M. Schrijvers, and G.R. De Meyer, *Pharmacological modulation of cell death in atherosclerosis: a promising approach towards plaque stabilization?* Br J Pharmacol, 2011. **164**(1): p. 1-13.
85. Tabas, I., *Macrophage apoptosis in atherosclerosis: consequences on plaque progression and the role of endoplasmic reticulum stress*. Antioxid Redox Signal, 2009. **11**(9): p. 2333-9.
86. Schrijvers, D.M., et al., *Phagocytosis of apoptotic cells by macrophages is impaired in atherosclerosis*. Arterioscler Thromb Vasc Biol, 2005. **25**(6): p. 1256-61.
87. Newby, A.C., et al., *Vulnerable atherosclerotic plaque metalloproteinases and foam cell phenotypes*. Thromb Haemost, 2009. **101**(6): p. 1006-11.
88. Kong, P., et al., *Inflammation and atherosclerosis: signaling pathways and therapeutic intervention*. Signal Transduct Target Ther, 2022. **7**(1): p. 131.
89. Tedgui, A. and Z. Mallat, *Apoptosis, a major determinant of atherothrombosis*.

- Arch Mal Coeur Vaiss, 2003. **96**(6): p. 671-5.
90. Bennett, M.R., *Apoptosis of vascular smooth muscle cells in vascular remodelling and atherosclerotic plaque rupture*. Cardiovasc Res, 1999. **41**(2): p. 361-8.
 91. Libby, P., et al., *Reassessing the Mechanisms of Acute Coronary Syndromes*. Circ Res, 2019. **124**(1): p. 150-160.
 92. Quillard, T., et al., *Mechanisms of erosion of atherosclerotic plaques*. Curr Opin Lipidol, 2017. **28**(5): p. 434-441.
 93. Manduteanu, I. and M. Simionescu, *Inflammation in atherosclerosis: a cause or a result of vascular disorders?* J Cell Mol Med, 2012. **16**(9): p. 1978-90.
 94. Seegers, L.M., et al., *Sex Differences in Culprit Plaque Characteristics Among Different Age Groups in Patients With Acute Coronary Syndromes*. Circ Cardiovasc Interv, 2022. **15**(6): p. e011612.
 95. Sun, H., et al., *In vivo detection of plaque erosion by intravascular optical coherence tomography using artificial intelligence*. Biomed Opt Express, 2022. **13**(7): p. 3922-3938.
 96. Mushenkova, N.V., et al., *Current Advances in the Diagnostic Imaging of Atherosclerosis: Insights into the Pathophysiology of Vulnerable Plaque*. Int J Mol Sci, 2020. **21**(8).
 97. Golfaroush, P., D.M. Yellon, and S.M. Davidson, *Mouse models of atherosclerosis and their suitability for the study of myocardial infarction*. Basic Res Cardiol, 2020. **115**(6): p. 73.
 98. Gisterå, A., et al., *Animal Models of Atherosclerosis-Supportive Notes and Tricks of the Trade*. Circ Res, 2022. **130**(12): p. 1869-1887.
 99. Véniant, M.M., S. Withycombe, and S.G. Young, *Lipoprotein size and atherosclerosis susceptibility in Apoe(-/-) and Ldlr(-/-) mice*. Arterioscler Thromb Vasc Biol, 2001. **21**(10): p. 1567-70.
 100. Getz, G.S. and C.A. Reardon, *Animal models of atherosclerosis*. Arterioscler Thromb Vasc Biol, 2012. **32**(5): p. 1104-15.
 101. Calleja, L., et al., *Low-cholesterol and high-fat diets reduce atherosclerotic lesion development in ApoE-knockout mice*. Arterioscler Thromb Vasc Biol, 1999. **19**(10): p. 2368-75.
 102. Aparicio-Vergara, M., et al., *Bone marrow transplantation in mice as a tool for studying the role of hematopoietic cells in metabolic and cardiovascular*

- diseases. *Atherosclerosis*, 2010. **213**(2): p. 335-44.
103. Herijgers, N., et al., *Effect of bone marrow transplantation on lipoprotein metabolism and atherosclerosis in LDL receptor-knockout mice*. *Arterioscler Thromb Vasc Biol*, 1997. **17**(10): p. 1995-2003.
 104. Lee, H., *Genetically engineered mouse models for drug development and preclinical trials*. *Biomol Ther (Seoul)*, 2014. **22**(4): p. 267-74.
 105. Khan, A.W., F. Paneni, and K.A.M. Jandeleit-Dahm, *Cell-specific epigenetic changes in atherosclerosis*. *Clin Sci (Lond)*, 2021. **135**(9): p. 1165-1187.
 106. Zhang, S.H., et al., *Spontaneous hypercholesterolemia and arterial lesions in mice lacking apolipoprotein E*. *Science*, 1992. **258**(5081): p. 468-71.
 107. Lo Sasso, G., et al., *The Apoe(-/-) mouse model: a suitable model to study cardiovascular and respiratory diseases in the context of cigarette smoke exposure and harm reduction*. *J Transl Med*, 2016. **14**(1): p. 146.
 108. Poznyak, A.V., et al., *Animal models of human atherosclerosis: current progress*. *Braz J Med Biol Res*, 2020. **53**(6): p. e9557.
 109. Huang, Y. and R.W. Mahley, *Apolipoprotein E: structure and function in lipid metabolism, neurobiology, and Alzheimer's diseases*. *Neurobiol Dis*, 2014. **72 Pt A**: p. 3-12.
 110. Hauser, P.S., V. Narayanaswami, and R.O. Ryan, *Apolipoprotein E: from lipid transport to neurobiology*. *Prog Lipid Res*, 2011. **50**(1): p. 62-74.
 111. Chang, T.Y., et al., *Cellular cholesterol homeostasis and Alzheimer's disease*. *J Lipid Res*, 2017. **58**(12): p. 2239-2254.
 112. Husain, M.A., B. Laurent, and M. Plourde, *APOE and Alzheimer's Disease: From Lipid Transport to Physiopathology and Therapeutics*. *Front Neurosci*, 2021. **15**: p. 630502.
 113. Blanchard, J.W., et al., *APOE4 impairs myelination via cholesterol dysregulation in oligodendrocytes*. *Nature*, 2022. **611**(7937): p. 769-779.
 114. Meir, K.S. and E. Leitersdorf, *Atherosclerosis in the apolipoprotein-E-deficient mouse: a decade of progress*. *Arterioscler Thromb Vasc Biol*, 2004. **24**(6): p. 1006-14.
 115. Getz, G.S. and C.A. Reardon, *Do the Apoe-/- and Ldlr-/- Mice Yield the Same Insight on Atherogenesis?* *Arterioscler Thromb Vasc Biol*, 2016. **36**(9): p. 1734-41.
 116. Y Nakashima, A.S.P., E W Raines, J L Breslow and R Ross, *ApoE-deficient*

- mice develop lesions of all phases of atherosclerosis throughout the arterial tree. Arteriosclerosis and Thrombosis: A Journal of Vascular Biology, 1994. 14(1): p. 133-140.*
117. Goldstein, J.L. and M.S. Brown, *The LDL receptor. Arterioscler Thromb Vasc Biol, 2009. 29(4): p. 431-8.*
 118. Harisa, G.I. and F.K. Alanazi, *Low density lipoprotein bionanoparticles: From cholesterol transport to delivery of anti-cancer drugs. Saudi Pharm J, 2014. 22(6): p. 504-15.*
 119. Bouhairie, V.E. and A.C. Goldberg, *Familial hypercholesterolemia. Cardiol Clin, 2015. 33(2): p. 169-79.*
 120. Ma, Y., et al., *Hyperlipidemia and atherosclerotic lesion development in Ldlr-deficient mice on a long-term high-fat diet. PLoS One, 2012. 7(4): p. e35835.*
 121. Oppi, S., T.F. Lüscher, and S. Stein, *Mouse Models for Atherosclerosis Research-Which Is My Line? Front Cardiovasc Med, 2019. 6: p. 46.*
 122. Libby, P. and B.M. Everett, *Novel Antiatherosclerotic Therapies. Arterioscler Thromb Vasc Biol, 2019. 39(4): p. 538-545.*
 123. Rabino, M., et al., *The Endocannabinoid System and Cannabidiol: Past, Present, and Prospective for Cardiovascular Diseases. Pharmaceuticals (Basel), 2021. 14(9).*
 124. Pacher, P. and G. Kunos, *Modulating the endocannabinoid system in human health and disease--successes and failures. Febs j, 2013. 280(9): p. 1918-43.*
 125. Zou, S. and U. Kumar, *Cannabinoid Receptors and the Endocannabinoid System: Signaling and Function in the Central Nervous System. Int J Mol Sci, 2018. 19(3).*
 126. Lu, H.C. and K. Mackie, *Review of the Endocannabinoid System. Biol Psychiatry Cogn Neurosci Neuroimaging, 2021. 6(6): p. 607-615.*
 127. Wilhelmsen, K., et al., *The endocannabinoid/endovanilloid N-arachidonoyl dopamine (NADA) and synthetic cannabinoid WIN55,212-2 abate the inflammatory activation of human endothelial cells. J Biol Chem, 2014. 289(19): p. 13079-100.*
 128. Guindon, J. and A.G. Hohmann, *The endocannabinoid system and pain. CNS Neurol Disord Drug Targets, 2009. 8(6): p. 403-21.*
 129. McKinney, M.K. and B.F. Cravatt, *Structure and function of fatty acid amide hydrolase. Annu Rev Biochem, 2005. 74: p. 411-32.*

130. Basavarajappa, B.S., *Critical enzymes involved in endocannabinoid metabolism*. Protein Pept Lett, 2007. **14**(3): p. 237-46.
131. Hourani, W. and S.P.H. Alexander, *Cannabinoid ligands, receptors and enzymes: Pharmacological tools and therapeutic potential*. Brain Neurosci Adv, 2018. **2**: p. 2398212818783908.
132. Biringer, R.G., *Endocannabinoid signaling pathways: beyond CB1R and CB2R*. J Cell Commun Signal, 2021. **15**(3): p. 335-360.
133. Morales, P. and P.H. Reggio, *An Update on Non-CB(1), Non-CB(2) Cannabinoid Related G-Protein-Coupled Receptors*. Cannabis Cannabinoid Res, 2017. **2**(1): p. 265-273.
134. An, D., et al., *Targeting Cannabinoid Receptors: Current Status and Prospects of Natural Products*. Int J Mol Sci, 2020. **21**(14).
135. Mach, F. and S. Steffens, *The role of the endocannabinoid system in atherosclerosis*. J Neuroendocrinol, 2008. **20 Suppl 1**: p. 53-7.
136. Howlett, A.C., L.C. Blume, and G.D. Dalton, *CB(1) cannabinoid receptors and their associated proteins*. Curr Med Chem, 2010. **17**(14): p. 1382-93.
137. Rajesh, M., et al., *Cannabinoid-1 receptor activation induces reactive oxygen species-dependent and -independent mitogen-activated protein kinase activation and cell death in human coronary artery endothelial cells*. Br J Pharmacol, 2010. **160**(3): p. 688-700.
138. Rajesh, M., et al., *Cannabinoid CB1 receptor inhibition decreases vascular smooth muscle migration and proliferation*. Biochem Biophys Res Commun, 2008. **377**(4): p. 1248-52.
139. Dol-Gleizes, F., et al., *Rimonabant, a selective cannabinoid CB1 receptor antagonist, inhibits atherosclerosis in LDL receptor-deficient mice*. Arterioscler Thromb Vasc Biol, 2009. **29**(1): p. 12-8.
140. Nguyen, T., et al., *Allosteric Modulation: An Alternate Approach Targeting the Cannabinoid CB1 Receptor*. Med Res Rev, 2017. **37**(3): p. 441-474.
141. Cinar, R., M.R. Iyer, and G. Kunos, *The therapeutic potential of second and third generation CB(1)R antagonists*. Pharmacol Ther, 2020. **208**: p. 107477.
142. Stasiulewicz, A., et al., *A Guide to Targeting the Endocannabinoid System in Drug Design*. Int J Mol Sci, 2020. **21**(8).
143. Stasiulewicz, A., et al., *Identification of CB1 Ligands among Drugs, Phytochemicals and Natural-Like Compounds: Virtual Screening and In Vitro*

- Verification*. ACS Chemical Neuroscience, 2022. **13**(20): p. 2991-3007.
144. Lu, D., et al., *Translational potential of allosteric modulators targeting the cannabinoid CB(1) receptor*. Acta Pharmacol Sin, 2019. **40**(3): p. 324-335.
 145. Nguyen, T., B.F. Thomas, and Y. Zhang, *Overcoming the Psychiatric Side Effects of the Cannabinoid CB1 Receptor Antagonists: Current Approaches for Therapeutics Development*. Curr Top Med Chem, 2019. **19**(16): p. 1418-1435.
 146. Palmer, S.L., G.A. Thakur, and A. Makriyannis, *Cannabinergic ligands*. Chemistry and Physics of Lipids, 2002. **121**(1-2): p. 3-19.
 147. Pertwee, R.G., *Ligands that target cannabinoid receptors in the brain: from THC to anandamide and beyond*. Addiction biology, 2008. **13**(2): p. 147-159.
 148. Sugiura, T., *Physiological roles of 2-arachidonoylglycerol, an endogenous cannabinoid receptor ligand*. Biofactors, 2009. **35**(1): p. 88-97.
 149. Vaseghi, G., M. Rabbani, and V. Hajhashemi, *The effect of AM281, a cannabinoid antagonist, on memory performance during spontaneous morphine withdrawal in mice*. Res Pharm Sci, 2013. **8**(1): p. 59-64.
 150. Kadoi, Y. and F. Goto, *Effects of AM281, a cannabinoid antagonist, on circulatory deterioration and cytokine production in an endotoxin shock model: comparison with norepinephrine*. J Anesth, 2006. **20**(4): p. 284-9.
 151. Murphy, T. and B. Le Foll, *Targeting the Endocannabinoid CB1 Receptor to Treat Body Weight Disorders: A Preclinical and Clinical Review of the Therapeutic Potential of Past and Present CB1 Drugs*. Biomolecules, 2020. **10**(6).
 152. Xie, S., et al., *The endocannabinoid system and rimonabant: a new drug with a novel mechanism of action involving cannabinoid CB1 receptor antagonism--or inverse agonism--as potential obesity treatment and other therapeutic use*. J Clin Pharm Ther, 2007. **32**(3): p. 209-31.
 153. Sam, A.H., V. Salem, and M.A. Ghatei, *Rimonabant: From RIO to Ban*. J Obes, 2011. **2011**: p. 432607.
 154. Carai, M.A., et al., *Efficacy of rimonabant and other cannabinoid CB1 receptor antagonists in reducing food intake and body weight: preclinical and clinical data*. CNS Drug Rev, 2006. **12**(2): p. 91-9.
 155. Chorvat, R.J., et al., *JD-5006 and JD-5037: peripherally restricted (PR) cannabinoid-1 receptor blockers related to SLV-319 (Ibipinabant) as metabolic*

- disorder therapeutics devoid of CNS liabilities*. *Bioorg Med Chem Lett*, 2012. **22**(19): p. 6173-80.
156. Ravinet Trillou, C., et al., *CB1 cannabinoid receptor knockout in mice leads to leanness, resistance to diet-induced obesity and enhanced leptin sensitivity*. *Int J Obes Relat Metab Disord*, 2004. **28**(4): p. 640-8.
157. Herling, A.W., et al., *Increased energy expenditure contributes more to the body weight-reducing effect of rimonabant than reduced food intake in candy-fed wistar rats*. *Endocrinology*, 2008. **149**(5): p. 2557-66.
158. Leija-Salazar, M., et al., *Arachidonyl-2'-chloroethylamide (ACEA), a synthetic agonist of cannabinoid receptor, increases CB(1)R gene expression and reduces dyskinesias in a rat model of Parkinson's disease*. *Pharmacol Biochem Behav*, 2020. **194**: p. 172950.
159. Howlett, A.C. and M.E. Abood, *CB(1) and CB(2) Receptor Pharmacology*. *Adv Pharmacol*, 2017. **80**: p. 169-206.
160. Aso, E., et al., *CB1 agonist ACEA protects neurons and reduces the cognitive impairment of A β PP/PS1 mice*. *J Alzheimers Dis*, 2012. **30**(2): p. 439-59.
161. Herrington, W., et al., *Epidemiology of Atherosclerosis and the Potential to Reduce the Global Burden of Atherothrombotic Disease*. *Circ Res*, 2016. **118**(4): p. 535-46.
162. Cabral, G.A. and L. Griffin-Thomas, *Emerging role of the cannabinoid receptor CB2 in immune regulation: therapeutic prospects for neuroinflammation*. *Expert Rev Mol Med*, 2009. **11**: p. e3.
163. McKenna, M. and J.J. McDougall, *Cannabinoid control of neurogenic inflammation*. *Br J Pharmacol*, 2020. **177**(19): p. 4386-4399.
164. Almogi-Hazan, O. and R. Or, *Cannabis, the Endocannabinoid System and Immunity-the Journey from the Bedside to the Bench and Back*. *Int J Mol Sci*, 2020. **21**(12).
165. Pacher, P., S. Bátkai, and G. Kunos, *Cardiovascular pharmacology of cannabinoids*. *Handb Exp Pharmacol*, 2005(168): p. 599-625.
166. Singla, S., R. Sachdeva, and J.L. Mehta, *Cannabinoids and atherosclerotic coronary heart disease*. *Clin Cardiol*, 2012. **35**(6): p. 329-35.
167. Tudorancea, I.M., et al., *The Therapeutic Potential of the Endocannabinoid System in Age-Related Diseases*. *Biomedicines*, 2022. **10**(10).
168. Sugamura, K., et al., *Activated endocannabinoid system in coronary artery*

- disease and antiinflammatory effects of cannabinoid 1 receptor blockade on macrophages*. *Circulation*, 2009. **119**(1): p. 28-36.
169. Marsicano, G., et al., *CB1 cannabinoid receptors and on-demand defense against excitotoxicity*. *Science*, 2003. **302**(5642): p. 84-8.
170. Janjic, A., et al., *Prime-seq, efficient and powerful bulk RNA sequencing*. *Genome Biol*, 2022. **23**(1): p. 88.
171. Love, M.I., W. Huber, and S. Anders, *Moderated estimation of fold change and dispersion for RNA-seq data with DESeq2*. *Genome Biol*, 2014. **15**(12): p. 550.
172. Yu, G. and Q.Y. He, *ReactomePA: an R/Bioconductor package for reactome pathway analysis and visualization*. *Mol Biosyst*, 2016. **12**(2): p. 477-9.
173. Subramanian, A., et al., *Gene set enrichment analysis: a knowledge-based approach for interpreting genome-wide expression profiles*. *Proc Natl Acad Sci U S A*, 2005. **102**(43): p. 15545-50.
174. Mootha, V.K., et al., *PGC-1alpha-responsive genes involved in oxidative phosphorylation are coordinately downregulated in human diabetes*. *Nat Genet*, 2003. **34**(3): p. 267-73.
175. Jiang, L.S., et al., *Role of activated endocannabinoid system in regulation of cellular cholesterol metabolism in macrophages*. *Cardiovasc Res*, 2009. **81**(4): p. 805-13.
176. Clausen, B.E., et al., *Conditional gene targeting in macrophages and granulocytes using LysMcre mice*. *Transgenic Res*, 1999. **8**(4): p. 265-77.
177. Roy, P., M. Orecchioni, and K. Ley, *How the immune system shapes atherosclerosis: roles of innate and adaptive immunity*. *Nature Reviews Immunology*, 2022. **22**(4): p. 251-265.
178. Hunter, M., et al., *Survival of monocytes and macrophages and their role in health and disease*. *Front Biosci (Landmark Ed)*, 2009. **14**(11): p. 4079-102.
179. Auffray, C., M.H. Sieweke, and F. Geissmann, *Blood monocytes: development, heterogeneity, and relationship with dendritic cells*. *Annu Rev Immunol*, 2009. **27**: p. 669-92.
180. Soehnlein, O., et al., *Distinct functions of chemokine receptor axes in the atherogenic mobilization and recruitment of classical monocytes*. *EMBO Mol Med*, 2013. **5**(3): p. 471-81.
181. Sinitiski, D., et al., *Macrophage Migration Inhibitory Factor (MIF)-Based Therapeutic Concepts in Atherosclerosis and Inflammation*. *Thromb Haemost*,

2019. **119**(4): p. 553-566.
182. Stelzer, G., et al., *The GeneCards Suite: From Gene Data Mining to Disease Genome Sequence Analyses*. Curr Protoc Bioinformatics, 2016. **54**: p. 1.30.1-1.30.33.
183. Gautier, E.L., et al., *Gene-expression profiles and transcriptional regulatory pathways that underlie the identity and diversity of mouse tissue macrophages*. Nat Immunol, 2012. **13**(11): p. 1118-28.
184. Roy, P., M. Orecchioni, and K. Ley, *How the immune system shapes atherosclerosis: roles of innate and adaptive immunity*. Nat Rev Immunol, 2022. **22**(4): p. 251-265.
185. Susser, L.I. and K.J. Rayner, *Through the layers: how macrophages drive atherosclerosis across the vessel wall*. J Clin Invest, 2022. **132**(9).
186. Vargas, R., et al., *Oestradiol inhibits smooth muscle cell proliferation of pig coronary artery*. Br J Pharmacol, 1993. **109**(3): p. 612-7.
187. Mossuz, P., et al., *Effects of two sex steroids (17beta estradiol and testosterone) on proliferation and clonal growth of the human monoblastic leukemia cell line, U937*. Leuk Res, 1998. **22**(11): p. 1063-72.
188. Tall, A.R., et al., *Cholesterol efflux: a novel regulator of myelopoiesis and atherogenesis*. Arterioscler Thromb Vasc Biol, 2012. **32**(11): p. 2547-52.
189. Yvan-Charvet, L., et al., *ATP-binding cassette transporters and HDL suppress hematopoietic stem cell proliferation*. Science, 2010. **328**(5986): p. 1689-93.
190. Murphy, A.J., et al., *ApoE regulates hematopoietic stem cell proliferation, monocytosis, and monocyte accumulation in atherosclerotic lesions in mice*. J Clin Invest, 2011. **121**(10): p. 4138-49.
191. Stark, C., et al., *BioGRID: a general repository for interaction datasets*. Nucleic Acids Res, 2006. **34**(Database issue): p. D535-9.
192. Feng, Q., et al., *A common functional promoter variant links CNR1 gene expression to HDL cholesterol level*. Nat Commun, 2013. **4**: p. 1973.
193. Jourdan, T., et al., *Activation of the Nlrp3 inflammasome in infiltrating macrophages by endocannabinoids mediates beta cell loss in type 2 diabetes*. Nat Med, 2013. **19**(9): p. 1132-40.
194. Tall, A.R. and L. Yvan-Charvet, *Cholesterol, inflammation and innate immunity*. Nat Rev Immunol, 2015. **15**(2): p. 104-16.
195. Moore, K.J. and I. Tabas, *Macrophages in the pathogenesis of atherosclerosis*.

- Cell, 2011. **145**(3): p. 341-55.
196. Rayner, K.J., *Cell Death in the Vessel Wall: The Good, the Bad, the Ugly*. Arterioscler Thromb Vasc Biol, 2017. **37**(7): p. e75-e81.
197. Taylor, W.R. and G.R. Stark, *Regulation of the G2/M transition by p53*. Oncogene, 2001. **20**(15): p. 1803-15.
198. Rivlin, N., et al., *Mutations in the p53 Tumor Suppressor Gene: Important Milestones at the Various Steps of Tumorigenesis*. Genes Cancer, 2011. **2**(4): p. 466-74.
199. Williams, A.B. and B. Schumacher, *p53 in the DNA-Damage-Repair Process*. Cold Spring Harb Perspect Med, 2016. **6**(5).
200. Azar, S., et al., *Reversal of diet-induced hepatic steatosis by peripheral CB1 receptor blockade in mice is p53/miRNA-22/SIRT1/PPAR α dependent*. Mol Metab, 2020. **42**: p. 101087.
201. Guevara, N.V., et al., *The absence of p53 accelerates atherosclerosis by increasing cell proliferation in vivo*. Nat Med, 1999. **5**(3): p. 335-9.
202. Merched, A.J., E. Williams, and L. Chan, *Macrophage-specific p53 expression plays a crucial role in atherosclerosis development and plaque remodeling*. Arterioscler Thromb Vasc Biol, 2003. **23**(9): p. 1608-14.
203. Chan, G.H., et al., *The role of p53 in the alternation of vascular functions*. Front Pharmacol, 2022. **13**: p. 981152.
204. Zekavat, S.M., et al., *TP53-mediated clonal hematopoiesis confers increased risk for incident atherosclerotic disease*. Nat Cardiovasc Res, 2023. **2**: p. 144-158.
205. Ding, L., et al., *The Roles of Cyclin-Dependent Kinases in Cell-Cycle Progression and Therapeutic Strategies in Human Breast Cancer*. Int J Mol Sci, 2020. **21**(6).
206. Galbraith, M.D., H. Bender, and J.M. Espinosa, *Therapeutic targeting of transcriptional cyclin-dependent kinases*. Transcription, 2019. **10**(2): p. 118-136.
207. Borghese, F. and F.I. Clanchy, *CD74: an emerging opportunity as a therapeutic target in cancer and autoimmune disease*. Expert Opin Ther Targets, 2011. **15**(3): p. 237-51.
208. Van den Bossche, J., et al., *Mitochondrial Dysfunction Prevents Repolarization of Inflammatory Macrophages*. Cell Rep, 2016. **17**(3): p. 684-696.

209. Gardiner, S.M., et al., *Involvement of CB1-receptors and beta-adrenoceptors in the regional hemodynamic responses to lipopolysaccharide infusion in conscious rats*. Am J Physiol Heart Circ Physiol, 2005. **288**(5): p. H2280-8.
210. Bénard, G., et al., *Mitochondrial CB₁ receptors regulate neuronal energy metabolism*. Nat Neurosci, 2012. **15**(4): p. 558-64.
211. Molica, F., et al., *Endogenous cannabinoid receptor CB1 activation promotes vascular smooth-muscle cell proliferation and neointima formation*. J Lipid Res, 2013. **54**(5): p. 1360-8.
212. Bátkai, S., et al., *Endocannabinoids acting at vascular CB1 receptors mediate the vasodilated state in advanced liver cirrhosis*. Nat Med, 2001. **7**(7): p. 827-32.
213. Guillamat Prats, R., et al., *Deficiency of Monoacylglycerol Lipase Enhances IgM Plasma Levels and Limits Atherogenesis in a CB2-Dependent Manner*. Thromb Haemost, 2019. **119**(2): p. 348-351.
214. Zhang, Q., et al., *Genotype effects contribute to variation in longitudinal methylome patterns in older people*. Genome Med, 2018. **10**(1): p. 75.
215. Navarro, D., et al., *Molecular Alterations of the Endocannabinoid System in Psychiatric Disorders*. Int J Mol Sci, 2022. **23**(9).
216. Chukwueke, C.C., et al., *The CB1R rs2023239 receptor gene variant significantly affects the reinforcing effects of nicotine, but not cue reactivity, in human smokers*. Brain Behav, 2021. **11**(2): p. e01982.
217. Yao, Y., et al., *Detection of Significant Association Between Variants in Cannabinoid Receptor 1 Gene (CNR1) and Personality in African-American Population*. Front Genet, 2018. **9**: p. 199.
218. Arnold, A.P. and X. Chen, *What does the "four core genotypes" mouse model tell us about sex differences in the brain and other tissues?* Front Neuroendocrinol, 2009. **30**(1): p. 1-9.

8. ACKNOWLEDGEMENTS

I extend my heartfelt appreciation to all those who played a role in the completion of this dissertation. Foremost, I would like to express my sincerest gratitude to my supervisor, Prof. Dr. Sabine Steffens, for her unwavering support and guidance throughout my Ph.D. journey. Her patience, vast knowledge, and trust in my abilities allowed me to work in my own unique way. Not only did Sabine provide academic guidance, but she also offered emotional encouragement during the challenging phases of this thesis. I am grateful for the opportunity to work in her laboratory and contribute to this remarkable project. Working with Sabine has always been a comfortable and enriching experience, and I couldn't have asked for a better supervisor.

I am immensely grateful to the cheerful and friendly group of colleagues I had the pleasure of working with. I would like to extend my thanks to each of them for their valuable assistance. Over the past few years, Dr. Raquel Guillamat Prats, an experienced and enthusiastic researcher in the field of endocannabinoids, provided intensive advice and support. Her supervision, contributions, and suggestions during my training and research were instrumental in the completion of this work. I would also like to acknowledge the significant contributions of Dr. Alexander Faussner, Dr. Sarah-Lena Puhl, and Dr. Martina Rami, whose involvement greatly influenced my work and training. I am also grateful to my fellow Ph.D. students, particularly Bingni Chen, who was not only a sincere friend but also shared the same lab with me for more than four years, providing invaluable assistance in both work and daily life. George Shakir and Guo Li also deserve my appreciation for their helpfulness, encouragement, and contributions to various aspects of this project.

The support and contributions of our technicians, Martina Geiger, Daniela Wagner, Silviya Wolkerstorfer, Rodrigo Carrasco, Yvonne Jansen, and Soyolmaa Bayasgalan, in conducting numerous experiments are deeply acknowledged. Their dedicated time and effort were crucial to the success of this research.

Furthermore, I would like to express gratitude to our assistant students, Seray Anak and Marleen Stremlau, who devoted considerable time and effort to various experiments, making significant contributions to the overall progress of this work.

Finally, I would like to extend my thanks to the China Scholarship Council (CSC) for providing funding throughout my doctoral studies, enabling me to pursue this research endeavor.

9. Confirmation of congruency



Confirmation of congruency between printed and electronic version of the doctoral thesis

Doctoral candidate: Yong Wang

I hereby declare that the electronic version of the submitted thesis, entitled
Role of macrophage CB1 in atherosclerosis
is congruent with the printed version both in content and format.

Munich 25.03.2024

Place, Date

Yong Wang

Signature doctoral candidate